The Hong Kong Polytechnic University

Department of Building Services Engineering

Development and Verification of Simulation Model of Hybrid Ground-Coupled Heat Pump Systems with Inclined Boreholes

Cui Ping

A thesis submitted in partial fulfillment of the requirements

for the Degree of Doctor of Philosophy

May 2008

CERTIFICATE OF ORIGINALITY

I hereby declare that this thesis is my own work and that, to the best of my knowledge and belief, it reproduces no material previously published or written, nor material that has been accepted for the award of any other degree or diploma, except where due acknowledgement has been made in the text.

Cui Ping

Department of Building Services Engineering

The Hong Kong Polytechnic University

Hong Kong, China

May 2008

ABSTRACT

Abstract of thesis entitled: Development and Verification of Simulation Model of Hybrid Ground-Coupled Heat Pump Systems with Inclined Boreholes

Submitted by : Cui Ping

For the degree of : Doctor of Philosophy
at The Hong Kong Polytechnic University in May, 2008.

The technology of the ground-coupled heat pump (GCHP) offers a high energy efficient way to provide space heating and cooling as well as domestic hot water. Based on the restrictions of the GCHP application in warm-climate areas, this thesis proposed a new hybrid GCHP (HGCHP) system with a desuperheater and inclined ground heat exchanger (GHE) for the possibility of improving the application of the GCHP system in cooling-dominated buildings. This thesis focuses on developing a new simulation model of the novel HGCHP system and analyzing the energy and exergy performances of the system applied in warm-climate areas.

Firstly, an analytical model of the inclined finite-line source has been developed to describe the transient and steady-state heat conduction processes in GHEs with inclined and vertical boreholes for long-term operation. An approximate method with satisfactory accuracy is proposed for the GHE design on the basis of the simulation model and recommended for engineering applications. The experimental validation shows that the analytical model is generally accurate to within ±12%, which is considered to be satisfactory for practical engineering.

To compensate for the inaccuracy of the finite line source model for short-time scale, a two-dimensional numerical finite element model has been established within the *ANSYS* simulation environment. Comparisons between the numerical and analytical results show that the finite line-source model is capable of modeling the GHEs except for a few hours because of the line-source assumption. The numerical finite element model was validated by the measured U-tube wall temperatures during a short-time period. The results demonstrate a reasonable agreement between the numerical and the measured data.

A steady-state, distributed parameter model of a water-to-water heat pump with a desuperheater (i.e. an HGCHP unit) has been developed. A comprehensive simulation program of the HGCHP system is thus developed, which is formed by the coupling of the heat pump unit and GHE models. A number of simulation cases were carried out, which demonstrate that the HGCHP system can offer considerable energy savings in the operating modes with DHW heating, especially in the case of using the desuperheater only to preheat hot water.

The simulation model of the HGCHP system was extensively validated by experiments, covering four different operation modes which are commonly used in practice, i.e. cooling only, cooling with DHW, heating with DHW and DHW heating modes. The results show, on the whole, the simulation model is accurate to within ±15% of the experimental data, which demonstrates that it is suitable for research study and engineering applications with an acceptable accuracy.

An exergy analysis of the HGCHP system is implemented on the basis of experimental data and the simulation model. Comparisons between the HGCHP and

conventional systems (air-source heat pump, electric heater and gas-fired boiler) show that the HGCHP system possesses the highest exergy and energy efficiencies. An optimum operating condition of the HGCHP system can be found, which behaves high energy efficiency and simultaneously remains high exergy efficiency through co-analysis of the first and second laws of thermodynamics.

Finally, an annual hourly simulation of the hybrid GCHP system is performed within the HVACSIM+ environment for a small residential apartment in Hong Kong. Compared with the conventional GCHP system, the hybrid system can effectively alleviate the imbalanced loads of the GHE on an annual basis. Furthermore, it can offer a significant energy saving of 67% for the DHW heating when compared with a conventional DHW heating system.

In summary, the simulation model of the GHE can be used to analyze or design the GHEs with inclined boreholes. The simulation model of the HGCHP with DHW system can provide a useful and effective tool to investigate the system performance in a variety of operating modes. The simulation and experimental results obtained in this thesis demonstrate that the HGCHP system can improve energy performance and occupy less ground area, as well as reduce the hot water heating capacity of boilers or electric heaters. Based on the substantial simulation results, it is feasible and desirable to apply this kind of system to cooling-dominated buildings in Hong Kong and other southern regions of China.

Keywords: Hybrid ground-coupled heat pump; inclined borehole; desuperheater; domestic hot water; exergy analysis; ground heat exchanger; thermal storage water tank; numerical method; heat transfer; finite line source.

PUBLICATIONS ARISING FROM THIS STUDY

Journal papers

P. Cui, H. Yang and Z. Fang， Numerical analysis and experimental validation of heat transfer in ground heat exchangers in alternative operation modes，*Energy and Buildings*, 2008, 40(6): 1060-1066

Ping Cui, Hongxing Yang, Zhaohong Fang. The Simulation Model and Design Optimization of Ground Source Heat Pump Systems. *HKIE Transactions*, 2007, 14(1):1-5.

Ping Cui, Hongxing Yang, Zhaohong Fang. Heat transfer analysis of ground heat exchangers with inclined boreholes. *Applied Thermal Engineering*, 2006, 26(11-12): 1169-1175.

Yang, H., C. Ren and P Cui, Study on performance correlations of an indirect evaporative cooler with condensation from primary airflow, *ASHRAE HVAC&R Research*, 2006, 12(3): 519-532.

Cui Ping, Man Yi, Fang Zhao-hong. Modeling of Heat Transfer in Geothermal Heat Exchangers. *Journal of Harbin Institute of Technology*, Volume 13 Number Sup. Oct. 2006, pp 313-318.

P. Cui, H. Yang, Z Fang, Energy and Exergy Analysis of Hybrid Ground Coupled Heat Pumps with Hot Water Supply, accepted by *International Journal of Exergy*.

Conference papers

Ping Cui, Hongxing Yang, Zhaohong Fang. Investigation on the Operating Performance of Hybrid Ground Coupled Heat Pump Systems: a Case Study in Hong Kong, 6th International Conference on Sustainable Energy Technologies. Santiago, Chile, 2007.

Ping Cui, Hongxing Yang, Zhaohong Fang. A Simulation Study on a New Hybrid GCHP System in Hong Kong. 5th International Conference on Sustainable Energy Technologies. P537-543 Vicenza, Italy, 2006

Z Fang, N Diao, M Yu and P Cui, Heat Transfer analysis of geothermal heat exchangers in ground-coupled heat pump systems, Proceedings of the 13th International Heat Transfer Conference, HEX-01, 2006.

Ping Cui, Hongxing Yang, Zhaohong Fang. A Systemic Simulation Model and Experiments on Vertical Ground Heat Exchangers in GCHP Systems. Proc. of 6th International Conference on Tall Buildings, pp881-887, Hong Kong, 2005.

Weicui Chen, Ping Cui and Zhaohong Fang, Analyses on Temperature Distribution around an Inclined Borehole in Ground Heat Exchangers, 4th International Conference on Sustainable Energy Technologies. Jinan, China, 23-25 September 2005.

ACKNOWLEDGEMENTS

This thesis could not be finished without the help and support of those who are gratefully acknowledged here.

First and foremost, I would like to express my deepest gratitude to my chief supervisor, Dr Yang Hongxing, for his invaluable guidance, support and continuous encouragement throughout the course of my research work.

My sincere gratitude is devoted to my co-supervisor Professor Fang Zhaohong who kept an eye on the progress of the research work. This thesis owes much to his thoughtful and helpful comments.

My special thanks go to Mr. H K Chan and his technicians for their hard work and useful suggestions in setting up the in-situ experimental rig.

I further express my gratitude to my colleagues in the renewable energy research group for their company and support throughout the PhD study.

My heartfelt appreciation goes to my beloved family members: my parents, my sisters and their lovely children, especially my husband, Sun Changliang. Their loving considerations and spiritual supports encouraged me to accomplish this work. This thesis is dedicated to all of them.

Finally I want to thank everyone who directly or indirectly offered his/her help and support to this thesis.

TABLE OF CONTENTS

LIST OF FIGURES

LIST OF TABLES

NOMENCLATURE

Symbols	Description	Unit
A	Heat transfer area	m^2
a	Ground thermal diffusivity	m^2 /s
B	Space between boreholes	m
Bo	Refrigerant boiling number	DL
B_r	Integrated refrigerant thermophysical property	DL
C_1~C_5	Constants in Equation (5.15)	DL
Co	Refrigerant convection number	DL
c_p	Water specific heat capacity	kJ/ (kg·K)
d	Diameter	m
d_e	Equivalent diameter	m
e (or E)	specific stream exergy of a fluid	kJ/kg
$\dot{E}$	Rate of exergy	kW
EWT	Entering water temperature from GHE to heat pump	˚C
$ExWT$	Exiting water temperature from Heat pump to GHE	˚C
f	Friction factor for single-phase flow	DL
	or correction factor	DL
F_{fl}	fluid-dependent parameter	DL
Fo	Fourier number	DL
Fr_{lo}	Froude number with all flow as liquid	DL

G	Mass velocity	kg/(m^2.s)
h	Refrigerant enthalpy or	kJ/kg
	convective heat transfer coefficient	W/(m^2.K)
H	Borehole depth	m
$\dot{I}$	Rate of irreversibility	kW
k	Thermal conductivity	W/ (m·K)
l	Variable of borehole depth	m
L	Length	m
$\dot{m}$	Mass flow rate	kg/s;
m	Re-expansion exponent	DL
M	Refrigerant mass	kg
n	Polytropic exponent	DL
P	Refrigerant pressure	kPa
Pr	Prandtl number	DL
Q	Heat transfer rate	W
q_l	Heat flow per unit length of borehole	W/m
r_b	Borehole radius	m
Re	Reynolds number	DL
r_p	Pipe wall thermal resistance	(m^2·K)/W
s	Specific entropy	kJ/kgK
	Or space between the pipe center and the borehole center	m
T *or* t	Temperature	˚C
U	Overall heat transfer coefficient	W/(m^2·K)

$Power$	Compressor power input	W
W_{th}	Theoretical work	W
x	Refrigerant quality	DL
X_{tt}	Martinelli parameter	DL
V	Volume	m^3
$\dot{V}_{th}$	Theoretical displacement volumetric flow rate	m^3/s

Greek

α	Inclined angle of borehole	°
β	direction angle of borehole	°
ε	Exergy efficiency	DL
ε_R	correction factor for the tube rows	DL
ε_v	Refrigerant vapor void fraction	DL
ξ	Coefficient of heat loss	DL
η	Compressor efficiency or Energy efficiency of electric heater	DL
η_{i}	Compressor indicated efficiency	DL
η_{m}	Compressor mechanical efficiency	DL
η_{mo}	Compressor motor efficiency	DL
θ	Angular coordinate	°
Θ	Dimensionless temperature	DL
λ	Volumetric efficiency	DL
λ_l	Compressor leakage coefficient	DL

λ_T	Compressor temperature coefficient	DL
λ_p	Compressor pressure loss coefficient	DL
λ_v	Compressor volumetric coefficient	DL
μ	Dynamic viscosity	Pa.s
ρ	Density	kg/m^3
τ	Time	s
ν	Specific volume	m^3/kg
φ	Ratio of the specific chemical exergy of the coal gas to its net calorific value	DL
w	Uncertainty of measured variable	DL
	Or angle in cross-section circle	°
σ	Relative uncertainty of variable	DL
Δt_m	Log-mean temperature difference	˚C
ΔP_{dis}	Pressure drop across the discharge valve	kPa

Subscript	**Description**
1	Refrigerant state 1 or inlet condition
2	Refrigerant state 2 or outlet condition
ambient	Ambient air
ASHP	Air source heat pump
b	Borehole
c	Condensing
	or mean temperature of cross-section circle

com	Compressor
con	Condenser
down	down pipe
dsp	Desuperheater
e	Evaporation
	or temperature of borehole wall in ground heat exchangers
Elc	Electric hot water heater
env	Environment
evp	Evaporator
f1	Inlet state of water
f2	Outlet state of water
far	far-field boundary
g	Grout
Gain	Exergy gain
GasB	Gas-fired boiler
i	Base borehole
in	Inner diameter/ inlet state
j	Adjacent borehole
l	Liquid
L	Mean temperature over borehole depth *L*
o	Out diameter
out	Outlet state
p	Pipe
r	Refrigerant

	or representative temperature
sc	Subcooling
sh	Superheating
Soil	Surrounding soil
tp	Two-phase
up	Up pipe
v	Vapor
w	Water
wo	Inner tube wall
ω	Temperature at the angle ω of a cross-section

Note: DL=Dimensionless

CHAPTER 1 INTRODUCTION

1.1 Ground Source Heat Pump

With the rapid economic development and increasing indoor comfort requirements in recent years, air conditioning (A/C) and hot water supply have been contributing to a significant percentage of the total energy consumption in Hong Kong. According to a report of the "Hong Kong Energy End-use Data" conducted by the Electrical and Mechanical Services Department (2006) of the Hong Kong SAR Government, the air-conditioning (A/C) plays a dominant role in energy consumption in Hong Kong, accounting for 28% and 22% of the total energy end-uses respectively in commercial and residential buildings in 2004. In addition, about 23% of the total energy end-use in residential buildings was consumed to heat domestic hot water (DHW) in 2004. The growing energy shortage has now become a worldwide crisis. Consequently, more efforts should be made to reduce the considerable energy consumption of air-conditioning and hot water heating.

Heat pumps offer the most energy efficient way to provide space heating and cooling as well as domestic hot water since they can utilize renewable heat sources, such as air, ground and surface water which contain useful energy that can be continuously replenished by the sun. The majority of heat pumps currently in operation utilize either ambient air or ground as heat source/sink, which are called air source heat pump system (ASHP) and ground source heat pump system (GSHP)

respectively. From a thermodynamic perspective, the overall energy efficiencies of the GSHP systems are much higher than those of the ASHPs because the underground environment experiences less temperature fluctuation compared with the ambient air temperature change. Besides the advantage of high efficiency, the GSHP systems offer other attractive benefits over conventional heating/cooling systems:

- Low maintenance cost and low noise

  The system eliminates the need for a cooling tower or any other outdoor equipment, which can significantly reduce the maintenance cost and noise.

- Environmental Friendliness

  This system produces less carbon dioxide and other pollutants than its conventional alternatives, thus reducing global warming and other environmental impacts.

- Building aesthetics and less required mechanical room

  Without boilers and cooling towers, the building aesthetics is improved by fewer external penetrations of the building envelope and the system requires less mechanical room, allowing for more profitable space use.

The GSHPs comprise a wide variety of systems that may use groundwater, ground, or surface water as heat sources or sinks. These systems have been basically grouped into three categories by ASHRAE (1999), i.e. (1) ground-water heat pump (GWHP) systems, (2) surface water heat pump (SWHP) systems, and (3) ground

coupled heat pump (GCHP) systems. The schematics of these different systems are shown in Figure 1.1.

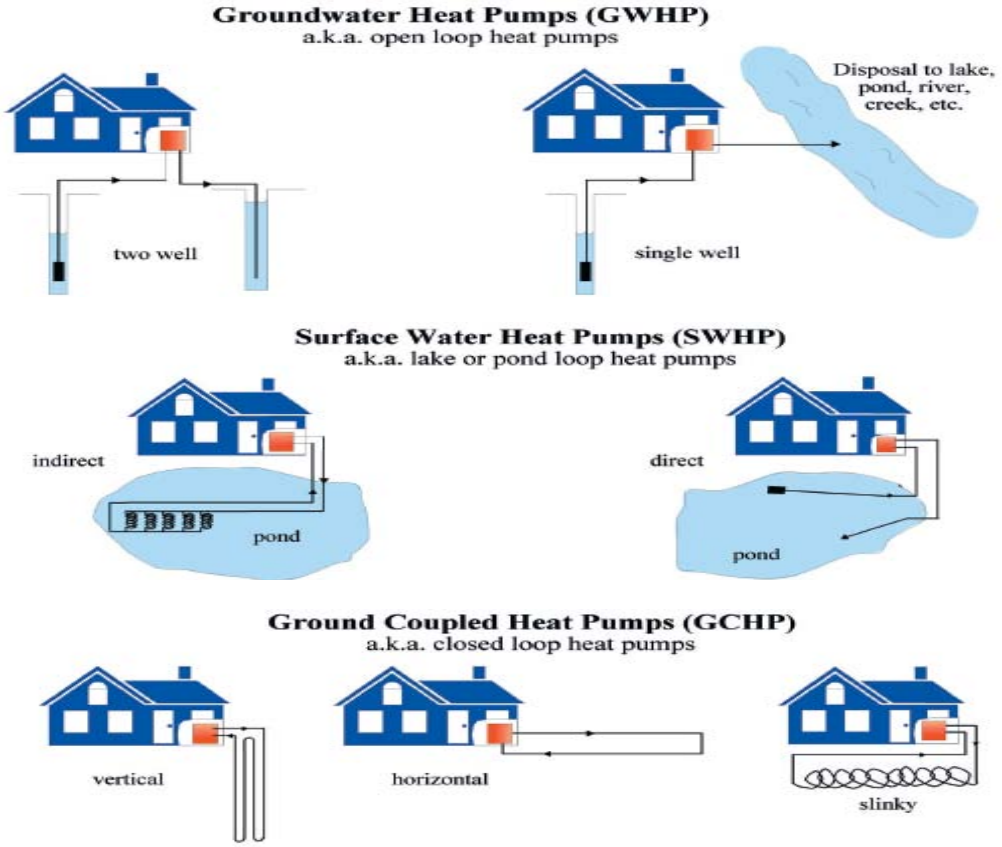

Figure 1.1 Schematics of different ground source heat pumps

(Cited from http://geoheat.oit.edu/ghp/survival.pdf)

The GWHP system, also referred to as open loop systems, is the original type of the GSHP systems, which utilizes ground water as heat source or heat sink. Ground water is supplied directly or indirectly to the heat pump units from a well or wells equipped with submersible pumps, and it can be discharged either on the subsurface through another well or the surface (ASHRAE, 1995). The GWHP systems have some marked advantages including low capital and operating costs, and minimal requirement for ground surface area over other GSHP systems. However, a number

of factors seriously restrict the wide application of the GWHP systems, among which the limited availability of ground water and the high maintenance cost due to the fouling corrosion are the most significant factors. In addition, many legal issues have arisen over ground water withdrawal and re-injection in some regions, which also restrict their applications to a large extent.

In a SWHP system, heat rejection/extraction is accomplished by circulating working fluid through high-density polyethylene (HDPE) pipes positioned at an adequate depth within a lake, pond, reservoir, or other suitable open channels. Natural convection becomes the primary role rather than heat conduction in the heat transfer process in a GCHP system, which tends to have higher heat exchange capability than a GCHP system. The major disadvantage of the system is that the surface water temperature is more affected by weather condition, especially in winter.

In a GCHP system, heat is extracted from or rejected to the ground via a closed loop through which pure water or an antifreeze solution circulates. The ground heat exchangers (GHEs) used in the closed loop systems typically consist of HDPE pipes installed in vertical boreholes or horizontal trenches, which are called vertical or horizontal GCHP systems, respectively.

1.2 Ground Coupled Heat Pump

In horizontal GCHP systems, the GHEs typically consist of a series of parallel pipe arrangements laid out in dug trenches approximately 1-2meters below the ground surface. A disadvantage is that the horizontal systems are more affected by ambient air temperature fluctuations because of their proximity to the ground surface. Other

disadvantage is that the installation of the horizontal systems needs much more ground area than vertical systems.

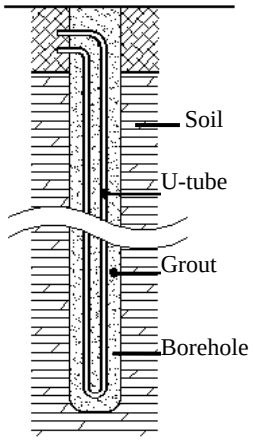

Figure 1.2 Schematic of a grouted borehole

In vertical GCHP systems, the GHE configurations may include one, tens, or even hundreds of boreholes, each containing one or double U-tubes through which the heat exchange fluid is circulated. Typical U-tubes have a diameter in the range of 19mm to 38mm and each borehole is normally 20m to 200m deep with a diameter ranging from 100mm to 200mm. The borehole annulus is generally backfilled with some special material (named as grout) that can prevent the contamination of ground water. A typical borehole with a single U-tube is illustrated in Figure 1.2.

The main advantage of the vertical GCHPs is that they require smaller land areas. Besides, the system can be installed at any location where drilling or earth trenching is feasible.

One of the main concerns in this project is to study the application of the GCHP systems with vertical boreholes in warm-climate areas like Hong Kong. The term

"GCHP" in the following chapters denotes the vertical GCHP systems.

1.3 Restrictions of GCHP Application in Warm-Climate Areas in China

Hundreds of vertical GCHP systems have been installed in China since 2000 due to the awareness on environment and growing energy crisis. It is well known that the GCHP system may achieve highest energy performance in specific locations where building heating and cooling loads are well balanced all the year round because of the long-term transient heat transfer in GHEs.

However, almost all buildings in hot or warm-climate areas are dominated by cooling loads. When the GCHP systems are used in cooling-dominated buildings in warm-climate areas, such as Hong Kong, they will reject more thermal energy to the ground than that they extract from the ground on an annual basis. For a system with a severely undersized GHE, the heat buildup within the ground will definitely increase the ground temperature, which consequently increases the temperature of the inlet water to the heat pump. As a result, the performance of the heat pump will greatly deteriorate over time. It is possible to avoid the problem and keep a better performance of the system by directly increasing the GHE size. As a result, larger GHEs will produce other unexpected problems such as high capital cost of the GHE installation and large required land area. Higher GHE installation cost may make the GCHP system less competitive compared with conventional A/C systems. Furthermore, there may be insufficient land areas for installing larger GHEs in densely-populated cities, especially in Hong Kong.

Therefore, higher capital cost of excessively larger GHEs and/or limited land area have restricted to a large extent the wider applications of this technology in cooling-dominated buildings in warm areas.

1.4 Aims and Objectives

An alternative to decrease the GCHP system capital cost and, at the same time, to improve the system performance is to employ a supplemental heat rejecter, which is called the hybrid GCHP (HGCHP) system. Incorporating a supplemental heat rejecter can reduce a fair amount of heat rejected into the ground and then effectively balance the ground thermal loads, which can consequently reduce the capital cost of the system and improve the operating performance.

In recent years, some concerns have been raised on the application of the HGCHP system with a supplemental heat rejecter in cooling-dominated buildings (Kavanaugh 1998; Yavuzturk and Spitler 2000; Ramamoorthy et al. 2001). Most researchers and engineers tend to add a fluid cooler or a cooling tower to handle the excess cooling requirement. Obviously, this method can reduce the GHE size and the capital cost; however, it is a waste of useful energy and may cause thermal pollution to the environment.

From another point of view, domestic hot water (DHW) is necessary for daily life in residential and some commercial buildings. Traditional hot water supply is usually produced by fossil fuel-fired or electrical boilers, which not only consume a great deal of energy but emit substantial volume of poisonous gases and greenhouse gases into the atmosphere. Considering the two issues together, an economical and

practical way to reduce the high capital cost of the GCHP system and simultaneously decrease the energy consumption for DHW heating is to preheat a portion of DHW using the excess condensation heat through addition of a desuperheater to the heat pump unit. The desuperheater is a small, auxiliary heat exchanger that uses superheated gas from the compressor to heat water. In cooling seasons, the desuperheater uses excess heat that would otherwise be expelled to the ground to heat domestic water virtually for free. In heating seasons, more heat can be extracted from the ground to simultaneously provide space heating and DHW heating, which can further balance the GHE cooling and heating loads in the ground. A schematic diagram can be referred to Figure 6.2.

The new HGCHP system with DHW can improve the operating performance, lower capital cost, and occupy less ground area, in addition to supplying hot water all the year round. The design challenge of the system lies in finding the optimum size of both the GHE and the desuperheater, which directly depends upon the heat transfers of the two components. However, limited performance studies of the new systems have been carried out based on experiments.

Another possible way for further reducing occupied land areas is drilling inclined boreholes rather than vertical ones in the peripheral borehole field as shown in Figure 1.3. It is known that the boreholes in the GHE field should be separated by certain space to reduce the thermal interference among them and ensure long term operation of the system. Inclined boreholes, which are evolved from the vertical borehole systems, can alleviate the thermal interference in the ground while occupying less land area on the ground surface than the vertical GHEs.

Unfortunately, the thermal analysis on the GHE with inclined boreholes is extremely complicated for engineering applications, for it is actually a transient and three-dimensional heat transfer problem. Few studies, therefore, have been carried out on heat transfer process of the GHE with inclined boreholes, except some discussions from a Swedish researcher who did some numerical simulation on the heat conduction of inclined boreholes in a specific GHE. However, the numerical solution of the transient three-dimensional heat transfer is too computationally intensive to be applied generally to engineering designs.

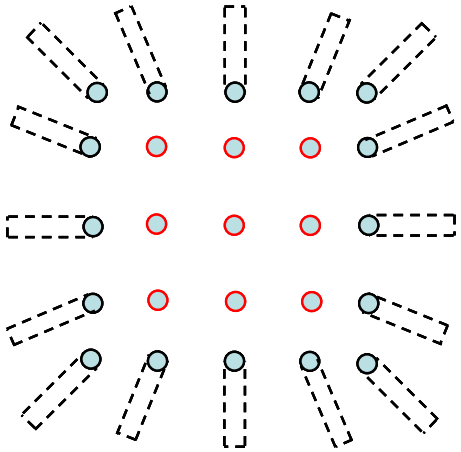

Figure 1.3 Cross section of the inclined GHE arrangement (5X5)

Based on the background discussed above, this thesis focuses on the development of a simulation model of the novel HGCHP system with a desuperheater and inclined GHE and on the analysis of the operating performance of the system to be used in warm-climate areas from energetic and exergetic perspectives.

The aims and objectives of this study are summarized as follows:

a) An analytical heat transfer model of the GHE with vertical and inclined boreholes will be first developed and solved for long-term operation. The

transient and steady-state heat transfer characteristics will be analyzed in terms of certain commonly practical aspects, such as the representative borehole wall temperatures and the thermal interferences among adjacent boreholes. An approximate method or simple algorithm with satisfactory accuracy will be proposed and recommended for engineering applications. The analytical model will be finally experimentally verified.

b) A two-dimensional numerical finite element model will be established in order to compensate for the inaccuracy of the analytical model in short-time scale. Comparisons between the analytical and numerical models will be performed. The numerical model will be finally validated through experimental data.

c) A steady-state deterministic model of a water-to-water heat pump unit with a desuperheater will be developed on the basis of the laws of energy conservation, mass balance, and pressure balance as well as heat transfer correlations. In addition, a comprehensive simulation algorithm of the HGCHP system which incorporates the heat pump and GHE models will be also established in this study. Finally, a program with a friendly interface for the simulation algorithm will be implemented for the purpose of convenient use in research and engineering applications.

d) An experimental rig will be set up for a pilot project of the HGCHP system with DHW. A series of experiments will be conducted to validate the simulation model and investigate the operating performance of the HGCHP system;

e) The comprehensive simulation model of the HGCHP system will be validated under different operating conditions by means of the experimental data collected from the pilot project.

f) The energetic and exergetic performances of the HGCHP system under different operating modes will be extensively discussed using the simulation model of the HGCHP system. A detailed exergy analysis for the DHW heating mode will be presented, which can reveal which component is efficient or inefficient in the system. The exergy performance of the HGCHP system in DHW heating mode will be compared with other conventional DHW heating systems.

g) Finally, an hourly simulation model for the HGCHP with DHW heating system will be performed for a small residential apartment. The HGCHP system performance related to the space cooling, heating and DHW heating will be compared with conventional systems on an hourly basis.

It follows that the results of this research can provide a useful tool for researchers and engineers to better apply the GCHP technology in warm climates.

1.5 Organization of the Thesis

The first chapter presents the basic concept of the GSHP system and its subset, especially the GCHP system. The application restrictions and problems of the GCHPs in cooling-dominated buildings in warm climates are subsequently discussed. Then, a novel HGCHP system with a desuperheater and inclined boreholes is proposed based on the aforementioned problems. The general objective is to develop

a systematic simulation model of the HGCHP system and further estimate the system operating performance when it is applied in warm climates. The detailed aims and objectives of this thesis are also discussed in this chapter.

A comprehensive and critical literature review is presented in Chapter 2. Various models and methods currently employed to analyze the heat transfer of GHEs are presented and compared. This is followed by reviewing the modeling of the heat pump unit without a desuperheater. The study on the HGCHP system is also reviewed here. Finally, the research purpose of this thesis is introduced.

In Chapter 3, the heat transfer characteristics of inclined GHEs including transient and steady-state processes are extensively analyzed by means of the analytical inclined finite line source. Based on the analysis results, the representative temperatures and simplified methods are proposed for engineering applications. Finally, the analytical model is experimentally validated for accurate use in engineering.

Chapter 4 presents a numerical model of GHEs, which is solved by the finite element method in order to investigate the heat transfer process of GHEs during a short-term operation. The simulation results of the analytical and numerical models are compared in this chapter. The numerical model is validated through experimental data as well.

Chapter 5 presents the detailed simulation model of a HGCHP unit equipped with a desuperheater which covers four sub-models of major components. The implementation of a computer simulation program that combines the HGCHP unit

model with the inclined GHE model is developed. The system performance under various operating modes is discussed using the simulation model.

Chapter 6 describes a pilot project of the novel HGCHP system which can provide space heating, cooling and domestic hot water as well. An experimental rig is set up for the project with the aim to validate the simulation models and investigate the system performance. An uncertainty analysis of the experimental data is implemented at the end of Chapter 6.

In Chapter 7, the simulation model of the HGCHP system is extensively validated using experimental data collected from the pilot project. Four operation modes which are commonly used in practice are discussed based on experiments.

In Chapter 8, an exergy analysis of the HGCHP system is implemented on the basis of experimental data and the simulation model developed in Chapter 5. Comparisons between the HGCHP and conventional DHW systems are made with respect to the exergy efficiency.

In Chapter 9, an hourly simulation model of the HGCHP system is performed within the HVACSIM+ environment for a small residential apartment located in Hong Kong. The conventional GCHP system for space cooling/heating and an electric heater for DHW supply are also modeled and simulated on the annual hourly basis for the purpose of comparisons.

Finally, Chapter 10 summarizes the main conclusions and achievements of this thesis and gives recommendations for the future work.

CHAPTER 2 LITERATURE REVIEW

2.1 Introduction

The first known record of the concept of using the ground as heat source for a heat pump occurred in a Swiss patent issued in 1912 (Ball et al. 1983). Thus, the research associated with GSHP systems has been undertaken for nearly a century. The first surge of interest in GSHP systems began in both North America and Europe after World War Two and lasted until the early 1950s when gas and oil became widely used as heating fuels. At that time, 12 major research projects involving laboratory investigations and field monitoring were undertaken by US electric utilities (Spitler 2005). In addition, some basic analytical theory for GSHP heat conduction was proposed by Ingersoll and Plass (1948), which served as a basis for some of the later design programs.

The next period of intense activity on GSHPs started in North America and Europe in 1970s after the first oil crisis, with an emphasis on experimental investigation. During this time period, the research was focused on the development of the vertical system due to the need of less land area for borehole installation. In the ensuing two decades, considerable efforts were made to establish the installation standard and develop some design methods (IGSHPA 1988; Kavanaugh and Rafferty 1997; Bose et al. 1985; Eskilson 1987).

To date, GSHP systems have been widely used in both residential and commercial buildings. It is estimated that GSHP system installations have grown continuously on a global basis with the range from 10 to 30% annually in recent years (Bose 2002). The rapid increase in the application of the GSHP system has driven more specific research in several areas, primarily related to reducing first cost and maintaining low operating costs.

Among the various GSHP systems, as discussed in Chapter 1, the vertical GCHP system has attracted the greatest interest in practical engineering and research field as well, owing to its advantages of less land area requirement and wide range of applicability. This chapter mainly presents a detailed literature-based review of the simulation models of the vertical GCHP system including the GHE and the heat pump unit.

2.2 Simulation Models of Ground Heat Exchangers

The major difference between the GCHP system and conventional A/C systems is the use of a special heat exchanger (i.e. GHE) instead of a cooling tower. The construction costs of GHEs are critical for the economical competitiveness of GCHP systems in the heating and air-conditioning market. On the other hand, the GHE size also plays a decisive role on the performance of GCHP systems. Thus, it is of great importance to work out sophisticated and validated tools by which the thermal behavior of any GCHP system can be assessed and then, optimized in technical and economical aspects.

The main objective of the GHE thermal analysis is to determine the temperature of the heat carrier fluid, which is circulated between the U-tubes and the heat pump, under certain operating conditions. A design goal is then to control the temperature rises of the ground and the circulating fluid within acceptable limits over the system lifespan. Several literature reviews on GHE models have been reported (Cane et al. 1991; Ball et al. 1983; Bose et al. 2002; Spitler 2005; Rawlings et al. 1999).

The “rule of thumb” approximations had been in vogue for a long time, which were discussed by Ball et al. (1983). Rules of thumb can serve well for specific localities where soil and weather conditions are fairly uniform because design specifications are based on the experience with related installations. However, some systems have suffered from the inability of the “rule of thumb” designer to properly assess the effect of varied design parameters, such as shallower burial depth, lower shank spacing between U-tube legs, and larger borehole space in ground surface.

In addition to the rule-of-thumb method, several models with different complexity have been developed for the design and performance prediction of GHEs in engineering applications.

Actually the heat transfer process in a GHE involves a number of uncertain factors, such as the ground thermal properties, the groundwater and building loads, over a long lifespan of several or even tens of years. In this case, the heat transfer process is rather complicated and must be treated, on the whole, as a transient one. In view of the complication of this problem and its long time scale, the heat transfer process may usually be analyzed in two separated regions. One is the solid soil/rock outside the borehole, where the heat conduction must be treated as a transient process. With

the knowledge of the temperature response in the ground, the temperature on the borehole wall can then be determined for any instant on specified operational conditions. Another sector often segregated for analysis is the region inside the borehole, including the grout, the U-tube pipes and the circulating fluid inside the pipes. This region is sometimes analyzed as being quasi-steady-state and sometimes analyzed as being transient. The analyses on the two spatial regions are interlinked on the borehole wall.

2.2.1 Heat conduction outside borehole

A number of simulation models for the heat transfer outside the borehole have been recently reported in open literature, most of which were based on either analytical methodologies or numerical methods. A few models were developed based on the incorporation of the analytical and numerical solutions, such as Eskilson's model (1987).

2.2.1.1 Kelvin's line source

The earliest approach to calculating the thermal transport around a heat exchange pipe in the ground is the Kelvin line source theory, i.e. the infinite line source (Ingersoll and Pass 1948; Ingersoll et al. 1950). In the Kelvin's line-source theory, the ground is regarded as an infinite medium with an initial uniform temperature, in which the borehole is assumed as an infinite line source. The heat transfer in the direction of the borehole axis, including the heat flux across the ground surface and down the bottom of the borehole, is neglected. The heat conduction process in the ground is, therefore, simplified as one-dimensional one. According to the Kelvin's

line-source theory, the temperature response in the ground caused by a constant heat rate is given:

$$t(r,\tau) - t_0 = \frac{q_l}{4\pi k} \int_{\frac{r^2}{4a\tau}}^{\infty} \frac{e^{-u}}{u} du \tag{2.1}$$

where, r is the distance from the line source and τ is the time since the start of the operation; t is the temperature of the ground at distance r and time τ; t_0 is the initial temperature of the ground; q_l is the heating rate per length of the line source; k and a are the thermal conductivity and diffusivity of the ground.

The solution to the integral term in Equation (2.1) can be found from the related references (Ingersoll et al. 1954; Hart and Couvillion 1986; Bose et al. 1985).

Although it is characterized by the simplicity and less computation time, this model can only be applied to small pipes within a narrow range of a few hours to months because of the assumption of the infinite line source (Eskilson 1987; Fang et al. 2002). It was estimated that using the Kelvin's line source may cause a noticeable error when $\frac{a\tau}{r_b^2} < 20$ (Ingersoll et al. 1954).

This approach has been widely utilized in some analytical design methods that are currently used to analyze the heat transfer of GHEs (Hackner et al. 1987; Hart and Couvillion 1986; Bose et al. 1985). A number of improvements for this approach have been proposed to account for some complicated factors so that the accuracy can be comparable to that of the numerical methods. Of all these methods employing

Kelvin's line-source theory, the Hart and Couvillion method (Hart and Couvillion 1986) may be more accurate than others.

2.2.1.2 Cylindrical source model

The cylindrical source solution for a constant heat transfer rate was first developed by Carslaw and Jaeger (1946), then refined by Ingersoll et al. (1954), and later employed in a number of research studies (Kavanaugh 1985; Deerman and Kavanaugh 1991; Bernier 2001; Liu et al. 2001). It is actually an exact solution for a buried cylindrical pipe with infinite length under the boundary condition of either a constant pipe surface temperature or a constant heat transfer rate between the buried pipe and the soil. In the cylindrical source model, the borehole is assumed as an infinite cylinder surrounded by the homogeneous medium with constant properties, i.e. the ground. It also assumes that the heat transfer between the borehole and soil with a perfect contact is pure heat conduction.

Based on the governing equation of the transient heat conduction along with the given boundary and initial conditions, the temperature distribution of the ground can be easily given in the cylindrical coordinate:

$$\begin{cases} \dfrac{\partial^2 t}{\partial r^2}+\dfrac{1}{r}\dfrac{\partial t}{\partial r}=\dfrac{1}{a}\dfrac{\partial t}{\partial \tau} & r_b < r < \infty \\ -2\pi r_b \lambda \dfrac{\partial t}{\partial r}=q_l & r=r_b, \tau>0 \\ t-t_0=0 & \tau=0, r>r_b \end{cases} \tag{2.2}$$

where r_b is the borehole radius.

The cylindrical source solution is given as follows:

$$t - t_0 = \frac{q_l}{k} G(z, p) \tag{2.3}$$

where, $z = \frac{a\tau}{r_b}$, $p = \frac{r}{r_b}$

As defined by Carslaw and Jaeger (1947), the expression *G(z,p)* is only a function of time and distance from the borehole center.

The temperature on the borehole wall, where $r = r_b$, i.e. p=1, is of interest as the representative temperature in the design of GHEs. However, the expression *G(z,p)* is relatively complex and involves integration from zero to infinity of a complicated function, which includes some Bessel functions. Fortunately, some graphical results and tabulated values for the *G(z,p)* function at p=1 are available in some related references (Kavanaugh 1985; Ingersoll et al. 1954). An approximate method for *G* is proposed by (Hellstrom 1991) and presented by Liu et al. (2001).

2.2.1.3 Eskilson's model

Both the one-dimensional model of the Kelvin's theory and the cylindrical source model neglect the axial heat flow; therefore they are inadequate for the long-term operation of GCHP systems. A major progress was made by Eskilson (1987) to account for the finite length of the borehole. In Eskilson's model, the ground is assumed to be homogeneous with constant initial and boundary temperatures, and the thermal capacitance of the borehole elements such as the pipe wall and the grout are neglected. The basic formulation of the ground temperature is governed by the heat conduction equation in cylindrical coordinates:

$$\begin{cases} \dfrac{\partial^2 t}{\partial r^2}+\dfrac{1}{r}\dfrac{\partial t}{\partial r}+\dfrac{\partial^2 t}{\partial z^2}=\dfrac{1}{a}\dfrac{\partial t}{\partial \tau} \\ t(r,0,\tau)=t_0 \\ t(r,z,0)=t_0 \\ q_l(\tau)=\dfrac{1}{H}\int_D^{D+H} 2\pi r\lambda \dfrac{\partial t}{\partial r}\Big|_{r=r_b} dz \end{cases} \tag{2.4}$$

where, D means the uppermost part of the borehole, which can be thermally neglected.

In Eskilson's model, numerical computation with the finite-difference method is used on a radial-axial coordinate system to obtain the temperature distribution of a single borehole with finite length. The final expression of the temperature response at the borehole wall to a unit step heat pulse is a function of τ/τ_s and r_b/H only:

$$t_b - t_0 = -\frac{q_l}{2\pi k} g(\tau/\tau_s, r_b/H) \tag{2.5}$$

where, H is the borehole length; $\tau_s = H^2/9a$ means the steady-state time. The *g*-function is essentially the dimensionless temperature response at the borehole wall, which was computed numerically.

An important achievement of Eskilson's model is that the special superimposition was employed to account for the temperature responses for multiple boreholes. In addition, the sequential temporal superimposition was used to calculate the temperature response (i.e. *g*-functions) to any arbitrary heat rejection/extraction which can be decomposed into a set of single pulses. In other words, the overall temperature response of the GHE to any heat rejection/extraction at any time can be determined by the special and temporal superimpositions.

The disadvantage of this approach, however, is time-consuming, and it can hardly be incorporated directly into a design and energy analysis program for practical applications, since the g-functions of the GHEs with different configurations have to be pre-computed and stored in the program as a massive database. The interpolation function is also needed in using the database which may lead to some computing errors.

2.2.1.4 Finite line-source model

Based on the Eskilson's model, an analytical solution to the finite line source has been developed by a research group which considers the influences of the finite length of the borehole and the ground surface as a boundary (Zeng et al. 2002). This analytical model approximates the borehole with the U-tube as a finite line source with radial heat flow. The computed results from the analytical solution were compared with the data from numerical solutions in references (Eskilson, 1987; Zeng et al. 2002), and they agreed with each other perfectly when $a\tau/r_b^2 \geq 5$.

The solution of the temperature excess was given by Zeng et al. (2002):

$$t(r,z,\tau)-t_0=\frac{q_l}{4k\pi}\int_0^H\left\{\frac{\operatorname{erfc}\left(\frac{\sqrt{r^2+(z-h)^2}}{2\sqrt{a\tau}}\right)}{\sqrt{r^2+(z-h)^2}}-\frac{\operatorname{erfc}\left(\frac{\sqrt{r^2+(z+h)^2}}{2\sqrt{a\tau}}\right)}{\sqrt{r^2+(z+h)^2}}\right\}\mathrm{d}h \qquad (2.6)$$

The temperature on the borehole wall, where $r = r_b$, varies with time and borehole depth. The temperature at the middle of the borehole depth (z=0.5H) is usually chosen as its representative temperature. An alternative is the integral mean

temperature along the borehole depth, which may be determined by numerical integration of Equation (2.6). For the convenience of applications, the former was accepted as the representative temperature in the design and analysis program, developed by the researchers (Zeng et al. 2002; Cui et al. 2007).

With respect to long duration, substantial discrepancy between the Kelvin's model and the finite line source may yield. When time tends to infinity, the temperature rise of the Kelvin's theory tends to infinity, whereas that of the finite line source model approaches a steady-state one, which corresponds to the actual heat transfer mechanism.

The integral of Equation (2.6) can be computed much faster than the numerical solution of the same heat conduction problem in the semi-infinite domain with long durations. The methodology has been complied in the later design and simulation software (Yu et al. 2002; Cui et al. 2007).

2.2.1.5 Yavuzturk and Spitler's model

Since both Eskilson's model and the finite line source model neglect the effect of the thermal capacity of the borehole including the U-tubes, circulating fluid, and the grout, the dimensionless temperature responses on the borehole wall are only valid for times greater than $\frac{5r_b^2}{a}$, estimated by Eskilson (1987). For a typical borehole with a radius of 55mm, the required time may be anywhere between 2 to 6 hours.

Yavuzturk and Spitler presented a numerical model for the simulation of the transient heat transfer in vertical GHEs, which can be accurate down to an hour and

below (Yavuzturk et al. 1999, 2001). The numerical results were expressed in terms of a short time-step response factor (i.e. g-function). The short time-step model is based on the two-dimensional, fully implicit finite volume formulation and utilizes an automated parametric grid generation algorithm for different pipe sizes, shank spacing and borehole geometry. The short time-step response factors are a very useful extension of the long time-step response factors developed by Eskilson. The numerical model was cast as a component model for TRNSYS (developed by Klein et al. 1996). The authors stated that it can evaluate the energy consumption and electrical demand of the GCHP system in hourly or shorter time intervals.

2.2.1.6 Other typical numerical models

Hellstrom (1989, 1991) and Thornton et al. (1997) proposed a simulation model for ground heat stores, which are densely packed ground loop heat exchangers used for seasonal thermal energy storage. This type of system may be directly used to heat buildings with or without a heat pump. The duct storage model (named as DST) divides the ground storage volume with multiple boreholes into tow regions: one is the volume that surrounds a single borehole, described as the “local” region; the other is called “global” region, which denotes the ground volume between the bulk of the heat store volume and the far field. A two-dimensional finite difference scheme was used to solve the ground temperature in the “global” region while the one-dimensional numerical method was employed to calculate the temperature in the “local” region. Since the ground heat storage is mainly used to provide heating function, the boreholes are generally spaced in a quite dense field, which may be not

suitable for some buildings with a considerable amount of cooling loads (Yavuzturk 1999).

Mei and Emerson (1985) proposed a numerical model for horizontal GHEs which took into account the effects of soil moisture freezing around the coil. A finite difference scheme was used to solve the mathematical model that was developed based on energy conservation. Since the mathematical equations were coupled to a one-dimensional partial differential equation representing the flow of heat along the coil, it was taken as a quasi-two-dimensional model. Finally, the model was partly validated by the field experimental results, which showed that the developed model well simulated the daily energy absorption from the ground.

Muraya, et al. (1996) developed a transient finite-element model of the heat transfer around a vertical U-tube heat exchanger for a ground-coupled heat pump to study the thermal interference that occurred between the adjacent legs of the U-tube. The thermal interference was quantified by defining a parameter of the heat exchanger effectiveness. The impacts of the separation distance, leg temperatures, different ambient soil temperatures, and backfills were all investigated.

Rottmayer, et al. (1997) presented a finite difference model that simulated the heat transfer process of a U-tube heat exchanger. A geometric factor was introduced to account for the noncircular geometry used to represent the pipes in the borehole. The model was validated for simple conditions and compared with an existing model, resulting in a good agreement.

2.2.2 Heat transfer inside borehole

The thermal resistance inside the borehole, which is defined by the thermal properties of the grouting materials and the arrangement of flow channels of the borehole, has a significant impact on the GHE performance. The main objective of this analysis is to determine the entering and leaving temperatures of the circulating fluid in the GHE according to the borehole wall temperature and its heat flow. A few models with varying degrees of complexity have been established to describe the heat transfer inside the GHE boreholes.

2.2.2.1 One-dimensional model

A simplified one-dimensional model has been recommended for GHE design, which considers the U-tube as a single “equivalent” pipe (Bose et al. 1985; Gu and O’Neal 1998). In this model, both the thermal capacitance of the borehole and the axial heat flow in the grout and pipe walls are negligible as the borehole dimensional scale is much smaller compared with the infinite ground outside the borehole. Thus, the heat transfer in this region is approximated as a steady-state one-dimensional process. The authors stated that the simplified one-dimensional model was appropriate and convenient for most engineering practices except for the analyses of dealing with dynamic responses within a few hours. However, this oversimplified model seems inadequate and unsatisfactory because it is incapable of evaluating the impact of the thermal “short circuiting” between the U-tube legs on the performance of the GHEs.

2.2.2.2 Two-dimensional model

Hellstrom (1991) derived analytical two-dimensional solutions of the thermal resistances among pipes in the cross section perpendicular to the borehole axis, which is superior to empirical expressions and one-dimensional model.

In the 2-D model, the temperature of the fluid in the U-tubes is expressed as a superposition of two separate temperature responses caused by the heat fluxes per unit length, q_1 and q_2, from the two pipes of the U-tube, as shown in Figure 2.1. If the temperature on the borehole wall, t_b, which is also considered as uniform along the borehole depth, is taken as a reference of the temperature excess, the fluid temperatures in the U-tubes can be obtained from the following equations:

$$\left.\begin{aligned} t_{f1} - t_b &= R_{11} q_1 + R_{12} q_2 \\ t_{f2} - t_b &= R_{12} q_1 + R_{22} q_2 \end{aligned}\right\} \tag{2.7}$$

where R_{11} and R_{22} are the thermal resistance between the circulating fluid and the borehole wall, and R_{12} is the resistance between the two pipes.

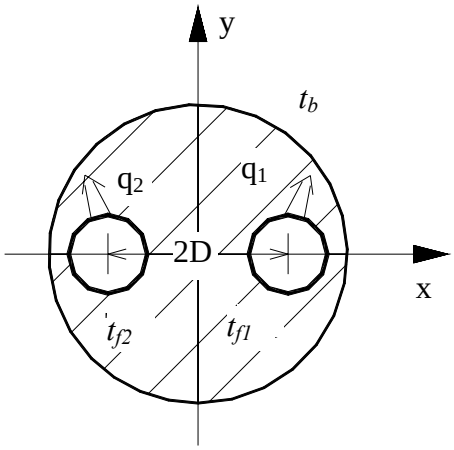

Figure 2.1 Configuration of a U-tube in a borehole

A linear transformation of Equation (2.7) leads to

$$\left.\begin{aligned} q_1 &= \frac{t_{f1} - t_b}{R_1^{\Delta}} + \frac{t_{f1} - t_{f2}}{R_{12}^{\Delta}} \\ q_2 &= \frac{t_{f2} - t_b}{R_2^{\Delta}} + \frac{t_{f2} - t_{f1}}{R_{12}^{\Delta}} \end{aligned}\right\} \tag{2.8}$$

where $R_1^{\Delta} = \frac{R_{11}R_{22} - R_{12}^2}{R_{22} - R_{12}}$, $R_2^{\Delta} = \frac{R_{11}R_{22} - R_{12}^2}{R_{11} - R_{12}}$, $R_{12}^{\Delta} = \frac{R_{11}R_{22} - R_{12}^2}{R_{12}}$。At the instance of the symmetric disposal of the U-tube inside the borehole (i.e. R_{11}= R_{22}), these resistances can be deduced as: $R_1^{\Delta} = R_2^{\Delta} = R_{11} + R_{12}$, $R_{12}^{\Delta} = \left(R_{11}^2 - R_{12}^2\right) \big/ R_{12}$.

The steady-state heat conduction problem in the cross section of a borehole was analyzed in detail by Hellstrom (1991) with the line-source and multipole approximation.

There is no distinction between the entering and exiting pipes since this model did not take into account the heat transmission by the axial flow of the circulating fluid. Therefore, the following assumptions were made to simplify the problem (Eskilson, 1987; Diao et al. 2003): $t_{f1} = t_{f2} = t_f$ and $q_1 = q_2 = q_l/2$.

The thermal resistance between the fluid and borehole wall can then be determined by:

$$R_{b2} = \left(R_{11} + R_{12}\right)/2 \tag{2.9}$$

With the aid of these assumptions the temperatures of the fluid entering and exiting the GHE can be calculated. Being superior to the model of an equivalent pipe, this two-dimensional model presented quantitative expressions of the thermal resistance in the cross section, and provided a basis for discussing the impact of the U-tube

disposal on the heat conduction. However, the fluid circulating through different legs of the U-tubes is, in fact, of varying temperatures. As a result, thermal interference, or thermal “short circuiting”, between the U-tube legs is inevitable, which degrades the effective heat transfer in the GHEs. With the assumption of identical temperature of all the pipes, it is impossible for these models to reveal the impact of this thermal interference on GHE performances.

2.2.2.3 Quasi-three dimensional model

On the basis of the 2-D model aforementioned, a quasi-three dimensional model was proposed by Zeng et al. (2003), which takes account of the fluid temperature variation along the borehole depth. Being minor in the order, the conductive heat flow in the grout and ground in axial direction, however, is still neglected so as to keep the model concise and analytically manageable. The energy equilibrium equations can be written for up-flow and down-flow of the circulating fluid:

$$\left.\begin{aligned} -Mc\frac{dt_{f1}}{dz} &= \frac{(t_{f1}-t_b)}{R_1^{\Delta}}+\frac{(t_{f1}-t_{f2})}{R_{12}^{\Delta}} \\ Mc\frac{dt_{f2}}{dz} &= \frac{(t_{f2}-t_b)}{R_2^{\Delta}}+\frac{(t_{f2}-t_{f1})}{R_{12}^{\Delta}} \end{aligned}\right\} \quad (0 \le z \le H) \tag{2.10}$$

Two conditions are necessary to complete the solution:

$$\left.\begin{aligned} z=0,\ t_{f1}=t'_f \\ z=H,\ t_{f1}=t_{f2} \end{aligned}\right\} \tag{2.11}$$

The general solution of this problem is derived by Laplace transformation, which is slightly complicated in form. At the instance of the symmetric placement of the

U-tube inside the borehole, the temperature profiles in the two pipes were illustrated by Diao et al. (2004).

For the purpose of practical applications an alternative parameter $\varepsilon = \left(t_f^{'} - t_f^{''}\right) / \left(t_f^{'} - t_b\right)$ is derived from the temperature profiles, which is named as the heat transfer efficiency of the borehole. It should be noticed that $t_f^{'}$ and $t_f^{''}$ are the entering /exiting fluid temperatures to /from the U-tube. From the derived temperature profile the more accurate heat conduction resistance between the fluid inside the U-tube and the borehole wall can be calculated by,

$$R_{b3} = \frac{H}{Mc}\left(\frac{1}{\varepsilon} - \frac{1}{2}\right) \tag{2.12}$$

The authors validated that the quasi-3-D model was more accurate than the other current models and recommended it for design and thermal analysis of GHEs.

2.2.3 Comparisons of the analytical and numerical models

Although the numerical models can offer a high degree of flexibility and accuracy (especially on short-term scales) compared with analytical models, most of them using polar or cylindrical grids may be computationally inefficient due to a large number of complex grids. Besides, the numerical models can hardly be incorporated directly into a design and energy analysis program, unless the simulated data are pre-computed and stored in programs as a massive database with some parameters.

The analytical models make a number of assumptions and simplifications in order to solve the complicated mathematical algorithms; therefore, the accuracy of analytical results will be slightly reduced but required computation time is much less. Another

advantage is that the straightforward algorithm deduced from analytical models can be readily integrated into a design/simulation program.

A summary of the characteristics of the numerical and analytical models of GHEs reviewed above is given in Table 2.1.

Table 2.1 Comparison of current models of GHEs

	Model	**Method**	**Thermal interference between boreholes**	**Boundary effects**
Outside borehole	Kelvin's line source	Infinite line source	Yes	No
	Cylindrical source	Infinite cylindrical source	Yes	No
	Finite line source solution	Finite line source	Yes	Yes
	Eskilson's model	Combination of numerical and analytical methods	Yes	Yes
	Yavuzturk and Spitler's model	Numerical methods	Yes	Yes
Inside borehole	**Model**		**Thermal interference between U-tube pipes**	**Heat flux along depth**
	One dimensional model (Equivalent pipe)		No	No
	Two dimensional model		Yes	No
	Quasi-three dimensional model		Yes	Yes

2.2.4 Inclined GHE

According to the comprehensive literature review aforementioned, a number of simulation models on vertical GHEs have been well developed over the last three

decades, whereas, few studies have been carried out on the GHE with inclined boreholes due to the complexity of its transient three-dimensional heat transfer process. Only Eskilson (1987) reported some studies on the heat conduction of inclined boreholes in a specific GHE on the basis of numerical simulation. However, the numerical solution of the transient three-dimensional heat transfer is too computationally intensive to be directly applied to engineering designs.

2.3 Modeling of HGCHP Unit with Desuperheater

The HGCHP system with a supplemental cooler or heater has been becoming attractive or popular in cooling or heating dominated buildings (Kavanaugh, 1998; Ramamoorthy et al., 2001; Chiasson et al., 2004). The HGCHP with domestic hot water (DHW) supply is one of the alternatives, which can provide space cooling or heating accompanied with hot water supply.

2.3.1 Performance study on desuperheaters

The concept of using a desuperheater as a heat recovery unit to preheat water has been widely accepted in air conditioning field. Some efforts have been recently made in the performance analysis of the desuperheater used in various systems, including ASHPs, chillers and GCHPs. Lee and Jones (1996) tested the thermal performance of a residential desuperheater/water heater system in a laboratory under controlled environmental conditions. Deng and Jiang (2003) reported a retrofitted hot water heating system using a water-to-water heat pump or an air-to-water heat pump. In their research, the heat pump was only used to produce hot water while chilled water became a free by-product. Shao et al. (2004) discussed the

configuration and principle of an ASHP system with domestic hot water. The authors claimed that the new design was able to reduce energy consumption by 31.1% and decreased the thermal pollution to the environment. A steady-state simulation model on a water chiller complete with a desuperheater and a reversibly used water cooling tower (RUWCT) for service hot water was developed by Tan and Deng (2001). In this system, a standard cooling tower was reversibly used, as an evaporator, to extract heat from ambient air in colder seasons in southern China, which can indirectly produce service hot water in desuperheater. The simulation results indicated that the use of a RUWCT would achieve a higher energy efficiency than the use of electrical heater for service water heating.

2.3.2 Modeling of heat pump unit

However, few simulation models of the heat pump with a desuperheater are found in the open literature that can evaluate the performance of the heat pump unit for all possible operating conditions. Compared with the few theoretical studies on heat pumps with desuperheater, a large number of simulation models for conventional heat pumps and water chillers have been developed primarily in the past two decades. Basically, the currently available simulation approaches for chillers and heat pumps can be classified into two groups (Hamilton and Miller 1990): one is the functional fit (i.e. equation-fit) model, which treats the system as a black box and fit the system performance into a few functional equations using catalog data; the other is the “first principle” model (deterministic model), which considers most component design parameters. In the deterministic model, the major components are separately modeled based on thermodynamics principles and fundamental heat and

mass transfer correlations, and then these models can be combined to form a systematic model.

A typical functional fit model of a reciprocating water chiller was proposed by Allen and Hamilton (1983). Other modeling algorithms employing the equation-fit approach are similar to this method. This steady state model did not consider individual component models and eliminated the internal variables by utilizing the functional relationships among variables and existing typical water chiller performance data. This approach is widely used in a few building-HVAC simulation programs for its good accuracy within the allowed operation range and its simplicity of computation. However, the valid application is limited to the manufacturer-supplied data range and conditions.

The majority of the models differed from the equation-fit method actually are near to the deterministic model but may still need to apply some fitting-equations to some of components. Stefanuk, et al. (1992) developed the superheat-controlled water-to-water heat pump model. The authors stated that the model was derived entirely from the basic conservative laws of mass, energy and momentum, and equations of state as well as fundamental correlations of heat transfer. The main significance of the detailed simulation model was that it can be used to simulate over a full operating range of a heat pump. Model predictions were compared with experimental data and good agreement was found for the cases studied in that paper.

A new simulation model of a water-to-water heat pump has been developed by Jin and Spitler (2002), based on the parameter estimated method to describe each heat pump component. Each of the fundamental equations describing the system

components may have one or more parameters, which were estimated simultaneously using catalog data only; no other experimental data were required. The parameter estimation was done with a multi-variable optimization method. Once the parameters were estimated, the heat pump model may be used as part of a multi-component system simulation. The author claimed that the predictions of the model were of similar or better accuracy than previously published deterministic models that required additional experimental data.

2.3.3 Field study on HGCHP unit with a desuperheater

Fanney and Dougherty (1992) first discussed the performance of a residential earth-coupled heat pump (i.e. GCHP) with an integral desuperheater water-heating circuit which located in a residential house. The recorded data showed that the desuperheater contributed to an average of 27% of the total energy supplied for heating water through the 24-month monitoring period. Kavanaugh (1992) reported a similar project of the GCHP system with a desuperheater and concluded that the cost savings were very considerable based on the utility bill. After that, some qualitative introduction and general concept on the HGCHP with hot water supply system were presented by Caneta Research Inc. (1995).

Compared with the relative fewer theoretical studies, the heat pump manufacturers show a great interest in the production of the heat pump unit with an integral desuperheater, which can simultaneously supply space cooling/ heating and hot water. Majority of manufactories, however, still depend to a large extent on repeated experiments to adjust the size of each component to search the optimal match

scheme with highest operating efficiency because of the absence of the comprehensive simulation model for the whole system including a heat pump unit and GHE as well.

2.4 Summary

This chapter presents a comprehensive literature review covering the simulation models of the GHEs in terms of analytical and numerical methods and the research studies on the heat pump unit with/without a desuperheater.

It can be found from the literature review that a great number of studies on the heat transfer analysis of vertical GHEs have been carried out. However, there is only one report on the modeling of GHEs with inclined boreholes, which presented the numerical results for some specific configurations of inclined boreholes. The numerical solution of the transient three-dimensional heat transfer is too computationally intensive to be directly applied to engineering designs. Thus, it is necessary to develop an analytical simulation model of inclined GHEs with acceptable precision which can be easily incorporated into many simulation/design programs available for engineering applications.

Although a fair amount of work has been done on modeling the GCHP unit, only a few studies have focused on evaluating the performance of the GCHP with a desuperheater based on experiments. Very little has been done modeling the HGCHP with DHW supply. Hence, it would be of interest to develop a simulation model of the HGCHP system and investigate the performance of such a practical system under various operation modes in warm-climate areas.

CHAPTER 3 ANALYTICAL MODEL OF INCLINED GROUND HEAT EXCHANGERS

3.1 Introduction

As is well known, for commercial or large residential applications, the GCHP systems require sufficient land area to accommodate enough vertical boreholes which should be separated by certain distances for the purpose of long-term operation of the system. The high cost of the GHE installation or the need for the large land area generally becomes a significant restriction against the GCHP applications in densely populated cities and towns.

As discussed in Chapter 1, drilling inclined boreholes in the peripheral borehole field can reduce the land areas required for the GHEs and further alleviate the thermal interference among them in the ground.

The main objective of the inclined GHE thermal analysis is to determine the temperature of heat carrier fluid based on certain operating conditions. A fundamental task is to explore the heat conduction process of a single borehole in the GHE. The heat transfer in a field with multiple boreholes can then be analyzed on this basis with the superposition principle. In the same way as the heat transfer analysis on a vertical borehole, the heat transfer process in an inclined borehole can

also be analyzed in two separated regions. One is the solid soil/rock outside the borehole, which are mainly discussed in Sections 3.2 through 3.3.

Another segregated sector for analysis is the region inside the borehole which can be approximately treated as that inside the vertical borehole. The quasi-three dimensional model is, therefore, cited here to calculate the inlet and outlet temperatures of the circulating fluid according to the borehole wall temperature, the thermal resistance inside the borehole and the heat rate of the GHE. The detailed governing equations and thermal resistance inside the borehole are presented in Chapter 2.

This chapter mainly focuses on the heat transfer analysis outside the boreholes, which plays a critical role in the whole heat transfer process of the GHE. Firstly, the transient heat transfer model of a single inclined borehole is developed and then the temperature response of a GHE with multi-inclined boreholes is discussed. Secondly, the steady-state heat transfer characteristics are also presented for the purpose of long-time thermal analysis. Finally, the simulation model is validated by experimental data which are collected from the pilot project.

3.2 Analytical Transient Heat Transfer Model of Inclined GHE

3.2.1 Assumptions

To develop the theoretical model of inclined GHEs, a basic and simple case is to first study a single inclined borehole and then to introduce other complications step by step. In a manner similar to the vertical borehole analysis (Yu et al. 2002; Diao et al. 2004, 2003; Zeng et al. 2003), the inclined borehole buried in the ground can be

approximated as an inclined line source with finite length in a semi-infinite medium. Some necessary assumptions are incorporated into the following model:

1) The ground is regarded as a homogeneous semi-infinite medium with constant thermophysical properties;

2) The boundary of the medium, i.e. the ground surface, keeps a constant temperature t_0 (same as its initial one) throughout the time period concerned;

3) The uppermost part of the borehole top, $0<z<D$, is treated as thermally insulated because the buried depth of D, generally less than 4m, is rather smaller than the borehole depth H.

4) The radial dimension of the inclined borehole is neglected so that it can be approximated as a line source stretching from the boundary to the bottom of the borehole depth, H;

A diagram of the physical model for a single inclined line source is illustrated in Figure 3.1. The coordinate of the line-source top at the ground surface is (x_0, y_0, 0); the inclined angle (obliquity) of the line source with the z-axis is denoted by α; the direction angle of the inclination with the positive X-axis is β; and the heating rate per length of the line source is q_l. To solve this problem, a virtual line-sink with the same length H but a negative heating rate $-q_l$ is set on the symmetric side of the line source on the boundary as shown in Figure 3.1. Thus, the concerned domain is extended to be an infinite medium by adding the mirror line sink.

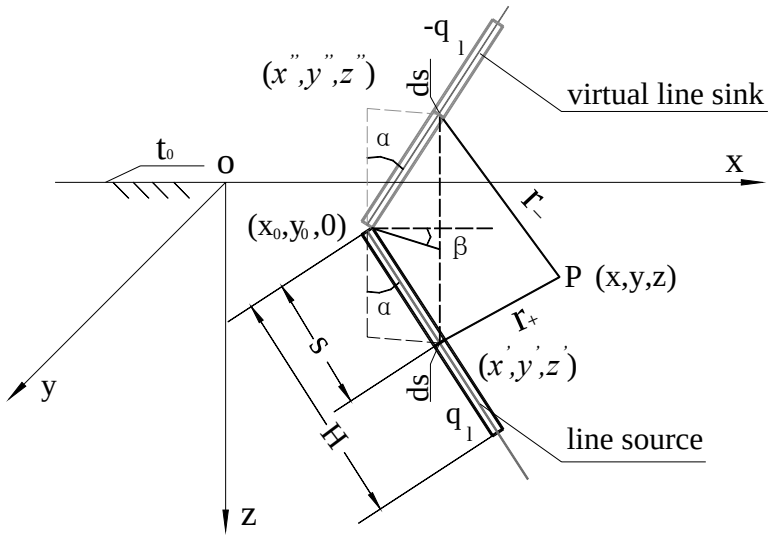

Figure 3.1 Schematic diagram of an inclined finite line source

3.2.2 Mathematical model of inclined finite line source

3.2.2.1 Applications of Green's functions in the heat conduction problem

Green's functions are very powerful tools for obtaining solutions of transient and steady-state linear heat conduction problems (Beck, et al. 1992). For a transient-state heat conduction problem, the Green's function can be taken as the temperature distribution caused by an instantaneous, local energy pulse.

In the case of the infinite medium initially at zero temperature with an instantaneous plane heat source of strength unity located at position x' at time τ', the Green's function can be written as,

$$\left.\begin{aligned} &\frac{\partial G}{\partial \tau} = a\frac{\partial^2 G}{\partial x^2} + \delta\left(x - x'\right)\delta\left(\tau - \tau'\right) && -\infty < x < \infty, \tau > \tau' \\ &G = 0 && -\infty < x < \infty, \tau = \tau' \\ &\frac{\partial G}{\partial x} = 0 && x \to \pm\infty \end{aligned}\right\} \tag{3.1}$$

The solution to the Green's function can be obtained by the method of separation of variables:

$$G\left(x, \tau, x', \tau'\right) = \frac{1}{\sqrt{4\pi a\left(\tau - \tau'\right)}} \exp\left(-\frac{\left(x - x'\right)^2}{4a\left(\tau - \tau'\right)}\right) \tag{3.2}$$

The temperature distribution of the infinite medium with an instantaneous heat source and nonhomogeneous initial temperature can then be deduced directly using the Green's function solution. Thus, the heat conduction problem with the initial temperature distribution *F(x)* and the volumetric energy generation of *g(x,t)* is described as follows:

$$\left.\begin{aligned} &\frac{\partial t}{\partial \tau} = a\frac{\partial^2 t}{\partial x^2} + g\left(x, \tau\right) && -\infty < x < \infty,\ \tau > 0 \\ &t = F\left(x\right) && -\infty < x < \infty,\ \tau = 0 \\ &\frac{\partial t}{\partial x} = 0 && x \to \pm\infty,\ \tau > 0 \end{aligned}\right\} \tag{3.3}$$

Thus, the temperature distribution can be calculated by:

$$t\left(x, \tau\right) = \int_{-\infty}^{\infty} F\left(x'\right) G\left(x, \tau; x', \tau' = 0\right) dx' + \int_{0}^{\tau} d\tau' \int_{-\infty}^{\infty} g\left(x', \tau'\right) G\left(x, \tau; x', \tau'\right) dx \tag{3.4}$$

Furthermore, the Green's function of the three-dimensional non-homogeneity transient heat conduction in the infinite medium can be expressed as the production of the one-dimensional Green's function (Eckert E R G, 1972).

$$G\left(x,y,z,\tau,x^{'},y^{'},z^{'},\tau^{'}\right)=\frac{1}{8\left[\pi a\left(\tau-\tau^{'}\right)\right]^{3/2}}\exp\left(-\frac{\left(x-x^{'}\right)^{2}+\left(y-y^{'}\right)^{2}+\left(z-z^{'}\right)^{2}}{4a\left(\tau-\tau^{'}\right)}\right)$$

(3.5)

3.2.2.2 Solution methods for the inclined finite line source model

As mentioned in section 3.2.2.1, the temperature response caused by the two instantaneous heat sources (line source and line sink) can be derived using the Green's function. Thus, the temperature rise at a random point $P(x, y, z)$ at time τ can be obtained by the linear superposition of the temperature responses generated by the line source and the line sink, respectively.

$$\begin{aligned}t(x,y,z,\tau)-t_0=&\frac{1}{\rho c}\int_0^{\tau}d\tau^{'}\int_0^{H}q_l\cdot\frac{1}{8\left[a\pi\left(\tau-\tau^{'}\right)\right]^{3/2}}\cdot\exp(-\frac{(x-x^{'})^2+(y-y^{'})^2+(z-z^{'})^2}{4\pi\left(\tau-\tau^{'}\right)})ds\\&+\frac{1}{\rho c}\int_0^{\tau}d\tau^{'}\int_0^{H}-q_l\cdot\frac{1}{8\left[a\pi\left(\tau-\tau^{'}\right)\right]^{3/2}}\cdot\exp(-\frac{(x-x^{''})^2+(y-y^{''})^2+(z-z^{''})^2}{4\pi\left(\tau-\tau^{'}\right)})ds\end{aligned}$$

(3.6)

where, $x^{'}=x^{''}=x_0+s\sin\alpha\cos\beta$, $y^{'}=y^{''}=y_0+s\sin\alpha\sin\beta$, $z^{'}=s\cos\alpha$ and $z^{''}=-s\cos\alpha$

Integrating Equation (3.6) with respect to the time from *0* to τ yields a more straightforward expression,

$$t-t_0=\frac{q_l}{4\pi k}\int_0^{H}\left(\frac{erfc\left(\frac{r_+}{2\sqrt{a\tau}}\right)}{r_+}-\frac{erfc\left(\frac{r_-}{2\sqrt{a\tau}}\right)}{r_-}\right)dS \qquad (3.7)$$

$$r_{+} = \sqrt{\left(x - x_0 - s\sin\alpha\cos\beta\right)^2 + \left(y - y_0 - s\sin\alpha\sin\beta\right)^2 + \left(z - s\cos\alpha\right)^2}$$
$$r_{-} = \sqrt{\left(x - x_0 - s\sin\alpha\cos\beta\right)^2 + \left(y - y_0 - s\sin\alpha\sin\beta\right)^2 + \left(z + s\cos\alpha\right)^2} .$$

It is noticed that Equation (3.7) becomes the solution of the vertical line source model when $\alpha=0$ and $\beta=0$.

Introducing the following dimensionless variables:

$$X = \frac{x}{H}, \quad Y = \frac{y}{H}, \quad Z = \frac{z}{H}, \quad S = \frac{s}{H} \quad X_0 = \frac{x_0}{H} \quad , \quad Y_0 = \frac{y_0}{H} \quad , \quad Fo = \frac{a\tau}{H^2} \quad ,$$

$$\Theta_p = \frac{4k\pi\left(t - t_0\right)}{q_l},$$

Then, the dimensionless temperature excess at point *P* caused by a single inclined line source can be expressed as a function of the following dimensionless variables:

$$\Theta_p\left(X, Y, Z, X_0, Y_0, \alpha, \beta, Fo\right) = \int_0^1 \left(\frac{erfc\left(\frac{r_+^*}{2\sqrt{Fo}}\right)}{r_+^*} - \frac{erfc\left(\frac{r_-^*}{2\sqrt{Fo}}\right)}{r_-^*} \right) dS \qquad (3.8)$$

where,

$$r_{+}^* = \sqrt{\left(X - X_0 - S\sin\alpha\cos\beta\right)^2 + \left(Y - Y_0 - S\sin\alpha\sin\beta\right)^2 + \left(Z - S\cos\alpha\right)^2} \quad ;$$

$$r_{-}^* = \sqrt{\left(X - X_0 - S\sin\alpha\cos\beta\right)^2 + \left(Y - Y_0 - S\sin\alpha\sin\beta\right)^2 + \left(Z + S\cos\alpha\right)^2}$$

3.2.3 Temperature response on an inclined borehole wall

A characteristic temperature response on the borehole wall is usually required in order to design or simulate GHEs in GCHP systems (Zeng et al. 2002). However, the temperature responses of the inclined borehole wall at any cross section perpendicular to its axis are unequal and vary with the borehole depth due to the three-dimensional heat transfer of the inclined line source.

3.2.3.1 Temperature response on the cross-section circle of the borehole

For simplicity, the borehole top is set on the origin of the coordinate (i.e. $x_0=y_0=0$) and situated in the plane *xoz* (i.e. $\beta=0$) since the direction of inclination has no effect on the temperature rise for a single borehole. The cross section of the borehole axis at the depth l is a tilted circle denoted by ADBE (see Figure 3.2). The coordinate of a certain point at the cross-section circle can be expressed by the following parameters:

$$\begin{cases} x = l\sin\alpha + r_b\cos\alpha\cos\omega \\ y = r_b\sin\omega \\ z = l\cos\alpha - r_b\sin\alpha\cos\omega \end{cases} \tag{3.9}$$

where, ω is the angle between the radius passing the concerned point on the circle and the specific radius at the plane *xoz* ($0\leq\omega<2\pi$).

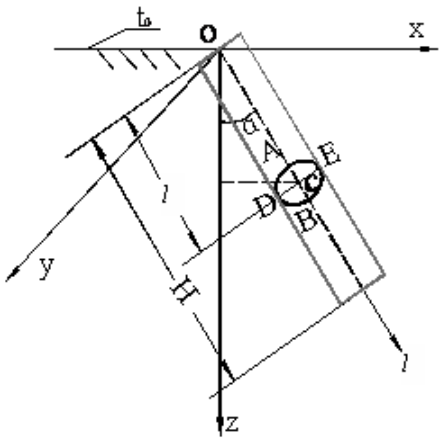

Figure 3.2 Geometry of a cross section at the borehole depth *l*

Substituting Equation (3.9) into Equation (3.7) yields the temperature response at the concerned point in the circle. Accordingly, the dimensionless expression is given as follows:

$$\Theta_{\omega}\left(L,R_b,Fo,\alpha,\omega\right)=\int_0^1\left(\frac{\operatorname{erfc}\left(\frac{r_{1+}^{\ *}}{2\sqrt{Fo}}\right)}{r_{1+}^{\ *}}-\frac{\operatorname{erfc}\left(\frac{r_{1-}^{\ *}}{2\sqrt{Fo}}\right)}{r_{1-}^{\ *}}\right)\mathrm{d}S \tag{3.10}$$

where

$$r_{1+}^{\ *}=\sqrt{\left(L\sin\alpha+R_b\cos\alpha\cos\omega-S\sin\alpha\right)^2+\left(R_b\sin\omega\right)^2+\left(L\cos\alpha-R_b\sin\alpha\cos\omega-S\cos\alpha\right)^2}$$

$$r_{1-}^{\ *}=\sqrt{\left(L\sin\alpha+R_b\cos\alpha\cos\omega-S\sin\alpha\right)^2+\left(R_b\sin\omega\right)^2+\left(L\cos\alpha-R_b\sin\alpha\cos\omega+S\cos\alpha\right)^2}$$

$$R_b=r_b/H\ ,\quad L=l/H\ ,\quad S=s/H\ .$$

Here S is an integral variable, i.e. the relative distance between a point on the wall and the top of the borehole, and L denotes the relative depth of the concerned cross-section circle.

According to the symmetry of the temperature field of the plane *xoz*, the dimensionless integral average temperature along the circle can be presented by,

$$\Theta_c\left(L, R_b, Fo, \alpha\right) = \frac{1}{\pi}\int_0^{\pi} \Theta_\omega d\omega \tag{3.11}$$

For fixed parameters of R_b, α and Fo, the borehole wall temperature varies with its depth, which is computed and plotted in Figure 3.3. The temperature variation on a vertical borehole (when α=0°) is also given in Figure 3.4 for the sake of comparison. It can be seen from Figures 3.3 and 3.4 that the variation of the temperature on the inclined borehole wall along its depth was almost similar to that on the vertical borehole. This illustrates that drilling the inclined borehole is unnecessary for such a GHE with a single borehole.

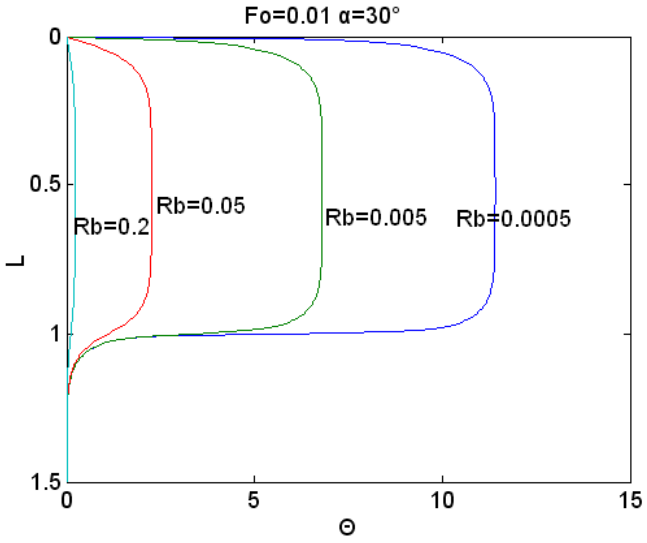

Figure 3.3 Temperature profiles along the borehole depth with different relative radii (with α =30°)

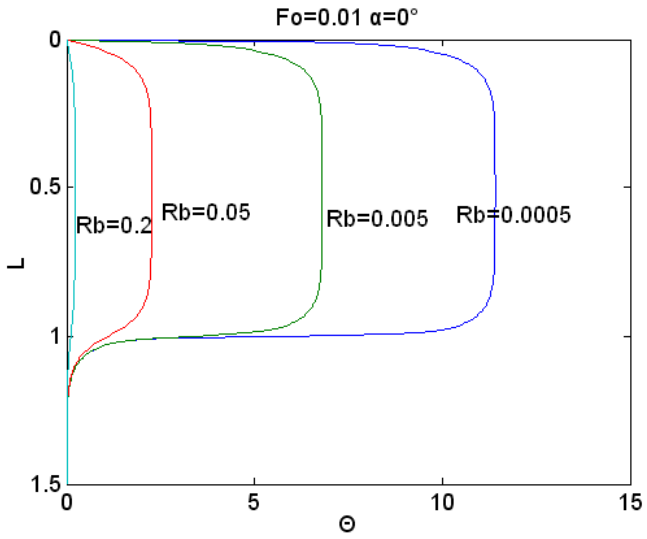

Figure 3.4 Temperature profiles along the borehole depth with different relative radii (with α =0°)

3.2.3.2 Representative temperature of the cross-section circle

For a specific cross-section circle of the borehole, the dimensionless temperature at any point on the circle is only a function of the variable ω. Since the borehole radius is relatively minor compared with its depth, the thermal influence of the boundary condition (ground surface) on the circle can be negligible. Hence, the temperature variation along the circle is quite insignificant. Take the middle cross section (i.e. $l = H/2$) as an example, computations showed that the temperature (named as Θ_r) at the point ($\omega = \pi/2$), i.e. its coordinate is $(H\sin\alpha/2, r_b, H\cos\alpha/2)$, can be recommended as the representative temperature instead of its average temperature (Θ_c). Table 3.1 lists the values of Θ_r and Θ_c for different conditions.

From Table 3.1, it can be found that the representative temperatures were almost equal to the average temperatures with different *Fo* and α for a borehole with

R_b=0.001, and the relative errors between the two temperatures were less than 0.001%. Thus, the representative temperature Θ_r, which is easier to be computed, can be used to replace the integral average temperature of the cross-section circle on the borehole wall in engineering applications.

Table 3.1 Comparisons of the representative and average temperatures (R_b=0.001)

Fo	α=10°		α=30°	
	Θ_r	Θ_c	Θ_r	Θ_c
0.01	10.002	10.002	10.022	10.022
0.1	12.048	12.048	12.012	12.012
1	12.662	12.662	12.550	12.550

3.2.3.3 Representative temperature of the borehole wall

In general, there are two characteristic temperatures of the borehole wall in the GHE design or simulation models. One is the integrated average temperature along the borehole depth:

$$\overline{\Theta}_b\left(R_b, Fo, \alpha\right) = \int_0^1 \Theta_c dL \tag{3.12}$$

The integrated temperature is regarded as a more reasonable characteristic temperature. However, it is too complicated and, therefore, inconvenient to be employed directly in engineering applications. A more common scheme is to use the temperature at the middle of the borehole wall as its representative temperature.

Thus, the representative temperature Θ_r at the middle cross-section circle can be employed instead of the integral average temperature $\overline{\Theta}_b$ over the borehole depth. The relative error between Θ_r and $\overline{\Theta}_b$, $\Delta = \Theta_r / \overline{\Theta}_b - 1$, is related with the variables α, R_b and *Fo*, since both of the two temperatures are the function of the three variables. The relative errors were analyzed under a wide range of conditions (α <50°, r_b =0.0005~0.005 and *Fo*= 0 ~0.6), which covers the commonly used data in practical engineering.

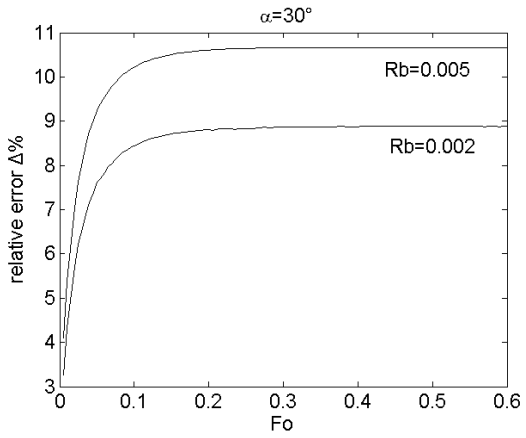

Figure 3.5 Relative errors between Θ_r and $\overline{\Theta}_b$ vs. *Fo*

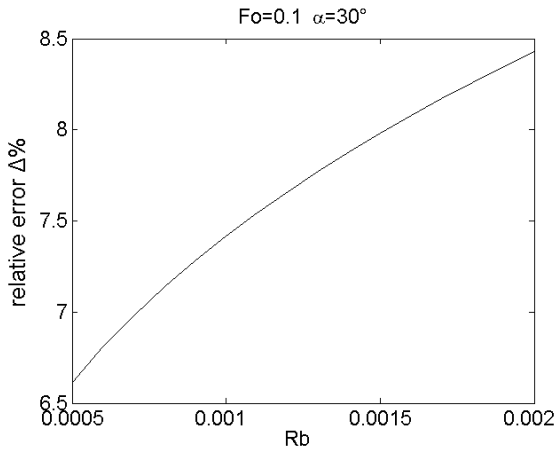

Figure 3.6 Relative errors between Θ_r and $\overline{\Theta}_b$ vs. R_b

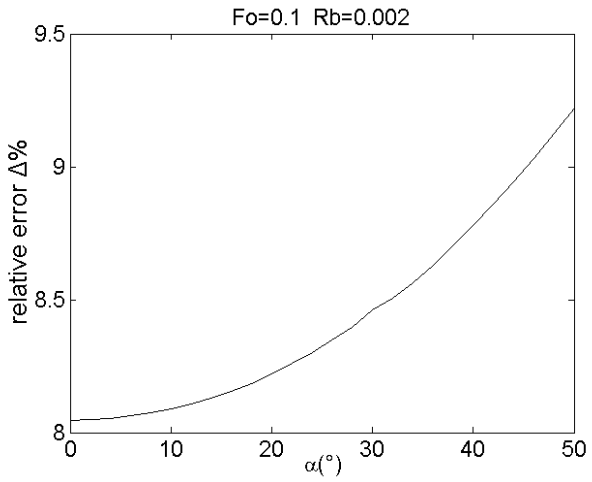

Figure 3.7 Relative error between Θ_r and $\overline{\Theta}_b$ vs. α

As can be found from Figures 3.5 to 3.7, the representative temperature Θ_r was generally higher than the average temperature. The maximum relative error between them was 10.6% in the studied ranges ($\alpha \le 50^o, R_b \le 0.005$), which is still acceptable for engineering applications. Compared with the complicated integral temperature, the representative temperature at the middle section as the characteristic temperature of the whole borehole can greatly simplify the process of the calculation in engineering practices. However, it should be noticed that the more reasonable integrated average temperature defined in Equation (3.12) may be incorporated into some sophisticated computer software for further research study.

3.2.3.4 Thermal interference among inclined boreholes

In engineering practice the radius of a borehole (typically ranging from 0.05m to 0.1m) is much smaller than the space between adjacent boreholes, which is usually above 3 meters. In view of this, the temperature response on the concerned borehole wall caused by its adjacent boreholes can be approximately treated as the response

on its axis due to the negligible influence of its radius. Take two boreholes (*i* and *j*) as an example, and suppose the borehole *i* is the one concerned, and *j* is its adjacent one as shown in Figure 3.8. The coordinates of the point at any axial distance *l* of the *i*-th borehole is given by,

$$\begin{cases} x = x_{0i} + l\sin\alpha_i\cos\beta_i \\ y = y_{0i} + l\sin\alpha_i\sin\beta_i \\ z = l\cos\alpha_i \end{cases} \tag{3.13}$$

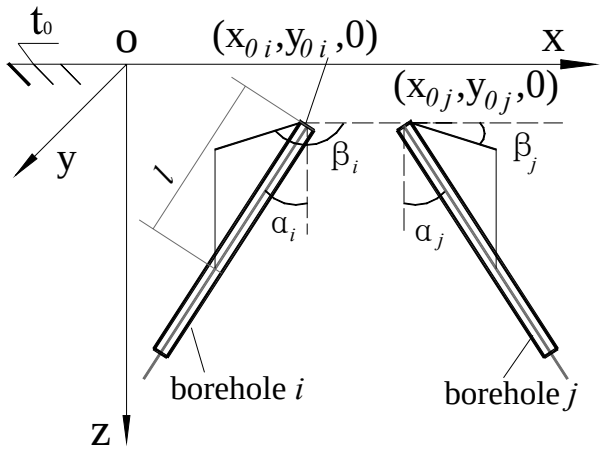

Figure 3.8 A schematic diagram of the two inclined boreholes

Substituting Equation (3.13) into Equation (3.7), the temperature response at any axial distance *l* of the *i*-th borehole caused by its adjacent *j*-th one can be derived accordingly. And, therefore, the dimensionless expression can be rearranged as a function of the following variables,

$$\Theta_{ij,L} = f_L\left(X_{0i}, Y_{0i}, L, \alpha_i, \beta_i, X_{0j}, Y_{0j}, \alpha_j, \beta_j, Fo\right) \tag{3.14}$$

A representative temperature rise on the borehole wall caused by its adjacent one is also required to characterize the thermal interference between them. Similar to a single inclined borehole, there are also two kinds of characteristic temperatures. One

is the average temperature rise, which can be obtained by integrating along the depth of the concerned borehole:

$$\overline{\Theta}_{ij} = \int_0^1 \Theta_{ij,L} dL \tag{3.15}$$

The other is a representative temperature response at the middle of the concerned borehole wall. Both of the two methods, however, are somewhat complicated for practical applications of GHEs with multiple inclined boreholes. Based on a great deal of computation and comparison, a simplified approach is proposed, which presents that the thermal interference between two inclined boreholes can be approximated as that of two supposed vertical boreholes disposed at a distance between the middle points of the inclined boreholes. Thus the temperature rise on the *i*-th inclined borehole caused by the *j*-th one can be obtained by the two supposed vertical boreholes, which is recommended as a new representative temperature ($\Theta_{ij,r}$). Involving a two-dimensional process, the expression of $\Theta_{ij,r}$ is much simpler, and can be found in the reference (Daio et al. 2004) ：

$$\Theta_{ij,r} = \int_0^1 \left\{ \frac{\operatorname{erfc}\left(\frac{\sqrt{(r_{i,j}/H)^2 + [0.5-(h/H)]^2}}{2\sqrt{a\tau/H^2}} \right)}{\sqrt{\left(\frac{r_{i,j}}{H}\right)^2 + \left[0.5-\left(\frac{h}{H}\right)\right]^2}} - \frac{\operatorname{erfc}\left(\frac{\sqrt{(r_{i,j}/H)^2 + [0.5+(h/H)]^2}}{2\sqrt{a\tau/H^2}} \right)}{\sqrt{\left(\frac{r_{i,j}}{H}\right)^2 + \left[0.5+\left(\frac{h}{H}\right)\right]^2}} \right\} \mathrm{d}\left(\frac{h}{H}\right) \tag{3.16}$$

where $r_{i,j}$ is the distance between the *i-th* and *j-th* boreholes.

Now take an example of the two inclined boreholes with the following parameters: $X_{0i}=0$, $Y_{0i}=Y_{0j}=0$, $\alpha_i=\alpha_j=20°$, and then the value of X_{0j} is obviously equal to the relative space B^* between them on the ground surface. Figure 3.9 presents the comparisons of the representative and the average temperatures against *Fo* in different inclining directions. As shown in Figure 3.9, the thermal influence between the boreholes was consistently increasing with the smaller *Fo* and, then, gradually approached constant with larger values of *Fo*. Though the maximum relative error resulted from the approximate approach reached nearly 17% when *Fo*=1.5 in the case of B^*=0.05 and $\alpha = 20°$, the temperature rise caused by the heat source in adjacent boreholes is much smaller than that caused by the heat source in the concerned borehole itself due to the significant space difference. Besides, the representative temperature is slightly higher than the average temperature, which can result in a conservative design for the GHEs. The approximate method therefore can be acceptable for engineering applications.

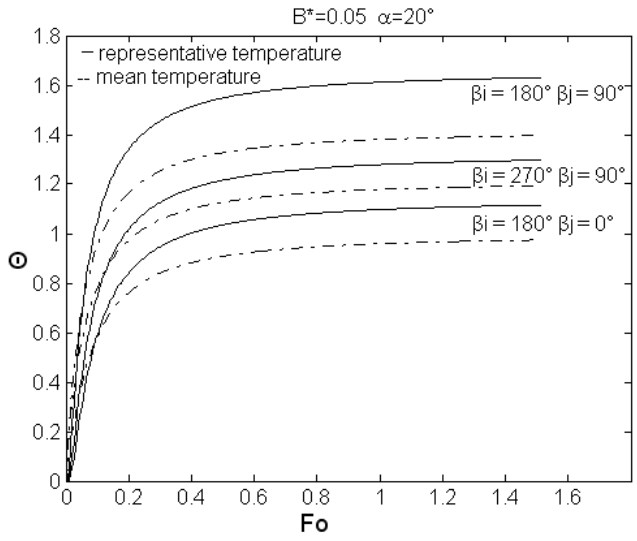

Figure 3.9 Comparisons of $\overline{\Theta}_{ij}$ and $\Theta_{ij,r}$

3.2.4 Temperature response on the borehole wall in a GHE

U-tubes in the multiple boreholes of a GHE are generally connected in parallel. The temperature responses on each borehole caused by its adjacent boreholes are obviously different, which primarily depend on the spacing and geometric placement of the boreholes. Hence, a basic borehole needs to be found out, which has the highest temperature rise or the worst heat transfer condition among all the boreholes, as a benchmark of the temperature rise on the borehole wall in a GHE. In this research, the same heat transfer rate per unit length of the borehole is assumed to calculate the borehole wall temperature of each individual borehole in a GHE. It is noteworthy that the thermal resistance of each borehole is different, which can finally determine the temperature response of each borehole.

For each borehole, its temperature response on the borehole wall basically consists of two parts: the primary temperature rise due to the line source (U-tube) in the borehole itself and the second one caused by the rest boreholes in the GHE. It should be noticed that the heat transfer rate per borehole is assumed to be constant. Thus, the representative temperature of a GHE with *n* boreholes can be determined through finding the maximum temperature rise on a specific borehole wall in the borehole field,

$$\Theta_e = \max\left(\Theta_i\right) = \max\left(\Theta_{ir} + \sum_{\substack{j=1 \\ j\neq i}}^{n} \Theta_{ij,r} \right) \tag{3.17}$$

where the function “max” means the maximum of the temperature responses among the *n* boreholes.

3.2.4.1 Case Study 1

A typical GHE configuration with multi-boreholes is the rectangle pattern in practical applications. Figure 3.10 depicts a layout of 20 boreholes on the ground surface in four rows each with 5 boreholes (4×5). The 6 inner boreholes are vertical, with relative space B^*_1=0.1 and the peripheral boreholes are inclined outwards with the equal obliquity and the relative space B^*_2 of 0.05. The temperature responses of such a GHE with two different obliquities ($\alpha = 10°$ and $\alpha = 20°$) are plotted in Figure 3.11. The curve for $\alpha = 0°$, i.e. the vertical GHE, is also plotted in Figure 3.11 for comparison purpose. It can be seen from Figure 3.11 that the temperature rises for cases of $\alpha = 10°$ and $\alpha = 20°$ were 16.3% and 27.3% lower, respectively, than that in the vertical GHE case when *Fo*=5.0.

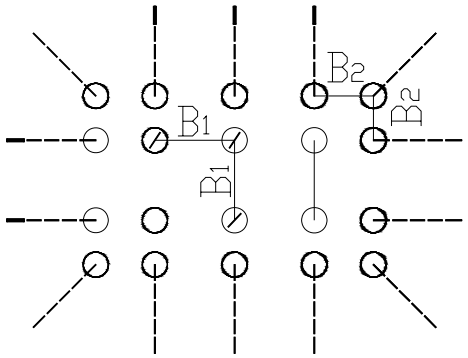

Figure 3.10 An inclined GHE with different spaces in a rectangle configuration

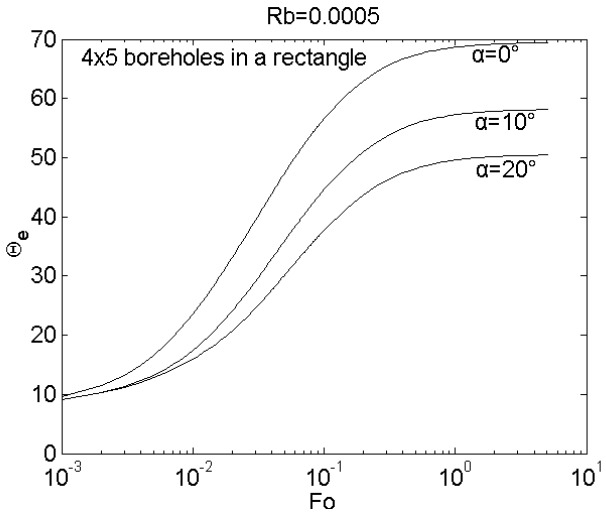

Figure 3.11 Comparisons of Θ_e between different GHEs (4×5)

3.2.4.2 Case Study 2

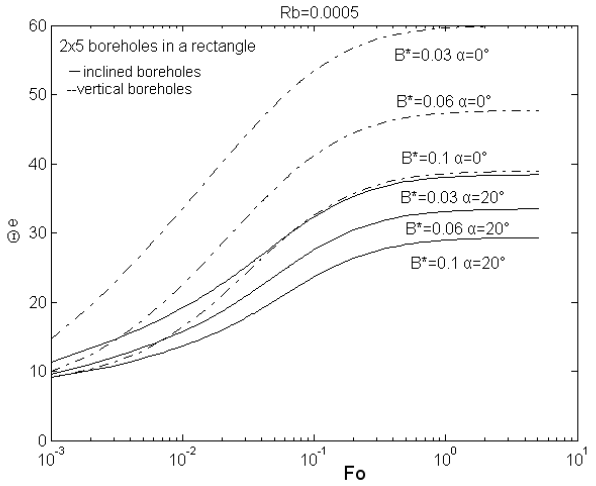

Figure 3.12 Comparisons of Θ_e between different GHEs (2×5)

Consider a GHE in a rectangle pattern (2×5) in two different cases of vertical and inclined boreholes with identical spacing. The obliquity of each borehole is 20° outward in the case of inclined boreholes. The dimensionless temperature responses of the two cases are illustrated in Figure 3.12 with different relative borehole space B^*. The results show that the temperature responses of both the inclined and the

vertical GHEs were increased with the decrease of the space between boreholes. Compared with the vertical GHE, the thermal influence of the boreholes in the inclined GHE was significantly reduced owing to its larger borehole space under the ground. For the case of B^*=0.03, the inclined GHE with $\alpha = 20°$ achieved a reduction of as much as 35% in the temperature response over the vertical GHE.

Figures 3.11 and 3.12 show that the thermal interference between boreholes can be substantially subdued by either expanding the planar spacing among boreholes or deviating the boreholes away from each other along their depth. Therefore, drilling inclined boreholes can be a favorable alternative to minimize the temperature rise of the GHEs in case of limited ground area for the installation of GHEs.

3.2.5 Comparison of representative and integral temperatures

It is well known that the inlet and outlet temperatures of the circulating water to/from a GHE (named as $t_f^{'}$ and $t_f^{''}$) can be calculated according to the borehole wall temperature, the heat rate of the GHE and the thermal resistance inside the borehole. The heat conduction resistance between the fluid inside the U-tube and the borehole wall can be determined using the quasi-three dimensional model, as shown in Equations (2.11, 2.12). The energy balances between the circulating water and the borehole wall can be expressed as:

$$\begin{cases} \left(t_f^{'}/2 + t_f^{''}/2\right) - t_b = q_l R_b \\ m_b c_p \left(t_f^{'} - t_f^{''}\right) = q_l H \end{cases} \tag{3.18}$$

where, m_b is the water mass flow rate in a single borehole.

The temperatures of $t_f^{'}$ and $t_f^{''}$ can then be easily calculated using Equation (3.18). From the viewpoint of a heat pump, $t_f^{'}$ also means the temperature of the water exiting the heat pump (called hereafter *ExWT*), and $t_f^{''}$ is the temperature of the water entering the heat pump (called hereafter *EWT*).

The main purpose of this case study is to compare the two characteristic *EWTs* which are calculated using the representative borehole wall temperature at the middle of the borehole and the integral average borehole wall temperature (see Equation 3.12), respectively. The pilot project presented in Chapter 6 is selected as the study objective in this case. The project was simulated for nearly 9 years under the assumption of constant heat transfer rate of 20W per meter of the borehole. Then the two characteristic *EWTs* can be obtained using Equation (3.18), which is illustrated in Figure 3.13. The relative errors between the two characteristic *EWTs* were also calculated and shown in Figure 3.14. In general, the representative *EWT* was slightly higher than the integral *EWT* except for the first one or two months. The maximum relative error during the long-term simulation was found to be 3.1%, which indicates that the representative temperature is completely acceptable for engineering applications.

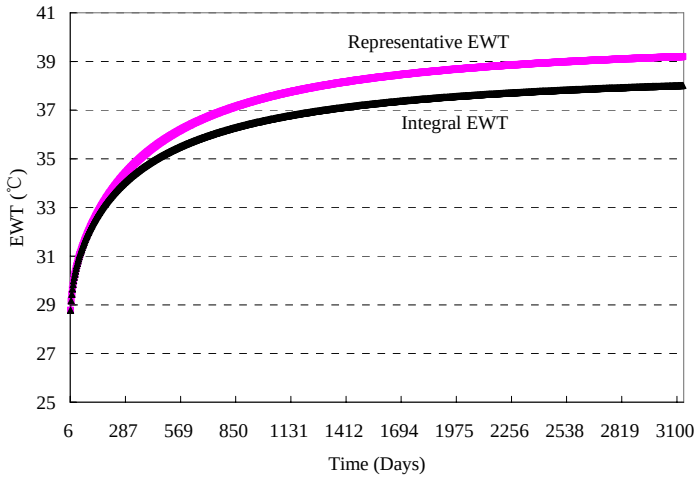

Figure 3.13 Comparisons of representative *EWT* and integral *EWT*

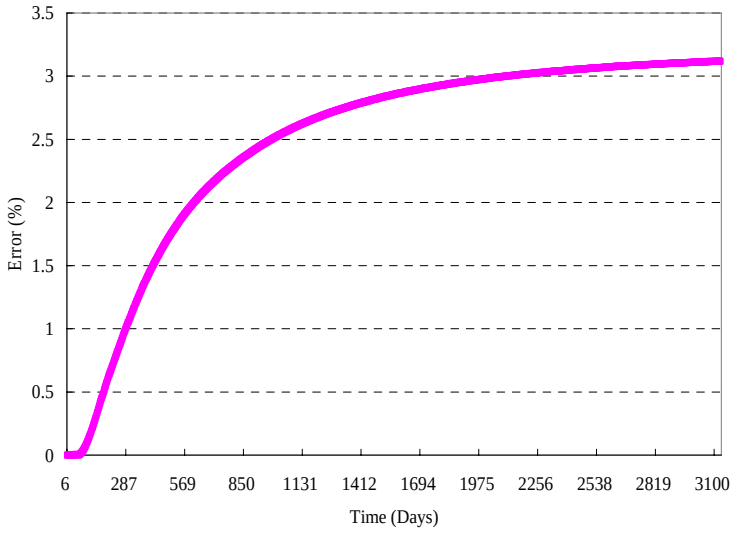

Figure 3.14 Relative errors between the two characteristic *EWTs*

3.2.6 Temperature distribution of the GHE in the pilot project

To further compare the vertical and inclined boreholes, the temperature distribution of the GHE in the pilot project which is presented in Chapter 6 are analyzed under the conditions of constant heat rejection rate: q_l=20W/m and initial soil temperature

of 22˚C. The configuration of the GHE is shown in Figure 3.15. Figure 3.16 illustrates the soil temperature distribution on the middle plane of the boreholes which was calculated at the time after 10-year continuous operation.

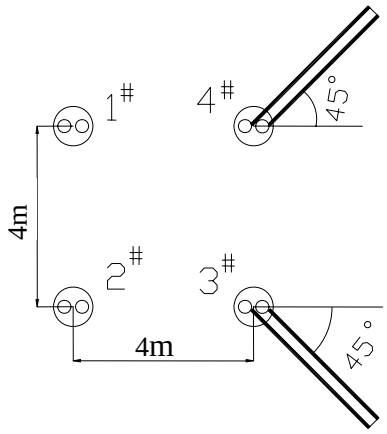

Figure 3.15 Borehole configuration

As shown in Figure 3.16, the distance between the inclined boreholes at this plane was much larger than that between the vertical ones due to the inclination of the boreholes away from each other. It can be noticed that the temperature rise around the vertical boreholes was significantly higher than that near the inclined boreholes due to the serious thermal influence between the vertical boreholes. This demonstrates that drilling inclined boreholes can effectively reduce the thermal influence and improve the heat transfer efficiency while occupying less ground area as compared with the vertical boreholes. On the other hand, the soil temperature about 15m away from the boreholes was increased by about 1˚C after 10-year continuous operation.

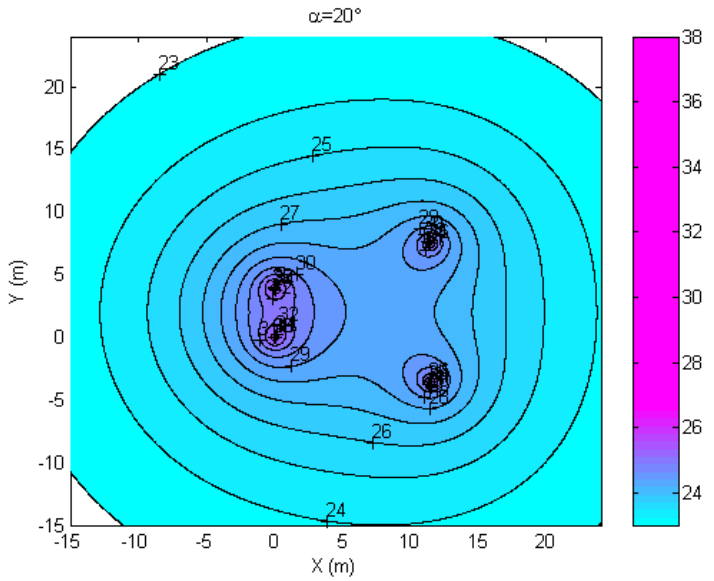

Figure 3.16 Temperature profile after 10 years' operation

3.3 Analytical Steady-State Heat Transfer Model of Inclined GHE

In general, a GHE is expected to have a lifespan of 50 years or more. To remain the GHE in adequate performance during its long lifespan, the borehole wall temperature and the circulating fluid temperature should be controlled within a certain limit in its design stage. If the amount of the heat injected to the ground in summer can be almost extracted from the ground by the GHE in winter, the soil mean temperature around the GHE will change little and thus the GHE performance will not deteriorate after its long-term operation for several years. However, in case that part of the heat injected in summer cannot be extracted in winter, the redundant heat will accumulate in the ground and thus lead to the increase in the annual mean temperature of the adjacent soil. Taking the effect of the heat transfer on the ground surface into account, the influence of the imbalanced heat will approach a relatively steady state after the GHE operates for a long enough period. This process normally

takes ten years or even more, depending mainly on the depth of the boreholes. The variation in the annual mean temperature of the soil around the GHE will affect its long-term behavior; and thus it must be taken into account when the ground loop is designed.

This section therefore is focused on the investigation of the heat transfer characteristics of the GHE when it approaches a steady state after several years' operation.

3.3.1 Modeling of the steady-state heat conduction of inclined GHEs

In the same way as the steady-state analysis of a vertical borehole (Zeng et al. 2002), the steady-state temperature distribution of an inclined finite line-source model can be solved based on the virtual heat source method and linear superposition principle. Employing the same geometry and assumptions as the transient heat transfer analysis on an inclined borehole as shown in Figure 3.1, the steady state temperature distribution of the inclined finite line source can be derived:

$$t(x,y,z)-t_0=\frac{q_l}{4k\pi}\int_0^H\left(\frac{1}{\sqrt{(x-x_0-s\sin\alpha\cos\beta)^2+(y-y_0-s\sin\alpha\sin\beta)^2+(z-s\cos\alpha)^2}}-\frac{1}{\sqrt{(x-x_0-s\sin\alpha\cos\beta)^2+(y-y_0-s\sin\alpha\sin\beta)^2+(z+s\cos\alpha)^2}}\right)ds \quad (3.19)$$

To simplify the problem, the borehole top is set on the origin of the coordinate and situated in the plane *xoz*, i.e. x_0=0, y_0=0 and β=0. Then equation (3.19) can be rewritten as

$$t(x,y,z)-t_0=\frac{q_l}{4k\pi}\int_0^H\left(\frac{1}{(x-s\sin\alpha)^2+y^2+(z-s\cos\alpha)^2}-\frac{1}{(x-s\sin\alpha)^2+y^2+(z+s\cos\alpha)^2}\right)ds \tag{3.20}$$

Integrating Equation (3.19) with respect to *s* along the borehole depth yields,

$$t(x,y,z)-t_0=\frac{q_l}{4\pi\lambda}\ln\left(\frac{H-x\sin\alpha-z\cos\alpha+r_{s+}}{H-x\sin\alpha+z\cos\alpha+r_{s-}}\cdot\frac{z\cos\alpha-x\sin\alpha+r}{-z\cos\alpha-x\sin\alpha+r}\right) \tag{3.21}$$

where, $r_{s+}=\sqrt{(x-H\sin\alpha)^2+y^2+(z-H\cos\alpha)^2}$;

$r_{s-}=\sqrt{(x-H\sin\alpha)^2+y^2+(z+H\cos\alpha)^2}$; $r=\sqrt{x^2+y^2+z^2}$

As can be seen in Equation (3.21), when $z=0$, $t(x,y,0)=t_0$, i.e. the temperature distribution accords with the boundary condition, where the temperature of the ground surface is assumed to be constant as the far-field ground temperature.

Equation (3.21) can be expressed in a dimensionless form as follows:

$$\Theta=\ln\left(\frac{1-X\sin\alpha-Z\cos\alpha+r^*_{s+}}{1-X\sin\alpha+Z\cos\alpha+r^*_{s-}}\cdot\frac{-X\sin\alpha+Z\cos\alpha+r^*}{-X\sin\alpha-Z\cos\alpha+r*}\right) \tag{3.22}$$

where $X=x/H$, $Y=y/H$, $Z=z/H$, $r^*_{s+}=r_{s+}/H=\sqrt{(X-\sin\alpha)^2+Y^2+(Z-\cos\alpha)^2}$,

$r^*_{s-}=r_{s-}/H=\sqrt{(X-\sin\alpha)^2+Y^2+(Z+\cos\alpha)^2}$, $r*=r/H=\sqrt{X^2+Y^2+Z^2}$.

When $\alpha=0$, Equation (3.22) becomes

$$\Theta=\ln\left(\frac{1-Z+\sqrt{X^2+Y^2+(Z-1)^2}}{1+Z+\sqrt{X^2+Y^2+(Z+1)^2}}\cdot\frac{Z+\sqrt{X^2+Y^2+Z^2}}{-Z+\sqrt{X^2+Y^2+Z^2}}\right) \tag{3.23}$$

This is identical to the solution obtained from the vertical finite line source (Zeng et al. 2002).

3.3.2 Characteristic steady-state temperatures of the borehole wall

Similarly, the steady-state temperature is not identical at a borehole wall circle on the cross section perpendicular to its axis and varies along the borehole depth because of the three-dimensional geometry. Based on the identical geometry of the inclined borehole as shown in Figure 3.2 and the same expressions for coordinates (Equation 3.9), the average temperature on a specific circle at the borehole depth L can be expressed by,

$$\Theta_{s,c} = \frac{1}{\pi}\int_0^{\pi} \Theta(L, R_b, \alpha, \omega) d\omega \tag{3.24}$$

Following the discussions on the representative temperature of the borehole wall in transient heat-transfer analysis, the temperature at the point $(H\sin\alpha/2, r_b, H\cos\alpha/2)$ with $\omega=\pi/2$ on the middle section of the borehole is recommended to substitute the integral average temperature on the cross section. The relative dimensionless expression is obtained:

$$\Theta_{s,r} = \ln\left(\frac{\sqrt{1+4R_b^2}+\cos 2\alpha}{\sqrt{1+4R_b^2+8\cos^2\alpha}+\cos 2\alpha+2}\cdot\frac{\sqrt{1+4R_b^2}+1}{\sqrt{1+4R_b^2}-1}\right) \tag{3.25}$$

Figure 3.17 indicates the variations of the relative errors between the representative temperature and the average temperature on the middle section circle with the borehole relative radius and obliquity change. It can be seen from the figure that all the relative errors between the two proposed temperatures were less than 1×10^{-5} for

a wide range of the obliquity (α<45°) as the relative radius ranged from 0.0001 to 0.01, which is commonly encountered in engineering practices of GHEs. This indicates that the representative temperature, Equation (3.25), can adequately replace the average temperature of the middle section circle on the borehole wall, which can further be recommended to be the unique characteristic temperature of the borehole wall.

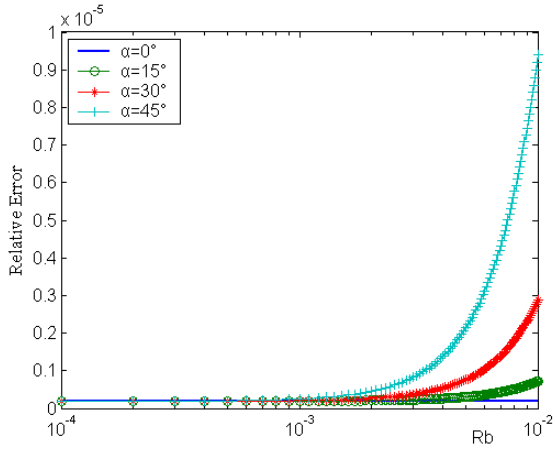

Figure 3.17 Relative errors between the representative and the integral average temperatures of the middle section circle

Equation (3.25) can be further simplified due to the much smaller borehole radius r_b compared with the borehole depth H (i.e. $r_b/H << 1$), and the representative temperature of the borehole wall can be deduced as:

$$\Theta_{s,r} \approx \ln\left[\frac{1+\cos 2\alpha}{\left(\sqrt{1+8\cos^2\alpha}+\cos 2\alpha+2\right)R_b^2}\right] \qquad (R_b << 1) \qquad (3.26)$$

Since the temperature along the length of the borehole wall varies significantly, it is not quite justified to use the temperature at the middle section of the borehole wall to

represent its temperature when calculating the heat transfer in the whole system. Consequently, the whole-length integral average temperature is recommended here as a more reasonable characteristic temperature of the inclined borehole wall in heat transfer analysis of GHEs. It is defined as,

$$\overline{\Theta}_{s,b} = \frac{1}{\pi}\int_0^1\int_0^\pi \Theta(R_b,\omega,L,\alpha)\mathrm{d}\omega\mathrm{d}L \tag{3.27}$$

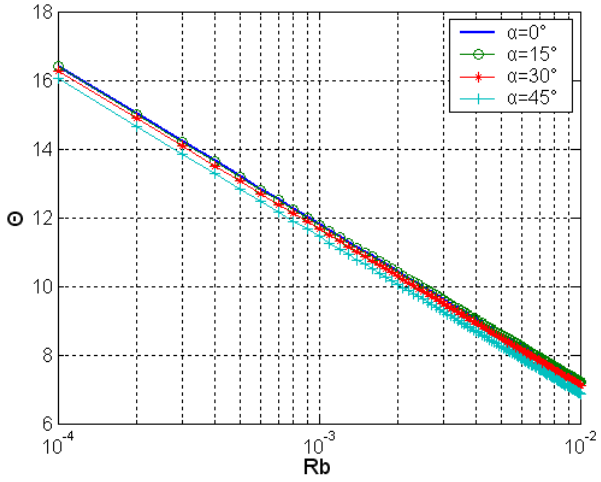

Figure 3.18 The integral average temperature at the borehole wall vs. R_b

Figure 3.18 presents the variations of the integral average temperatures at the borehole wall with relative borehole radius under conditions of different obliquities.

Figure 3.19 shows the variations of the relative errors between the two characteristic temperatures (defined as $\varepsilon = \Theta_{s,r}/\overline{\Theta}_{s,b} - 1$) against the obliquity and the relative radius of the inclined borehole. As can be seen from Figure 3.19, the relative discrepancy between the two characteristic temperatures ranged from 5.5 % to 13% under the conditions of $R_b \le 0.02$ and $\alpha \le 45^o$.

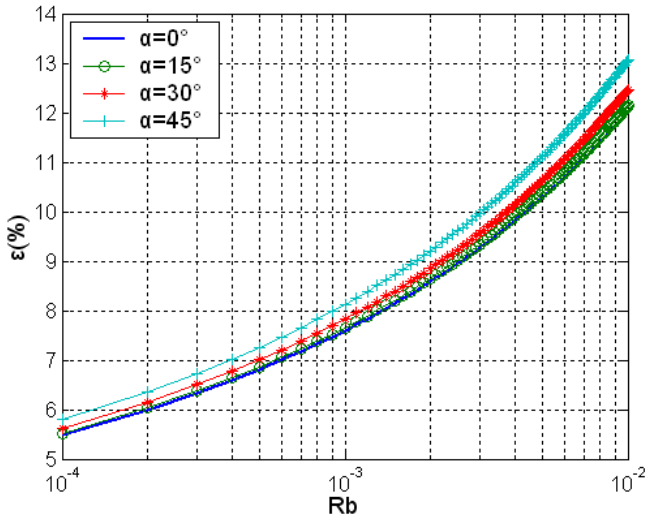

Figure 3.19 Relative errors between the representative and integral average temperatures at the borehole wall vs. R_b

3.3.3 Approximate method for the integral average temperature over whole length of the borehole

Although it is defined more reasonably, the whole-length integral average temperature is difficult to calculate, and inconvenient to practical applications. It can be detected from Figure 3.16 that the integral average temperature has an almost linear relation to the logarithm of the borehole relative radius. Thus, a simpler semi-empirical expression is derived by means of linear regression of the data computed with Equation (3.27). The approximate expression is given in the following form,

$$\Theta_{s,b} \approx -3.2073 - 1.9910 \ln(R_b) + 1.2809 \cos\alpha \quad \left(1e-4 < R_b < 1e-2, \alpha \le 45^\circ\right) \tag{3.28}$$

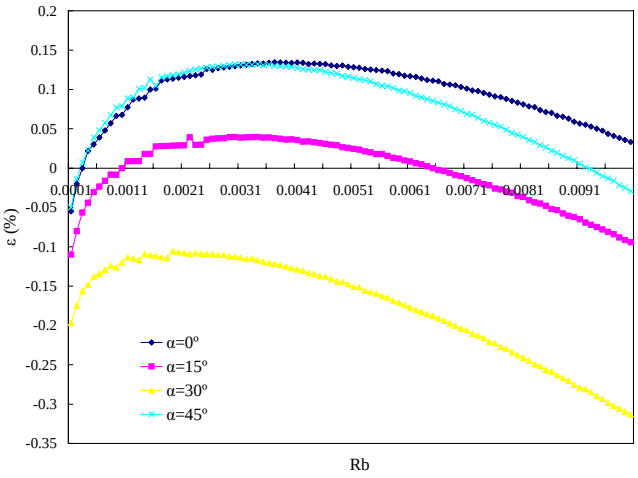

Figure 3.20 Relative errors between the approximate and integral average temperatures at the borehole wall vs. R_b

As shown in Figure 3.20, the relative deviation of approximate temperature was within -0.35%~0.15% from the whole-length integral average temperature under the ranges of $0.0001 \le R_b \le 0.01$ and $\alpha \le 45^\circ$. Obviously, the explicit expression of Equation (3.28) is quite convenient, and accurate enough for engineering applications.

3.4 Model Validation

This section is focused on the comparisons of the calculated *EWT* and *ExWT* with the experimental data, which can be used to verify the accuracy of the simulation model of the GHE.

3.4.1 Experimental description

The detailed parameters and configuration of the GHE of the pilot project are described in Chapter 6. To experimentally validate the simulation mode of the

inclined GHE, a set of experiments were continuously conducted under cooling mode over two different periods (from 7:30 24th to 15:00 26th May 2007 and from 6:30 to 15:00 27th May 2007).

3.4.2 Results and discussion

Based on the measured water flow rates and water temperatures on the GHE side, the heat transfer rates between the GHE and the ground (i.e. the heat rejection to the ground) can be easily calculated. Figure 3.21 presents the average heat transfer rate per unit length of the borehole with operating time. The heat flux of the borehole was significantly varied with time, resulting in an average value of about 60W/m in daytime, and less than 30W/m at night, which reflected the large difference of building cooling loads between daytime and nighttime.

The comparisons between the predicted and measured *EWT* and *ExWT* are presented in Figures 3.22 and 3.23, respectively. The relative errors were calculated and also presented in the two figures. In general, the model prediction and measurement experiments showed an acceptable agreement throughout the operating period. The temperature differences between the predicted and measured data were found be within 3˚C. The discrepancies between the predicted and measured temperatures were within the range of ±12%.

It should be pointed out that the compressor was turned on and off frequently during the most time of the experiments because of the small cooling loads of the conditioned space, which may result in large variations of the temperatures in short time. Since the collection time interval was set to be two minutes, there must be

some inevitable deviations of the calculated heat transfer rates from the real values, which may cause a wide fluctuation in the calculated temperatures, as shown in the figures.

It can be detected from the figures that both *EWT* and *ExWT* were increased during the daytime and then decreased gradually at night owing to the less heat rejection to the ground. As expected, when the system was re-operated after 15 hours of off time, the temperatures were evidently lower than the last operation. This means that the discontinuous operation mode can effectively increase the heat transfer efficiency of the GHE and the performance of the whole system.

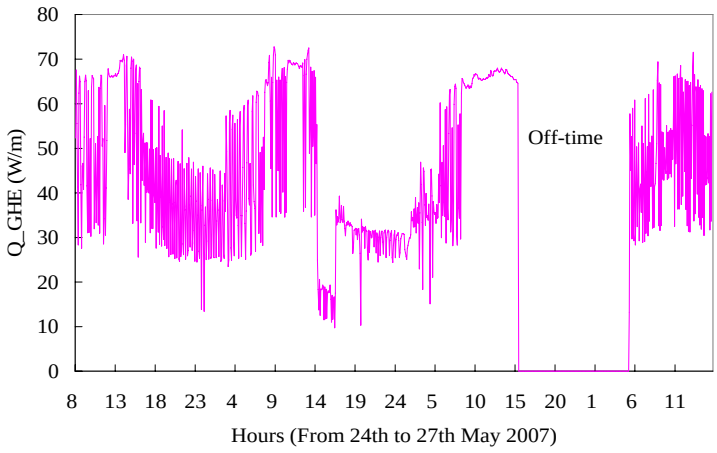

Figure 3.21 GHE load per borehole length

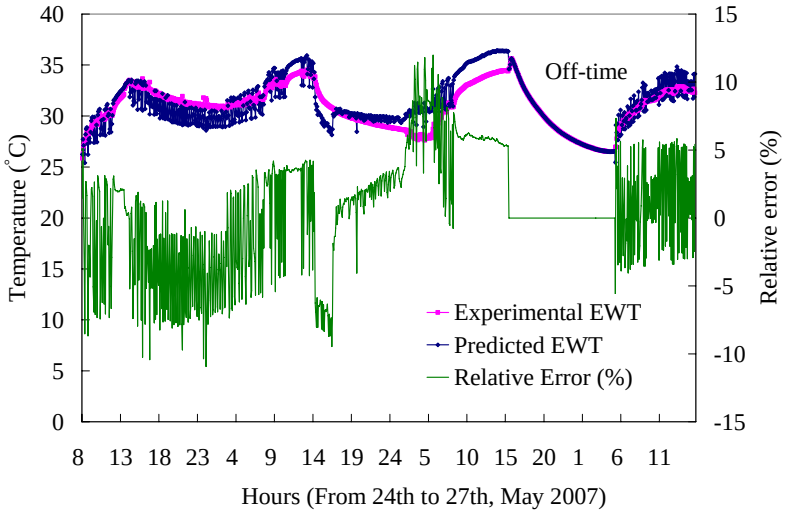

Figure 3.22 Comparisons of experimental and predicted *EWT*s along with the relative error

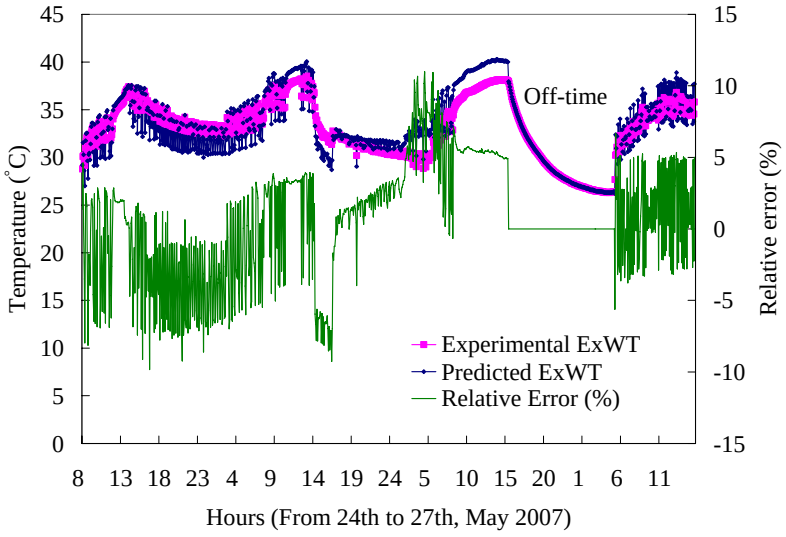

Figure 3.23 Comparisons of experimental and predicted *ExWT* along with the relative error

3.5 Summary

This chapter has presented an extensive analysis on the heat transfer of the inclined GHEs from a basic case of a single inclined borehole to practical cases of the GHEs with vertical and inclined boreholes. An inclined finite line-source model in a semi-infinite medium has been developed to describe the transient and steady-state heat conduction processes in GHEs for long-term operation. The following conclusions are drawn.

1. The representative temperature at a specific point on the middle cross-section circle of the borehole wall is recommended for the design of GHEs instead of its integral average temperature along the cross-section circle and the borehole depth.

2. The thermal interference between two inclined boreholes can be approximately simplified as that of two supposed vertical boreholes disposed at a distance between the middle points of the inclined boreholes. The representative temperature obtained from the approximate method is recommended for engineering design.

3. A semi-empirical function with satisfactory accuracy is presented, describing the steady-state integral average temperature of the inclined borehole wall.

4. Comparisons between the inclined and vertical GHEs of typical rectangular patterns show that the temperature rise on the borehole wall of the inclined GHE can be 10%~35% lower than that of the vertical GHE for long-term performance under commonly encountered conditions in engineering practice.

Finally, the analytical model of the inclined finite line source has been experimentally validated through the pilot project. The comparisons show that the analytical model was generally accurate to within ±12%, which is considered to be satisfactory for practical engineering.

To sum up, inclusion of inclined boreholes in the GHE configuration can improve its thermal performance especially for the GCHP systems with imbalanced annual loads and limited land allowance to install the GHE. The benefit from drilling inclined boreholes is evident in such situations.

CHAPTER 4 NUMERICAL MODEL OF GHEs

4.1 Necessity of Numerical Analysis

The HGCHP system with triple functions can flexibly change the operation modes to provide cooling, heating or hot water heating according to different requirements of owners in short time scales. In summer, the system can be converted alternatively into heating mode for a few hours to produce hot water when the cooling requirement is insignificant or zero. In winter or the transitional seasons when the cooling requirement is unnecessary, the main function of the system is to satisfy the domestic hot water demand. Such systems may experience at least two different operating modes during a short time period, which can accordingly cause significant variations of the amount of heat transferred to/from the soil surrounding the GHE. As a result, the corresponding fluctuations are observed in temperatures of the surrounding soil and the heat carrier (water) to the heat pump, which directly impacts the operating performance of the system. Therefore, it is vital to design and analyze the thermal performance of the GHEs in short-time scales.

Neither the inclined finite line source model nor the vertical one is capable of modeling the heat transfer of GHEs in short time intervals (usually less than a few hours) due to the assumption of neglecting the thermal capacitance of the borehole elements. It is estimated that the concerned radius of the thermal influence by a single borehole is about 3-4 meters away from the borehole center after a few

months of continuous operation. Furthermore, according to the simulation results obtained from Chapter 3, there is insignificant difference of the heat transfer between a vertical borehole and an inclined one, especially for short-time scale. In view of these factors, also for simplicity, a single vertical borehole will be studied here in terms of its heat transfer characteristics for short-time scale, which can represent the general case.

A number of researchers have recently paid more attention to analyzing the effect of the short-term performance of the GHEs using various numerical methods which have been elaborated in Chapter 2.

This chapter is focused on the study of the transient heat transfer behavior of the GHE in alternative operation modes in short-time scale. The numerical finite element method (FEM) is used to analyze the temperature distribution in the borehole.

4.2 Model Development

4.2.1 Assumptions

The modeling of the transient heat transfer process of a GHE in a short time period is a complex mathematical problem. Simplifying assumptions are necessary to obtain the solution. The ground is regarded to be homogeneous in its thermal properties and initial temperature. The heat flux through the top and the end of the borehole is neglected because the size of the borehole diameter is much smaller than its depth. A two-dimensional transient heat conduction model, therefore, is employed to represent the actual heat transfer process in the borehole domain.

4.2.2 Governing equations

To simplify the analysis, a symmetrical placement of the two legs of the U-tube inside the borehole is assumed. Thus, only half of the borehole domain is modeled because of the axisymmetric configuration, as shown in Figure 4.1. An adiabatic boundary condition is applied to the symmetric plane on the center of the borehole. The borehole domain is physically divided into three regions according to the categories of the material: the inner one is the pipe wall; the middle is the grout backfilled in the borehole and the outer region is the soil surrounding the borehole.

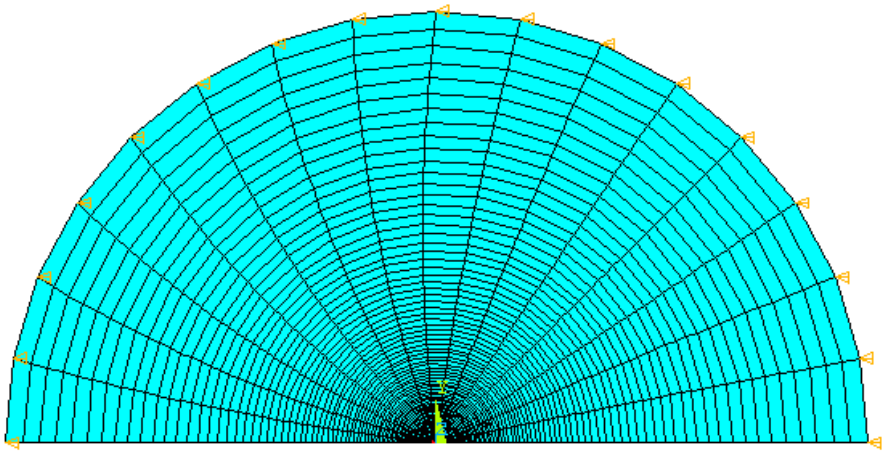

Figure 4.1 (a) Meshed model of the borehole domain

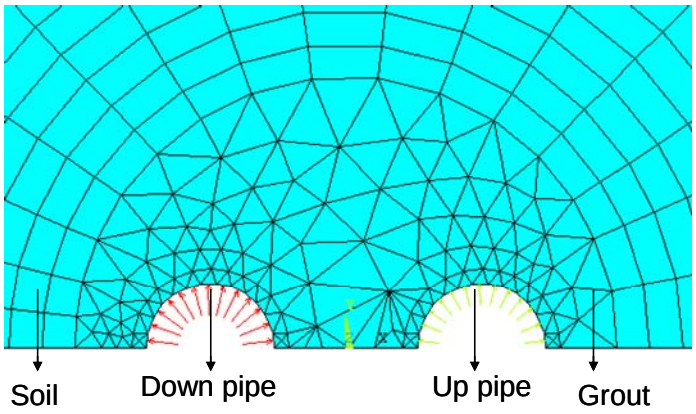

Figure 4.1 (b) Magnification of the meshes adjacent to the U-tube

The governing equation for each region in the borehole domain can be represented with cylindrical coordinates.

$$\frac{1}{a_i}\frac{\partial t_i}{\partial \tau}=\frac{\partial^2 t_i}{\partial r^2}+\frac{1}{r}\frac{\partial t_i}{\partial r}+\frac{1}{r^2}\frac{\partial^2 t_i}{\partial \theta^2} \tag{4.1}$$

where the subscript $i=p$ means the pipe; $i=g$ is the grout; $i=s$ is the soil.

Introducing the following dimensionless variables:

$$\Theta_i^*=2\pi k_s\frac{t_i-t_0}{q_l},\quad r^*=\frac{r}{r_b},\quad Fo_r=\frac{a_s\tau}{r_b^2},a_i^*=\frac{a_i}{a_s},\quad k_i^*=\frac{k_i}{k_s}$$

Equation (4.1) can be transformed into the nondimensionalized expression:

$$\frac{1}{a_i^*}\frac{\partial \Theta_i^*}{\partial Fo_r}=\frac{\partial^2 \Theta_i^*}{\partial r^{*2}}+\frac{1}{r^*}\frac{\partial \Theta_i^*}{\partial r^*}+\frac{1}{r^{*2}}\frac{\partial^2 \Theta_i^*}{\partial \theta^2} \tag{4.2}$$

Taking the boundary conditions into consideration for each region, the dimensionless temperature rise in each region can be determined by a number of dimensionless parameters.

For the pipe section:

$$\Theta_i^*=f\left(r^*,\theta,Fo_r,k_p^*,a_p^*,k_g^*,\alpha_g^*,r_{p,in}^*,r_{p,out}^*,s^*\right) \tag{4.3}$$

where, $r_{p,in}^*=\frac{r_{p,in}}{r_b}$, $r_{p,out}^*=\frac{r_{p,out}}{r_b}$, $s^*=\frac{s}{r_b}$, $r_{far}^*=\frac{r_{far}}{r_b}$, s means the space between the pipe center and the borehole center and r_{far} means the far-field boundary away from the borehole center.

4.2.3 Boundary conditions

For numerical heat transfer calculation, an outer boundary condition must be given to obtain the closed-form solution to the heat transfer problem. The outer extent of the domain defined here is large enough to ensure the boundary temperature maintains consistently at the value of the far-field temperature during the concerned time, i.e., the amount of the heat flux at the outer edge of the domain is zero or insignificantly small.

The convective heat transfer between the water in the U-tube and the pipe wall is not simulated in the model for the purpose of simplicity and it is approximately considered in the conductive heat transfer of the pipes by adding a convective heat transfer resistance. Therefore, the inner boundary condition at the inner pipe wall is set to be the heat flux. It is noticed that the heat flux and fluid temperatures along the two legs of the U-tube are actually varied due to the thermal interference between the two legs. Zeng et al. (2003) proposed the quasi-three dimensional transient model which illustrated the fluid temperature variation along the flow direction in the two pipes of a U-tube. In the case of the project mentioned below, computations show that about 60% of the total heat flux in a single borehole was transferred through the down pipe and only 40% was released through the up pipe when $Fo_r = a\tau / r_b^2 = 4.5$ (about 6 hours for a typical borehole). Figure 4.2 illustrates the dimensionless fluid temperature distribution in the down and up pipes of a U-tube in the case of the cooling mode.

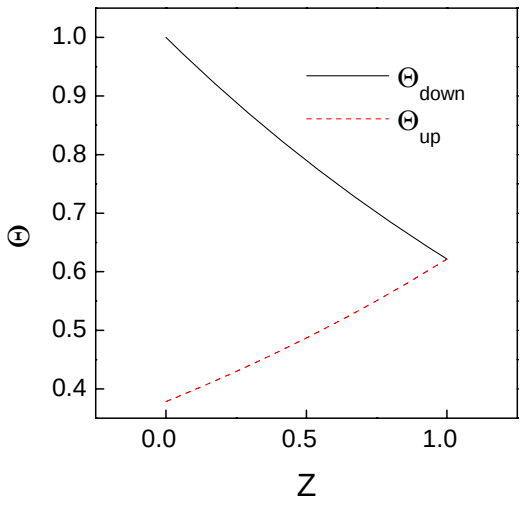

Figure 4.2 Fluid temperature profiles of the two pipes along the borehole depth at $Fo_r=4.5$

4.2.4 Finite element method (FEM)

In the simulation model, the numerical FEM is employed to solve the problem and the commercial code *ANSYS* is used to perform the transient heat transfer simulation in the borehole domain. One of the important advantages of the FEM is the ability to deal with the heat transfer process with arbitrary geometries and non-homogenous media. After building the geometric model and defining the necessary parameters including the material thermal properties, the element size and type as well as the boundary conditions, the *ANSYS* program can automatically generate a finite element model which consists of nodes and elements, as shown in Figures 4.1 (a) and (b). The region nearest to the pipes, where the temperature gradient is the steepest, is meshed finer to ensure the temperatures to be accurately predicted, as shown in Figure 4.1 (b). In contrast, a coarser mesh is sufficient for the region

outside the borehole. Once the finite element model is built with the mesh discretization, the heat transfer problem can be solved numerically.

4.3 Numerical Results

A case study was established in order to better investigate the heat transfer process and temperature distribution in the borehole region. All the necessary dimensionless variables including the geometric parameters and the material thermal properties are summarized in Table 4.1. This case was simulated using the numerical method under the *ANSYS* simulation environment over a period of operation time (Fo_r *=4e-2 ~4e+2*), which may be corresponding to the time steps of 4 minutes and 670 hours (about one month) for a typical borehole.

Table 4.1 Dimensionless parameters of the case study

k_p^*=0.25	a_p^*=0.23	k_g^*=0.8	a_g^*=0.67
$r_{p,in}^*$=0.24	$r_{p,out}^*$=0.29	r_{far}^*=73	

Figure 4.3 shows the dimensionless temperature distribution in the whole region under study when Fo_r *=4e+2* (i.e. after about one month simulation). It can be seen from Figure 4.3 (a) that the heat flux released from the borehole center only reached about half region of the whole domain, which equaled about 2 meter away from the center of a typical borehole. This demonstrates that neglecting the thermal interference between adjacent boreholes is completely suitable for short-term simulation (such as, less than one month).

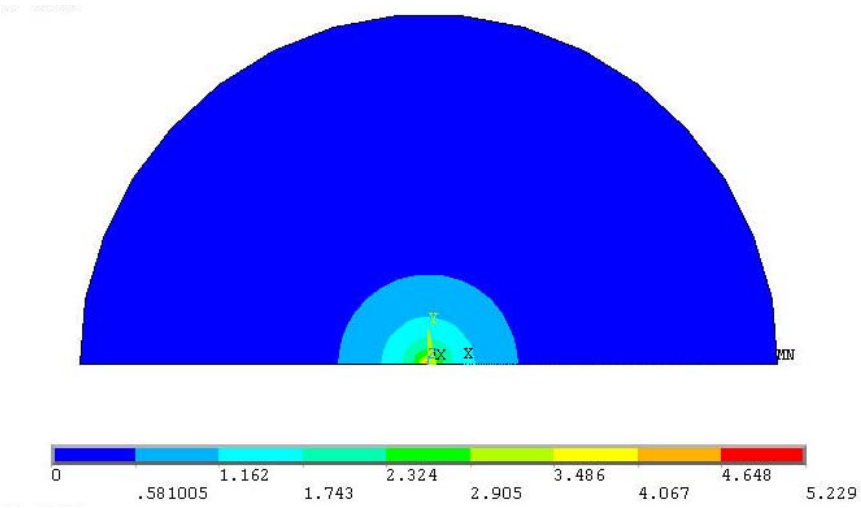

Figure 4.3 (a) Dimensionless temperature contours of the whole region

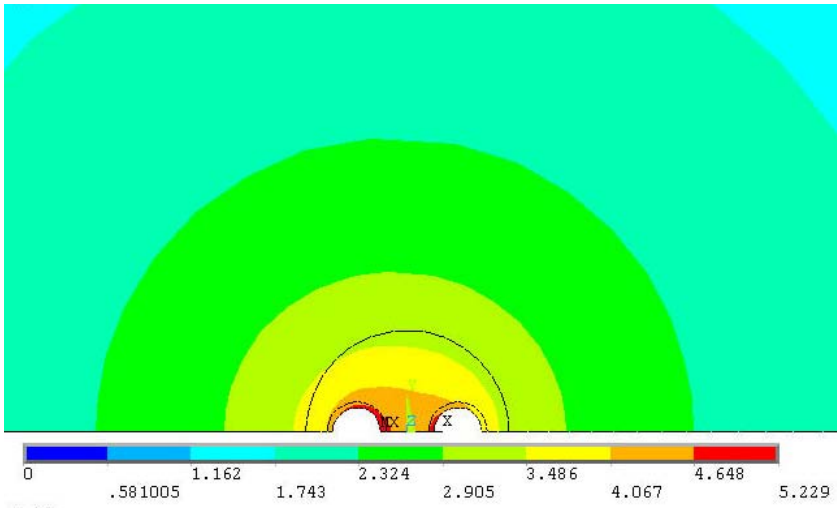

Figure 4.3 (b) Magnification of the dimensionless temperature contours around the borehole

As is shown in Figure 4.3 (b) which illustrates the temperature distribution around the borehole, the imbalanced heat fluxes in the two legs of the U-tube did influence the heat transfer around the borehole wall. Thus it is necessary to take the heat flux disequilibrium within the borehole into consideration in the modeling of the GHE.

4.4 Comparison of Analytical and Numerical Models of GHE

In order to make a meaningful comparison between the finite element (numerical) method and the finite line source (analytical) method, the same case simulated using the numerical method in section 4.3 is also investigated using the finite line source. It is noted that the borehole depth H should be considered in the analytical method although its effect is insignificant on the analytical solution in a short-time scale, then, adding another dimensionless variable, H / r_b =2000.

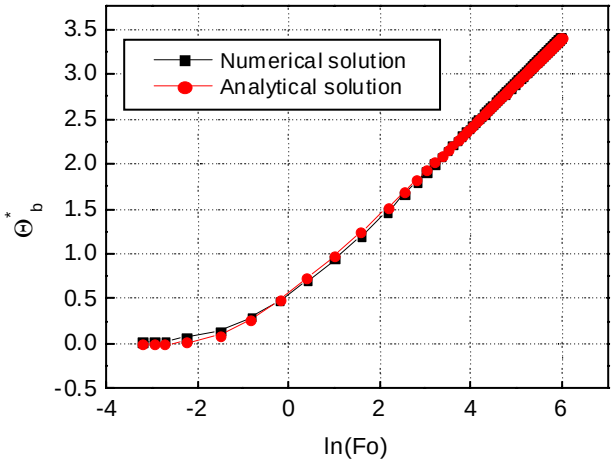

Figure 4.4 Comparison of the numerical and analytical results

Figure 4.4 illustrates the variations of the average dimensionless temperature rises on the borehole wall obtained from the numerical and analytical methods, respectively. According to Figure 4.4, the general varying trends of the numerical and analytical results exhibited a good agreement during the operating time. To better analyze the difference between the two methods, the relative error which is defined in Equation (4.4) is also calculated and depicted in Figure 4.5.

$$relative\,error = \frac{Analytical\,value - Numerical\,value}{Numerical\,value - Initial\,value} \times 100\% \tag{4.4}$$

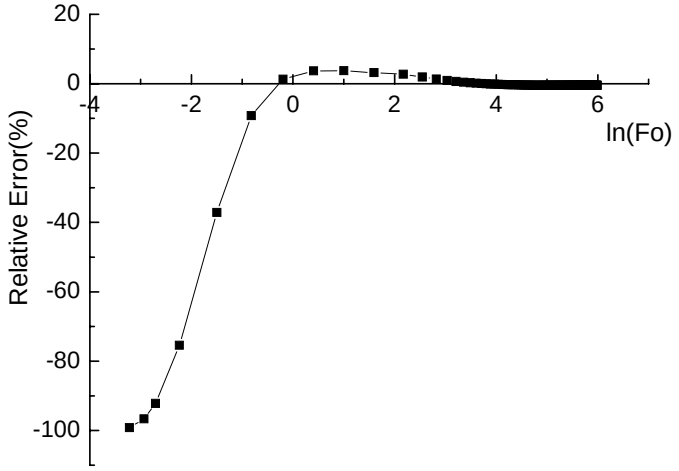

Figure 4.5 Relative error profile between the numerical and analytical results

It can be seen from Figures 4.4 and 4.5 that the analytical value of the temperature rise on the borehole wall was markedly smaller than the numerical value at the beginning of the simulation (generally within an hour for a typical borehole). This was due to the assumption of the line source in the center of the borehole, which neglected the physical size of the U-tube in the borehole. The significant relative error with a maximum value of nearly 100% proves that the finite line-source method is not accurate enough for the simulation or design of the GHEs for short time operation. However, after the initiative period of a short time, the deviation between the two values rapidly attenuated with time, resulting in a small average error of less than 4%. This indicates that the finite line-source method is completely acceptable for the practicable engineering except for the case of short-time simulation/design.

4.5 Experimental Validation of the Numerical Model

4.5.1 Experimental description

Two vertical boreholes in the GHE of the pilot project (noted as B1 and B2) were used for the experimental validation. Verifying the short-time numerical model of the GHEs can be implemented through comparisons of the predicted and experimental pipe wall temperatures. The temperature sensor disposal along the U-tubes in the two boreholes is given in Figure 6.4.

A series of experiments were conducted under the alternative cooling and heating modes during May 17th to 18th in 2007, as shown in Table 4.2.

Table 4.2 The experimental operating schedule of the HGCHP system

No.	Operating Time	Operating mode
Ⅰ	17th 11:00~14:27	Cooling mode
Ⅱ	17th 14:32~14:58	Heating mode
Ⅲ	17th 15:00~16:54	Cooling mode
Ⅳ	17th 16:55 ~18th 8:59	Off-time
Ⅴ	18th 9:00~10:55	Cooling Mode
Ⅵ	18th 11:07~11:39	Heating mode
Ⅶ	18th 12:44~16:00	Cooling Mode

4.5.2 Results and discussion

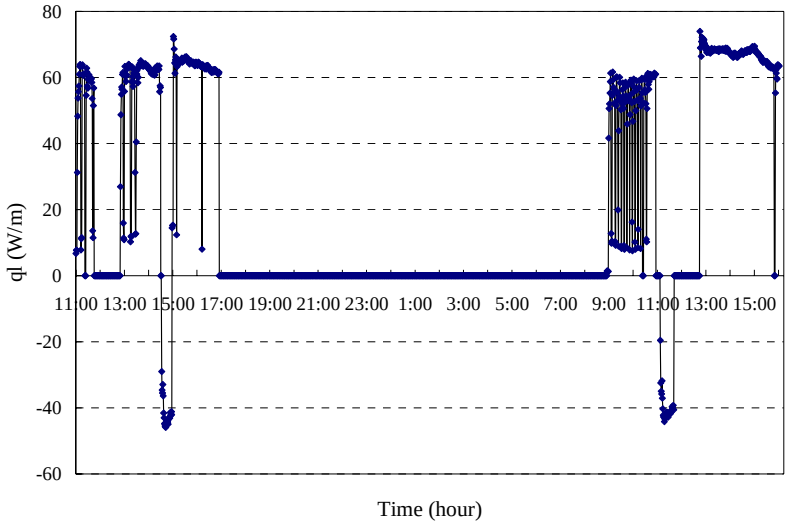

Figure 4.6 Average heat transfer rate per unit length of the borehole

According to the recorded data resulting from the experiments, the total heat transfer rate per borehole during the operation period was calculated using the water flow rate and the temperature difference between the borehole inlet and outlet, similar to Equation (6.2). Figure 4.6 illustrates the minutely heat transfer rate per unit length of the borehole with operating time, where the heat rejection is shown as positive and heat extraction as negative. A higher heat rejection was observed in cooling mode, which had an average value of about 60W/m. However, the heat transfer rate in the heating mode was approximated to be 45W/m, which was due to the low heat requirement for DHW heating.

The comparisons between the predicted and measured pipe wall temperatures in the two concerned boreholes are presented in Figures 4.7 and 4.8. The temperature differences between the predicted and measured temperatures are also plotted in Figure 4.9. The predicted and measured temperatures on the two U-tubes showed, on the whole, a great agreement during the operating time. It should be noticed that the

temperature deviations in the two down pipes were obviously larger than that in the up pipes. This phenomenon may be caused by several uncertain factors, such as the heat flux sharing ratio between the two pipes of the U-tubes or the temperature sensor sensitivity. The maximum temperature difference between the predicted and measured data was less than 1.6˚C.

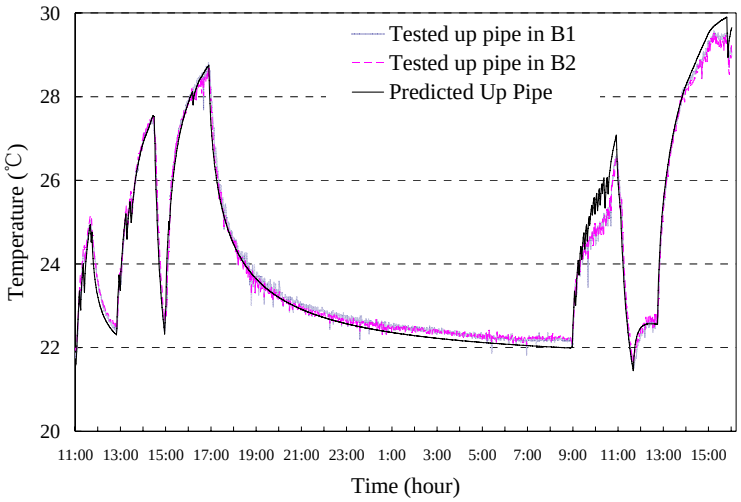

Figure 4.7 Comparison of the predicted and measured up pipe wall temperatures

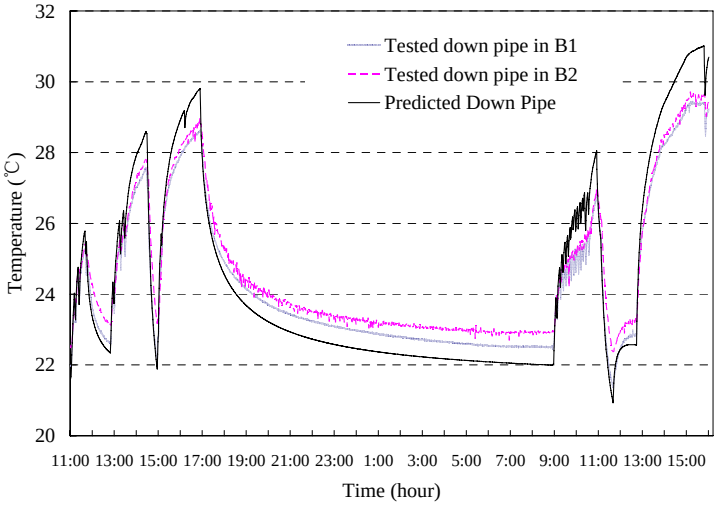

Figure 4.8 Comparison of the predicted and measured down pipe wall temperatures

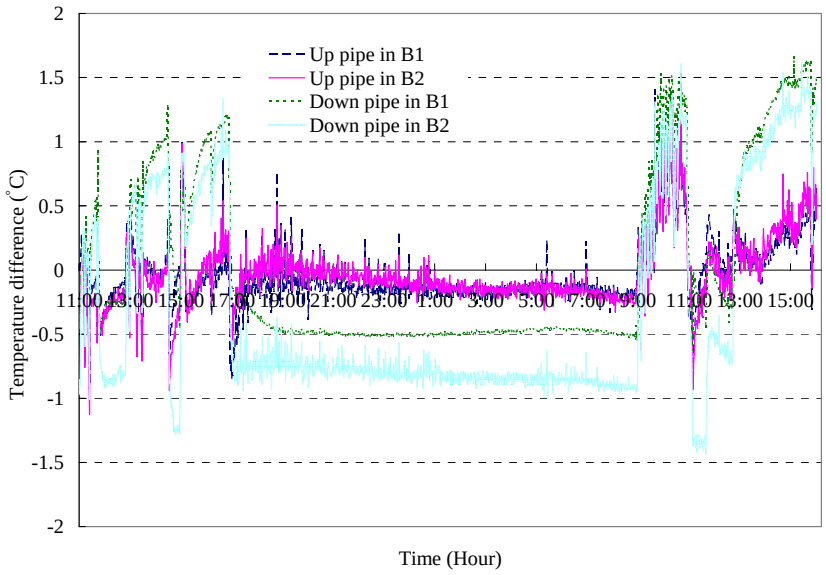

Figure 4.9 Temperature differences between predicted and measured pipe wall temperatures

In addition, it can be detected from Figures 4.7 and 4.8 that the pipe wall temperatures oscillated significantly during the cooling and heating alternative modes and then gradually approached the far-field ground temperature after the system was shut down. After 12 hours of off time at night, the pipe wall temperature was almost close to the initial value before the system restarted. This means that both the alternative modes and the discontinuous operation mode can significantly increase the heat transfer efficiency of the GHE and therefore improve the performance of the whole system.

4.6 Summary

A finite element numerical model has been developed to analyze the performance of the GHEs during the short-time scale operation. Comparisons between the numerical

and analytical results indicate that the finite line-source model can be capable of modeling the GHEs except a few hours because of the line-source assumption.

The numerical finite element model has been experimentally validated by means of the measured U-tube wall temperatures under the conditions of the alternative cooling and heating modes during a short-time period. The comparisons showed a reasonable agreement between the numerical and the measured data. This illustrates that the finite element numerical model can be used to simulate the heat transfer behavior of the GHEs in short time scale instead of the typical finite line-source model.

Finally, the variations of the U-tube pipe wall temperatures demonstrate that the discontinuous operation mode and the alternative cooling/heating modes can effectively alleviate the heat buildup in the surrounding soil, which can ultimately improve the system performance. Thus, the discontinuous operation mode (such as operating during daytime while shut down at night or vice versa) is also recommended and it is feasible for commercial or residential buildings.

CHAPTER 5 MODELING OF THE HGCHP SYSTEM WITH DESUPERHEATER

5.1 Introduction

A great number of heat pump units with desuperheaters have been produced by manufacturers, which can simultaneously supply space cooling/ heating and hot water. However, few manufacturers can provide a wide range of performance data for such equipment under various operation modes. An effective and practical simulation model is strongly desirable in order to accurately evaluate the operating performance of the HGCHP systems. The objective of this chapter is to develop a comprehensive simulation model for the HGCHP system with DHW supply and to further analyze the performance of the system under various conditions using the simulation model.

According to the literature review on the heat pump models in Chapter 2, the heat pump simulation models are basically classified as either functional fit or deterministic models. One of the primary advantages of the deterministic model is the convenience of designing an efficient and cost-effective heat pump unit by varying the design parameters of each component and conditions. Besides, it can be capable of simulating the system responses for a variety of external and internal conditions which may be beyond the range of catalog data.

It is worth noticing that the deterministic models consist of the dynamic and steady-state models. The dynamic model is mainly used to analyze the dynamic behavior during the start-up or shutdown period of a system or to investigate the operating performance of a complicated system with variable speed pumps or compressors. Besides, for a heat pump system with constant speed water pumps and compressor, the characteristic time to approach the steady-state operation (usually a few hours) is quite smaller compared with the characteristic steady-state time (i.e. a few years) of the heat transfer of GHEs. In the studied heat pump unit, the compressor together with the water pumps is constant speed. The steady-state deterministic model is therefore employed here to develop the simulation model of the HGCHP unit which incorporates laws of thermodynamics, fluid mechanics and heat transfer correlations into a network of simulation algorithms.

The simulation model of the HGCHP unit consists of five sub-models: a rolling piston compressor, evaporator, desuperheater, condenser and a thermostatic expansion valve. A lumped-parameter model is used to evaluate the performance of the compressor in view of the high speed of the compression process. An adiabatic process is assumed in the expansion valve model. The three heat exchangers of the evaporator, desuperheater and condenser, which are copper tube-in-tube heat exchangers, are modeled by means of a zone-based distributed parameter method.

5.2 System Description

A water-to-water heat pump with an integral desuperheater is presented in Chapter 6 and the schematic configuration is also shown in Figure 6.2.

It is worthwhile to point out that the pressure drop across the compressor inlet Δp_{suc} is set to be zero owing to the absence of the suction valve in the rolling piston compressor. Since the sizes of the connecting tubes are much smaller than the heat exchangers, the pressure and temperature drops in the connection tubes can then be negligible, which can simplify the modeling procedure to some extent.

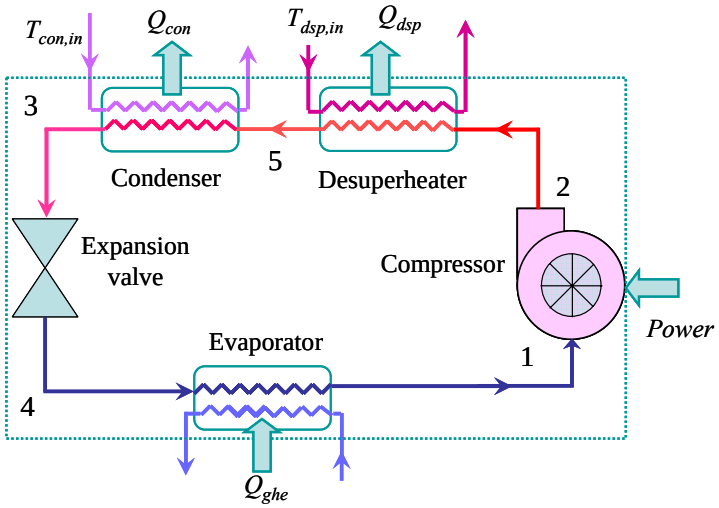

Figure 5.1 Schematic diagram of the refrigerant flow chart

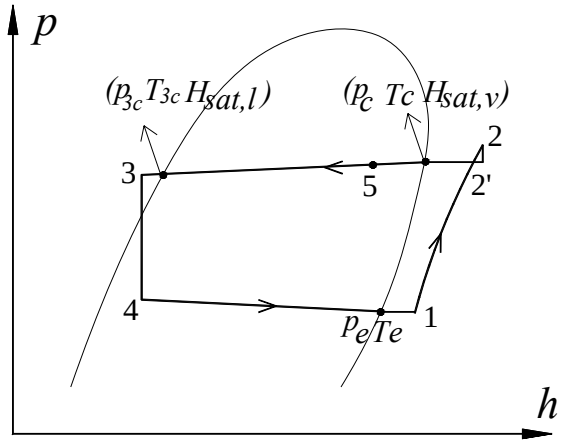

Figure 5.2 Pressure-enthalpy diagram of the refrigerant cycle

The basic working principle of the heat pump unit is illustrated in Figure 5.1 and the corresponding refrigerant cycle is also described in a pressure-enthalpy diagram, as shown in Figure 5.2. As can be seen from the two figures, the refrigerant cycle is represented by 5 state points. Point 1 means the compressor inlet state; Point 2 is the discharge state; Point $2'$ is the desuperheater inlet state; Point 5 is the condenser inlet (i.e. desuperheater outlet); Point 3 is the condenser outlet (i.e. expansion valve inlet) and Point 4 is the evaporator inlet.

5.3 Compressor Module

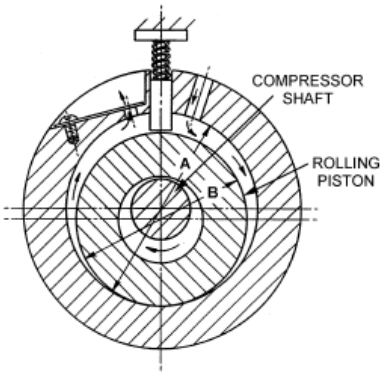

Figure 5.3 A rolling-piston rotary compressor

(From ASHRAE handbook 2000)

The working principle of the rolling piston compressor is illustrated in Figure 5.3. This type of compressor uses a roller mounted on an eccentric shaft to compress vapor refrigerant entering the compression chamber through the suction inlet. When the rolling piston is in contact with the top of the cylindrical housing, the high pressure and temperature gas is squeezed out through the discharge valve. The rolling-piston rotary compressor behaves a high volumetric efficiency because of its

small clearance volume and correspondingly low re-expansion losses inherent in the design. It is therefore widely used in air-conditioning units or smaller unitary hermetic heat pump.

The main objectives of the rolling piston compressor model are to provide predictions of the mass flow rate and of the electrical power of the compression process transferred to the refrigerant. The following assumptions are made:

- The compression and expansion in the compressor are assumed to be isentropic processes with constant isentropic exponents.
- The oil has negligible effects on refrigerant properties and compressor operations.
- The thermal properties of the refrigerant in the compressor are uniform at any time.

In accordance with the assumptions, the lumped-parameter method is employed in the compressor model.

Firstly, the general relationship between the refrigerant temperatures and pressures at the suction inlet and discharge outlet of the compressor is given as follows:

$$T_2 = T_1 \cdot \left(\frac{P_2}{P_1} \right)^{\frac{n-1}{n}} \tag{5.1}$$

where, T_1 and T_2 are the refrigerant suction and discharge temperatures; P_1 and P_2 are the refrigerant suction and discharge pressures; n is the polytropic exponent, which is set to be isentropic exponent in the model.

The refrigerant mass-flow rate which is critical for the performance of the compressor can be determined by:

$$\dot{m}_r = \lambda \frac{\dot{V}_{th}}{v_1} \tag{5.2}$$

where, $\dot{m}_r$ = refrigerant mass flow rate, kg/s;

$\dot{V}_{th}$ = theoretical displacement volumetric flow rate, m^3/s;

v_1 = specific volume at suction state (i.e. point *1*), m^3/kg.

λ = volumetric efficiency, which is given:

$$\lambda = \lambda_v \cdot \lambda_p \cdot \lambda_T \cdot \lambda_l \tag{5.3}$$

where，λ_v is the compressor volumetric coefficient, given by:

$$\lambda_v = 1 - c\left[\left(\frac{p_2}{p_1}\right)^{\frac{1}{m}} - 1\right] \tag{5.4}$$

c = clearance factor with the recommended value of 0.015 by the compressor manufacturer;

m = re-expansion exponent, which is assumed to be isentropic exponent;

λ_p = pressure loss coefficient with a value of approximately 1 due to the absence of the suction valve;

λ_T = temperature coefficient with a range of 0.82-0.95;

λ_l = leakage coefficient with a range of 0.98-0.92.

The theoretical work of the compressor in an isentropic process can be determined from:

$$W_{th} = \dot{m}_r \cdot \upsilon_1 \cdot p_e \cdot \frac{n}{n-1}\left[\left(\frac{p_c}{p_e}\right)^{\frac{n-1}{n}} - 1\right] \tag{5.5}$$

where, W_{th}= theoretical work, kW

p_c and p_e are the condensing and evaporation pressures, respectively.

The compressor power input can then be obtained when taking into account the various efficiencies:

$$Power = \frac{W_{th}}{\eta} = \frac{W_{th}}{\eta_i \cdot \eta_m \cdot \eta_{mo}} \tag{5.6}$$

where, η_i, η_m and η_{mo} are the indicated efficiency, mechanical efficiency and motor efficiency, respectively, and η_m=95% and η_{mo}=83.6% as provided by the compressor manufacturer. The indicated efficiency is given,

$$\eta_i = \frac{\lambda_T \lambda_l}{1 + \dfrac{1.5\left(\Delta p_{dis}\left(p_2 / P_1\right)^{1/n}\right)}{\left(h_2 - h_1\right)/\upsilon_1}} \tag{5.7}$$

The pressure drop across the discharge valve (kPa):

$$\Delta p_{dis} = 25\left(T_c^{-1.01} - 273.15\right)10^{-0.15\frac{P_2}{P_1}} \tag{5.8}$$

If the compressor inlet temperature (or the degree of superheating) and the condensing and evaporation temperatures (or pressures) are known, the refrigerant

mass flow rate and the power input together with the inlet and outlet refrigerant thermal properties can be determined by the aforementioned equations. The refrigerant thermodynamic parameters at the inlet and outlet of the compressor can be calculated by means of the Martin-Hou equation.

5.4 Evaporator Module

A great deal of research work on heat exchangers has been presented in the open literature during the past a few decades. The existing models generally fall into two broad categories: zone-based (i.e. lumped-parameter) and distributed-parameter models (Bensafi et al. 1997). The zone-based model divides a heat exchanger into several parts, depending on the number of the phases that the refrigerant exhibits throughout the heat exchanger (vapor, liquid and two-phase). Each zone is treated as a separate heat exchanger (Chi and Didion 1982). The zone-based models are hardly used to evaluate the detailed variations of the refrigerant along its flow direction because of their oversimplifying assumptions. On the other hand, the distributed-parameter model divides the heat exchanger into a great number of small elements each of which can be solved using local values of thermal properties and heat transfer coefficients. Although it is more rigorous and accurate compared with the zone-based method, the distributed-parameter method is extremely time-consuming.

Considering the advantages and disadvantages of the two methods, a zone-based distributed-parameter model is employed here to analyze the performance of the heat exchangers in the HGCHP system. In this model, the heat exchanger is first divided

into a few sections according to the number of refrigerant phases throughout the heat exchanger. Then, each section is further divided into several segments, each of which is treated as a small heat exchanger. Thus, this method can not only evaluate well the distribution characteristic of parameters along the heat exchanger but also shorten the computing time.

For simplicity, the following assumptions are incorporated into the simulation model.

- The heat transfer within the evaporator is assumed as a steady-state and one-dimensional process;
- The two streams are taken as counterflow in cooling mode, and parallel flow in heating mode.

Two possible heat transfer modes that the refrigerant can exhibit in the evaporator are considered here: forced convective boiling of the two-phase refrigerant and forced convection of the superheated refrigerant vapor which depends to a large extent on the amount of heat absorbed by the external fluid. Corresponding to the two heat transfer modes, the evaporator can be divided into two sections, i.e. two-phase and superheat sections. Then, the two-phase section can be subdivided into a number of small elements with assumed equal enthalpy change, while the superheat section is segregated into several elements with assumed equal temperature change. The lumped-parameter model and the log mean temperature difference (LMTD) are used to solve the heat transfer process in each element.

5.4.1 Energy balance

The energy balance between the refrigerant and water sides in each element can be described by the following equation with a coefficient of heat loss that accounts for the heat transferred from the evaporator to the environment.

$$\dot{m}_w c_p (t_{w1} - t_{w2}) = \xi_{evp} \dot{m}_r (h_{r2} - h_{r1}) \tag{5.9}$$

where,

m_w = water mass flow rate, kg/s;

c_p = water heat capacity, kJ/ (kg·K);

t_{w1} = inlet water temperature of an element, ℃;

t_{w2} = outlet water temperature of an element, ℃;

h_{r1} = inlet refrigerant enthalpy of an element, (kJ/kg);

h_{r2} = outlet refrigerant enthalpy of an element, (kJ/kg);

ξ_{evp} = coefficient of heat loss, which varies according to the evaporator configuration and the insulation, usually within a range of $0.8<\xi_{evp}<1$.

On the other hand, the heat transfer rate between the counter flows in a given element can be determined by:

$$Q = U \Delta t_m A \tag{5.10}$$

The log-mean temperature difference (LMTD) is defined as:

$$\Delta t_m = \frac{(t_{w,1} - t_{r,2}) - (t_{w,2} - t_{r,1})}{\ln\left(\frac{t_{w,1} - t_{r,2}}{t_{w,2} - t_{r,1}}\right)} \tag{5.11}$$

U is the overall heat transfer coefficient evaluated at the mean properties of the element, which incorporates the influences of the water-side and refrigerant-side heat transfer coefficients, and the tube thermal resistance. Equation (5.12) gives the expression of the overall heat transfer coefficient of each element based on the outside heat transfer area of the inner tube:

$$U = \frac{1}{\frac{1}{h_w} + \frac{d_o}{2k_p}\ln\left(\frac{d_o}{d_{in}}\right) + \frac{d_o}{h_r d_{in}}} \tag{5.12}$$

where,

h_r = refrigerant heat transfer coefficient, (W/m^{2}K).

h_w = water heat transfer coefficient, (W/m^{2}K).

k_p = pipe wall thermal conductivity, (W/m.K).

d_{in} = the inner diameter of the inner tube (m).

d_0 = the outer diameter of the inner tube (m).

The calculation procedures of the heat transfer coefficients of the water and refrigerant are presented in detail in the following section.

5.4.2 Heat transfer coefficients

5.4.2.1 Water heat transfer coefficient

The water flow in the evaporator is usually in the fully developed turbulent flow region with the single phase, which undertakes the forced convective heat transfer

process. Thus, the water heat transfer coefficient can be determined by Dittus-Boelter correlation (Incropera and DeWitt, 1990):

$$h_w = 0.023 Re_w^{0.8} Pr_w^{0.4} k_w / d_e \cdot \varepsilon_R \tag{5.13}$$

where, Re_w and Pr_w are the Reynolds and Prandlt numbers of the water respectively;

k_w = water thermal conductivity, W/(m·K);

ε_R = correction factor for the tube rows;

d_e = equivalent diameter of the annular region (m).

5.4.2.2 Heat transfer coefficient of superheated refrigerant vapor

In the superheated refrigerant vapor region, the heat transfer is dominated by the forced convective mechanism, which can also be approximately evaluated by Dittus-Boelter correlation.

$$h_r = 0.023 Re_r^{0.8} Pr_r^{0.4} k_r / d_{in} \cdot \varepsilon_R \tag{5.14}$$

where,

k_r = thermal conductivity of the refrigerant, W/(m·K).

Re_r and Pr_r are the Reynolds and Prandlt numbers of the refrigerant respectively.

5.4.2.3 Boiling heat transfer coefficient of two-phase refrigerant

The heat transfer in the flow boiling area has been studied for decades. There are over 30 saturated flow boiling correlations available in the literature. In general, the flow boiling correlations can be classified into two categories. Under the first

category, the correlations are developed by experimental investigators to represent their own data. After ascertaining the accuracy of the experiments conducted, these individual correlations may be used within the same range of parameters. The correlations under the second category are developed based on a larger number of data sets involving a number of fluids over a wide range of parameters. A general correlation proposed by Kandlikar (1990) is used in the present work. The Kandlikar's correlation can be widely used in a number of refrigerants, e.g. water, R11, R12, R22, R113, and R114, by incorporating a fluid-dependent parameter F_{fl}. The general correlation is expressed as a sum of the convective and nucleate boiling terms.

$$h_r = \left(C_1 (Co)^{C_2} \left(25 Fr_{lo}\right)^{C_5} + C_3 (Bo)^{C_4} F_{fl}\right) h_l \tag{5.15}$$

where,

h_l = single-phase liquid-only heat transfer coefficient;

Co = refrigerant convection number;

Bo = refrigerant boiling number

Fr_{lo} = Froude number with all flow as liquid

F_{fl} = fluid-dependent parameter

The detailed calculation procedure along with the values of constants ($C_1 \sim C_5$) can be found in the references (Kandlikar 1990; 1983).

5.4.3 Heat transfer area

The heat transfer area of a certain element *i* under the given condition can be calculated from the energy balance in the element as follows:

$$A_i = \frac{m_r(h_{r2} - h_{r1})}{U\Delta t_m} \tag{5.16}$$

Thus, the total calculated area of the evaporator is a sum of areas of all the elements.

$$A_{evp,cal} = \sum A_i \tag{5.17}$$

5.4.4 Pressure drop prediction

To simplify the simulation procedure, the pressure drops in all single-phase regions are negligible owing to their relatively small sizes compared with the two-phase regions.

The overall pressure drop for a one-dimensional two-phase flow in tubes consists of friction, change in momentum, and gravitational components (ASHRAE, 2005).

$$\frac{dP}{dz} = \left(\frac{dP}{dz}\right)_f + \left(\frac{dP}{dz}\right)_m + \left(\frac{dP}{dz}\right)_g \tag{5.18}$$

where z is the coordinate in the flow direction. The gravitational component is set to be zero in this analysis because of the horizontal tubes. The momentum pressure drop accounts for the acceleration of the flow usually caused by evaporation of liquid or condensation of vapor. In this case, it can be calculated with the conservation of momentum and its expression is given by:

$$\left(\frac{dP}{dz}\right)_m = G^2\left\{\left[\frac{(1-x)^2}{\rho_l(1-\varepsilon_v)} + \frac{x^2}{\rho_v\varepsilon_v}\right]_{in} - \left[\frac{(1-x)^2}{\rho_l(1-\varepsilon_v)} + \frac{x^2}{\rho_v\varepsilon_v}\right]_{out}\right\} \tag{5.19}$$

where G is total mass velocity; *in* and *out* represent the inlet and outlet of the element; ρ is the refrigerant density; ε_v is the void fraction which will be discussed in section 5.7.

A number of empirical correlations for computing frictional pressure drop in two-phase internal flow have been formulated based on the single-phase model. Among them, a Muller-steinhagen and Heck correlation (1986) is recommended due to the more accuracy and wide range of applications.

$$\left(\frac{dP}{dz}\right)_f = \left\{\left(\frac{dP}{dz}\right)_{lo} + 2\left[\left(\frac{dP}{dz}\right)_{vo} - \left(\frac{dP}{dz}\right)_{lo}\right]x\right\}\cdot(1-x)^{1/3} + \left(\frac{dP}{dz}\right)_{lo} x^3 \tag{5.20}$$

where $\left(\frac{dP}{dz}\right)_{lo} = f_l \frac{2G^2}{d_{in}\rho_l}$ and $\left(\frac{dP}{dz}\right)_{vo} = f_v \frac{2G^2}{d_{in}\rho_v}$

f_l is the friction factor of liquid refrigerant and f_v is the friction factor of vapor.

5.4.5 Simulation algorithm

In the modeling procedure, the following parameters should be given first: evaporator configuration, water inlet temperature and mass flow rate, the inlet state of the refrigerant and the refrigerant mass flow rate. Based on the aforementioned equations, an iterative method is established here to determine the outlet states of the water and refrigerant together with the refrigerant mass in the evaporator for the given operating conditions.

The constraint condition of the model is that the calculated heat transfer area of the evaporator should equal the actual physical area. The detailed procedures in the simulation model are summarized as follows.

1) Input the inlet variables in both the water and refrigerant sides and assume the refrigerant outlet enthalpy (or the degree of the superheat) and evaporation pressure drop.

2) Determine the two-phase and superheat regions respectively and divide them into a number of small elements.

3) Calculate the intermediate and outlet temperatures of the water and refrigerant using the principle of energy balance (Equation 5.9).

4) Determine the log-mean temperature difference and the overall heat transfer coefficient (Equations 5.11-5.15).

5) Calculate the required heat transfer area corresponding to the heat transfer rate in each element (Equations 5.16 and 5.17).

6) Evaluate the total pressure drop of the refrigerant in the two-phase section (Equation 5.18-5.20);

7) Resume the model with an updated guess of the pressure drop until the difference between the calculated and guessed values is within the allowable error.

8) Determine the total required heat transfer area of the evaporator by adding up the heat transfer areas of all the elements (Equation 5.17).

9) Update the guess of refrigerant outlet enthalpy and repeat steps 1-8 until the calculated area converges to the actual area within an allowable error tolerance.

10) Calculate the total mass of the refrigerant in the evaporator.

Figure 5.4 shows the basic flow chart of the evaporator module.

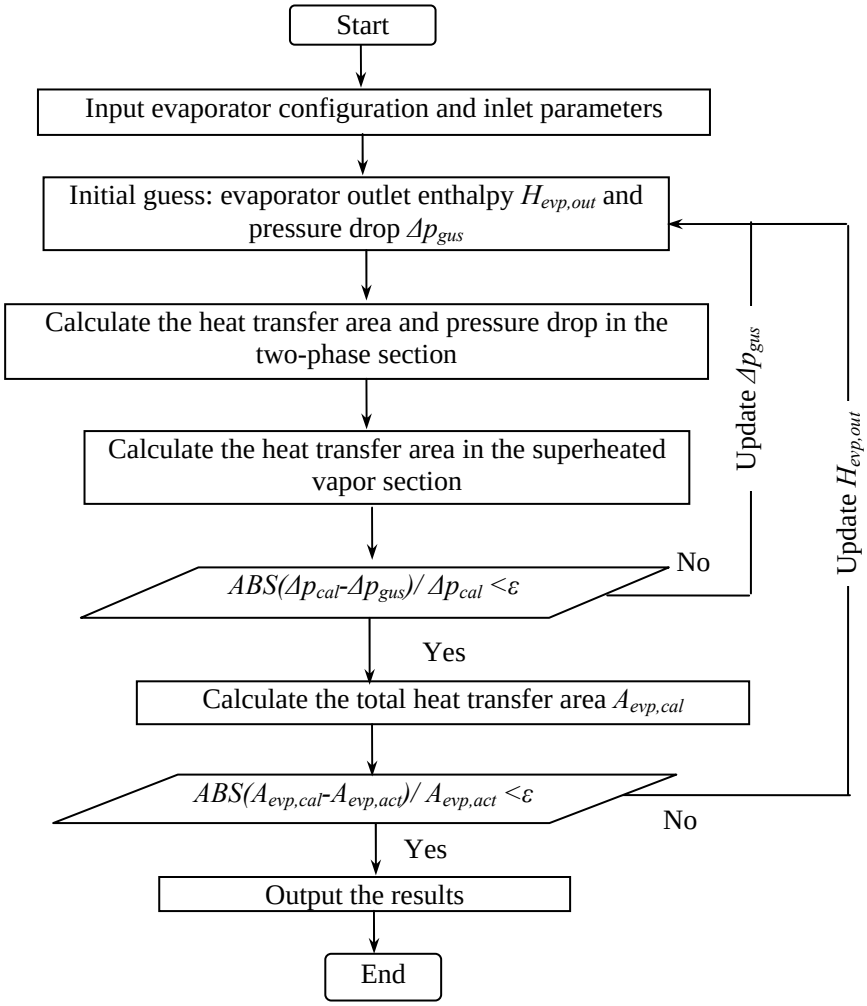

Figure 5.4 Flow chart of the evaporator module

5.5 Desuperheater Module

The desuperheater and condenser can actually be considered as two similar heat exchangers connected in series from the viewpoint of the refrigerant cycle. The

purpose of the desuperheater in the heat pump is to recover the heat at temperatures substantially above the condensing temperature (superheated vapor) and then to reduce the heat rate released into the ground through the condenser. In some actual operating conditions, the desuperheater may contribute both the cooling of the superheated vapor and part condensing of the saturated refrigerant. Accordingly, the refrigerant in the desuperaheater may have two states (superheat and two-phase) or one state (superheat) depending on its outlet enthalpy. The steady-state zone-based distributed-parameter method together with the LMTD method used in the evaporator is also employed in the models of the desuperheater and condenser.

5.5.1 Heat transfer coefficients

The heat transfer coefficients in the water side and in the superheated vapor in the desuperheater have the same characteristics and formulas as those in the evaporator. For the condensation heat transfer coefficient, an empirical correlation is given by Wu (1997):

$$h_r = 0.725 B_r d_{in}^{-0.25} (T_c - T_{wo})^{-0.25} \tag{5.21}$$

where， B_r is the integrated refrigerant thermophysical property related to the condensing temperature T_c. T_{wo} is the inner tube wall temperature, which can be obtained using the *Newton* iteration method.

5.5.2 Simulation algorithm

In general, the simulation model of the desuperheater is quite similar to that of the evaporator. Similarly, the desuperheater is divided into one or two heat transfer

sections connected in series that correspond to the different phases of the refrigerant. Each section is subdivided into several elements of assumed equal enthalpy change or equal temperature change.

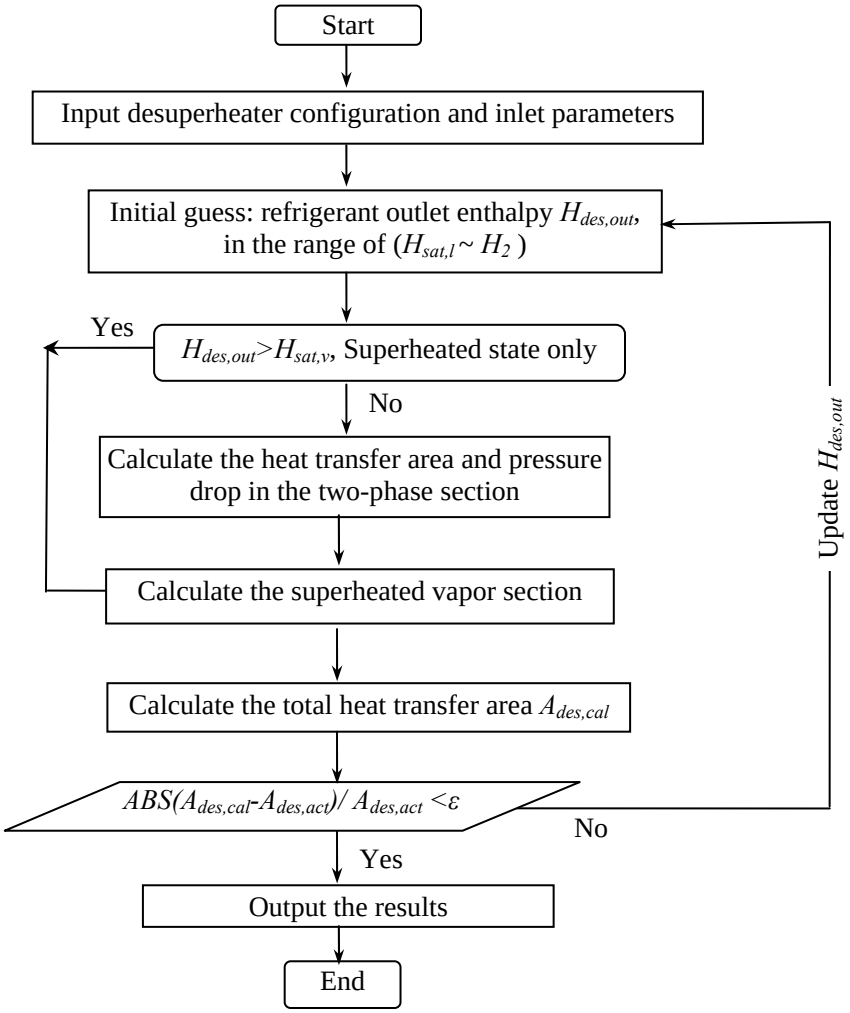

Figure 5.5 Flow chart of the desuperheater module

The simulation model begins with an assumption of the outlet enthalpy of the refrigerant leaving the desuperheater. Then, the heat transfer area can be estimated using the formulas and given parameters. Finally, based on an iteration procedure, an appropriate value of the refrigerant enthalpy will be found, which satisfies the

constraint condition that the error between the calculated and actual heat transfer areas is within the prespecified error. The simulation flow chart is shown in Figure 5.5.

5.6 Condenser Module

In actual operation conditions, three possible heat transfer modes of the refrigerant may occur in the condenser depending on the outlet enthalpy of the refrigerant leaving the desuperheater and the external fluid. They are the forced convection of the superheated vapor, force-convective condensation of the two-phase refrigerant and forced convection of the subcooled liquid.

The heat transfer coefficients associated with the condensation and superheat in the elements can be estimated using the correlations employed in the desuperheater. For the subcooled section, the heat transfer coefficient is calculated in the same way as that used in superheated refrigerant vapor because of the identical single-phase characteristics of the subcooled and superheated refrigerants.

The flow chart of the simulation model is depicted in Figure 5.6.

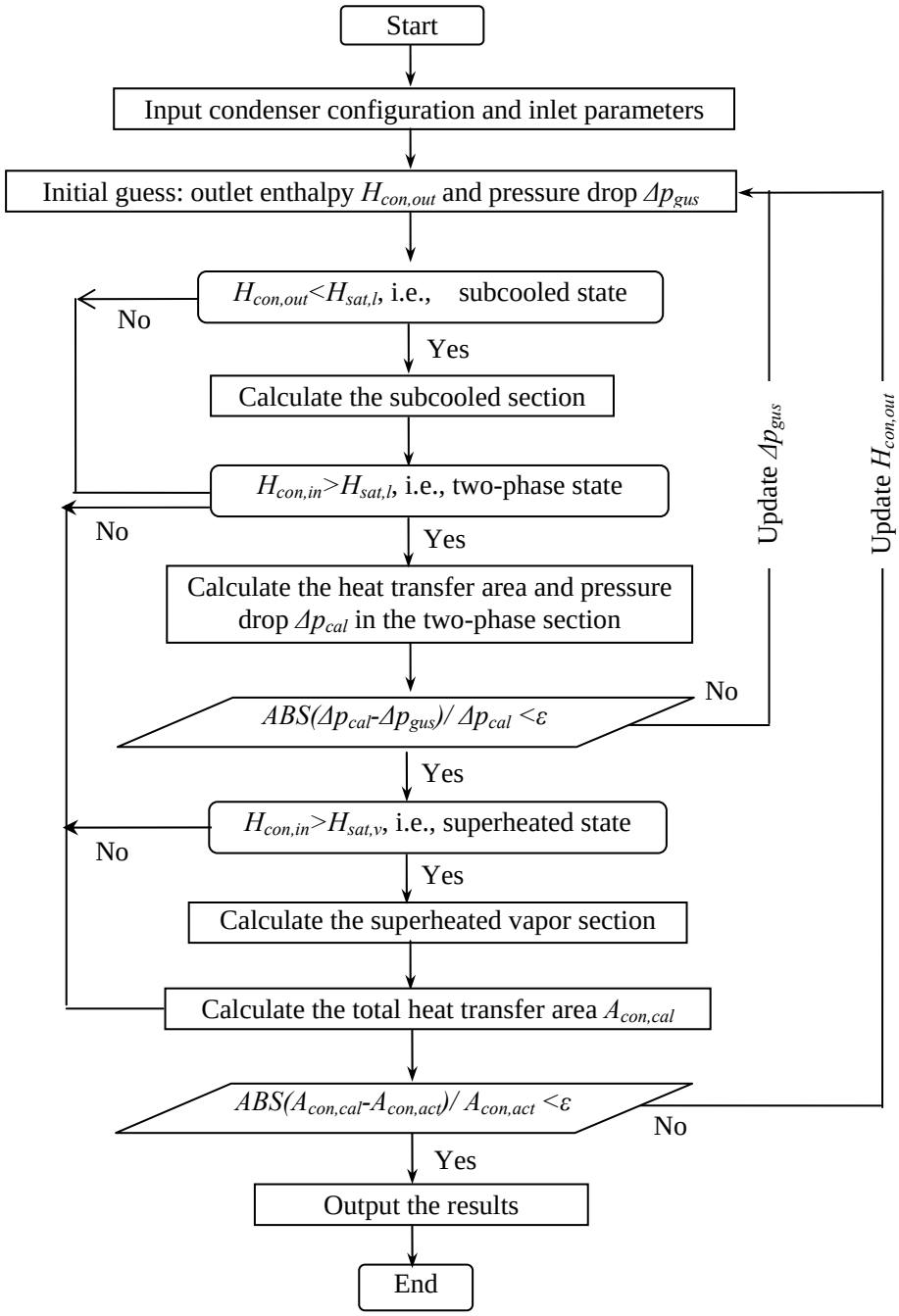

Figure 5.6 Flow chart of the condenser module

5.7 Expansion Valve

This research project employed a thermostatic expansion valve (TEV) which is used to meter the flow of liquid refrigerant entering the evaporator at a rate that matches the amount of refrigerant being boiled off in the evaporator. Like all the other metering devices it also provides a pressure drop in the system, separating the high pressure side of the system from the low pressure side, thus allowing low pressure refrigerant to absorb heat. To simplify the TEV simulation model, a constant degree of superheat and the refrigerant mass flow rate obtained in the compressor are directly used in the simulation model. The thermal process in the expansion device is assumed to be adiabatic, and, therefore, it is isenthalpic from the first law of thermodynamics:

$$H_3=H_4 \tag{5.22}$$

5.8 Modeling of the HGCHP Unit

5.8.1 System energy balance

For the refrigerant system under study, according to the first-law thermodynamic, the amount of energy absorbed by the refrigerant in the evaporator and compressor theoretically equals the energy released from the refrigerant in the condenser and the desuperheater. Based on this theory, the energy balance can be given as follows：

$$Q_{dsp}+Q_{con}= Q_{evp}+Power \tag{5.23}$$

In cooling with DHW mode, an alternative expression of the COP is given by taking into account the free production of hot water in the desuperheater.

$$COP_{cool} = \frac{Q_{evp} + Q_{dsp}}{Power} \tag{5.24}$$

Similarly, in heating mode, it can be rewritten as follows:

$$COP_{heat} = \frac{Q_{dsp} + Q_{con}}{Power} \tag{5.25}$$

where, Q_{dsp} is the heat absorbed by the hot water in the desuperheater; Q_{con} is the heat released into the condenser; Q_{evp} is the heat absorbed in the evaporator and *Power* is the compressor power input.

5.8.2 System refrigerant mass balance

The principle of mass conservation states that the amount of the refrigerant in the system is always maintained constant for all operating conditions. For simplicity, the refrigerant mass in the compressor is negligible due to its relatively low density. Hence, the refrigerant charge in the system is distributed within the evaporator, condenser, desuperheater and the connecting tubes. The system refrigerant mass balance is described by the following equation.

$$M_{char} = M_{con} + M_{evp} + M_{des} + M_{line} \tag{5.26}$$

The following subsections present the detailed calculation procedure of the refrigerant mass with different phases.

5.8.2.1 Single-phase refrigerant mass

The mass of the single-phase refrigerant can be conveniently determined by the mean density and internal volume.

For the subcooled liquid: $$M_{sc} = \int_0^{L_{sc}} A \ \rho_l dx \tag{5.27}$$

For the superheated vapor: $M_{sh} = \int_0^{L_{Ssh}} A\,\rho_v dx$ (5.28)

where，M is the refrigerant mass, kg; L is the length of the section, m; ρ is the refrigerant density, kg/m^3; the subscripts of *sc* and *sh* denote the subcooling and superheating sections, respectively.

5.8.2.2 Two-phase refrigerant mass

For the two-phase flow region, mean density is evaluated by the saturated liquid density, saturated vapor density, and the void fraction which is defined as the ratio of the cross-sectional area occupied by vapor to the total cross-sectional area.

The X_{tt},-correlated model is used to calculate the void fraction, which was developed by Wallis (1969) and refined by Domanski and Didion (1983) for X_{tt} >10. The equations are:

$$\begin{cases} \varepsilon_v = (1+X_{tt}^{0.8})^{-0.378} & (X_{tt} \le 10) \\ \varepsilon_v = 0.823 - 0.157 \ln X_{tt} & (X_{tt} > 10) \end{cases} \quad (5.29)$$

X_{tt} is the square root ratio of the liquid-only pressure gradient to the vapor-only pressure gradient, which is employed the Lockhart-Martinelli correlation (1949).

$$X_{tt} = \left(\frac{1-x}{x}\right)^{0.9} \left(\frac{\rho_v}{\rho_l}\right)^{0.5} \left(\frac{\mu_l}{\mu_v}\right)^{0.1} \quad (5.30)$$

Based on the definition of the void fraction, the two-phase refrigerant mass can be consequently determined using the following equation,

$$M_{tp} = \int_0^{L_{tp}} A\,[(1-\varepsilon_v)\rho_l + \varepsilon_v \rho_v]\,dx \tag{5.31}$$

where, M_{tp} is the two-phase refrigerant mass, kg; L_{tp} is the length of the two-phase section, m.

5.8.3 Simulation algorithm

The main purpose of the simulation model of the HGCHP unit is to determine the operating performance, refrigerant states and water outlet properties which are corresponding to pre-specified operating conditions. For a specified condition, there is only one refrigerant state against one water state at any location within the system. This unique set of refrigerant state and flow conditions can be sought by a HGCHP simulation program using the iteration method.

It is well known that the thermodynamic cycle of the heat pump is a closed loop, which makes it convenient to incorporate the component modules into an overall systematic model by means of the pressure balance, energy balance and mass balance.

The systematic model consists of four main iterative convergence loops: evaporator, desuperheater, condenser and mass inventory loops. The iterative convergence loops begin with the initial guesses of the unknown variables which will finally converge to the true values through the iterative process. There are a total of six variables to be solved, by which the unique refrigerant state at any point can be determined. They are:

1) The evaporation pressure drop Δp_{evp};

2) The evaporation temperature T_e at saturated vapor line (solved by evaporator loop);

3) The condensing pressure drop in the condenser and/or desuperheater Δp_{con} and/or Δp_{dsp}.

4) The refrigerant outlet enthalpy from the desuperheater $H_{dsp,out}$ (solved by desuperheater loop);

5) Condensing temperature T_c at saturated vapor line (solved by condenser loop);

6) The inlet refrigerant quality to the evaporator X (solved by the mass inventory loop)

It is worth noticing that the exact pressure drops in the evaporation and condensing sections can be finally sought once the convergences of the calculated values are achieved through the iterative method in the evaporator, condenser and/or desuperheater models.

The simulation model, consisting of four iterative convergence loops, is summarized below.

1) Input the inlet parameters of the external fluid (water), the refrigerant charge (M_{act}) and the structure parameters of each component.

2) Specify a convergence error tolerance and the initial guesses of the six unknown variables: Δp_{evp}, Δp_{con}, T_e, $H_{dsp,out}$, T_c, and X.

3) Use compressor and expansion valve models to determine the refrigerant properties at states 1~5 and the refrigerant mass flow rate along with the

compressor power input.

4) Run the evaporator module to calculate the evaporator heat transfer area ($A_{evp,cal}$) and Δp_{evp}. Compare the calculated pressure drop with the guessed value to check whether they are converged; if not, repeat steps 3 and 4 with a new guessed pressure drop.

   If the calculated area is within the error tolerance of the actual area of the evaporator ($A_{evp,act}$), go to next step. Otherwise, update the guess of T_e based on the error and repeat steps 3 and 4 until $A_{evp,cal}$ converges to $A_{evp,act}$ within the error tolerance.

5) Run the desuperheater module to calculate the heat transfer area ($A_{dsp,cal}$) and Δp_{dsp} (if possible). Adjust $H_{dsp,out}$ and repeat step 5 until the relative error between the calculated area A_w and the actual area $A_{dsp,act}$ is less than the error tolerance.

6) Run the condenser module to calculate the condenser area ($A_{con,cal}$) and the total condensing pressure drop Δp_{con} including the possible pressure drop in the desuperheater. Compare the calculated pressure drop with the guessed value to check whether they are converged; if not, go to step 3 to resume the computation with an updated pressure drop.

   Reset T_c, and go back to step 3 until the calculated area approaches the actual area $A_{con,act}$ within the allowable error.

7) Calculate the refrigerant mass in the heat pump (M_{char}). Adjust X and go to step 3 until the error between the calculated mass and the actual mass of

refrigerant (M_{act}) is within the specified error tolerance. This is the outermost convergence loop of the simulation algorithm.

8) Calculate the heat transfer rates and the coefficient of performance (*COP*) of the heat pump.

The flow chart of the computing procedure for the model implementation is described in Figure 5.7.

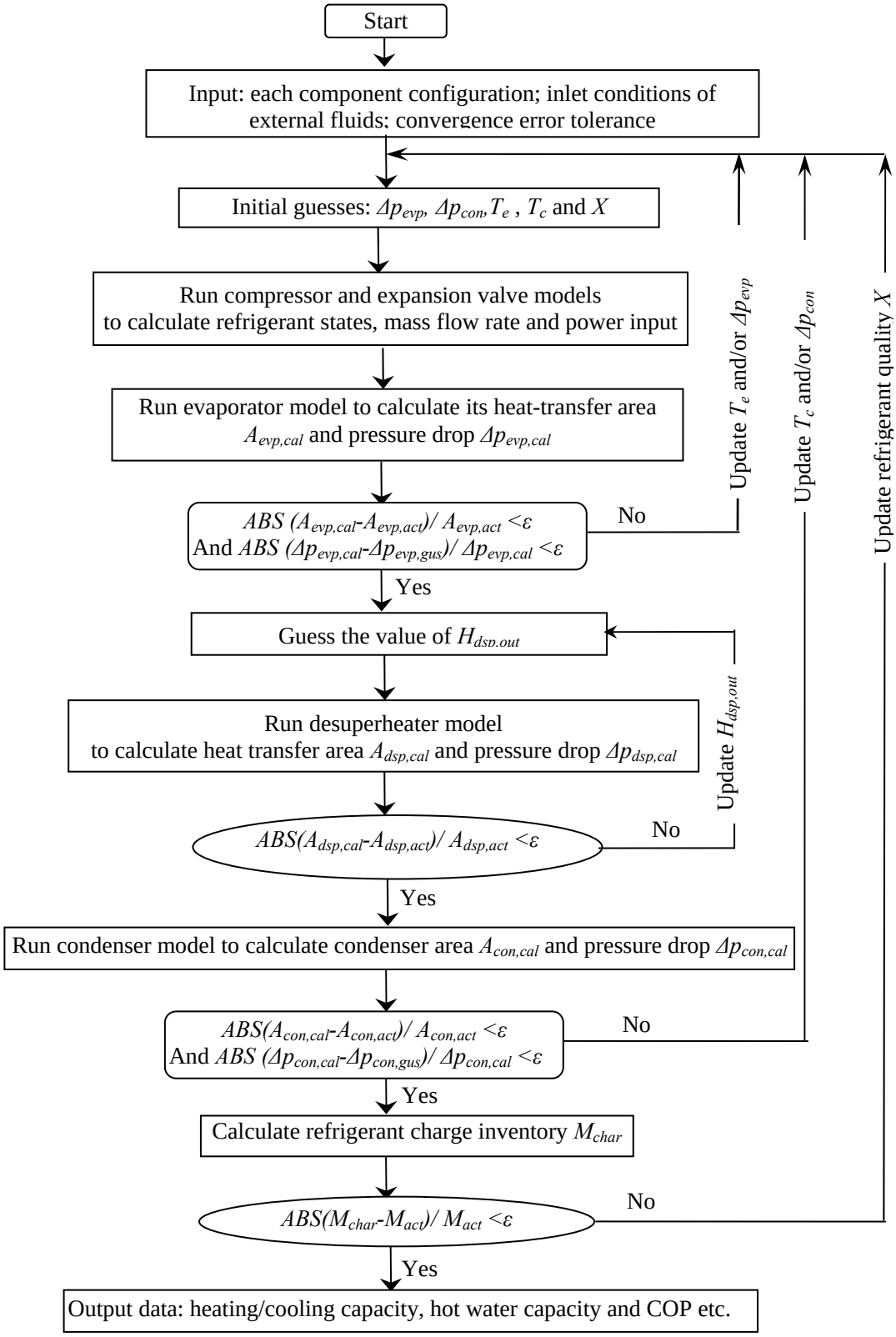

Figure 5.7 Flow chart of the computation procedure for the model implementation

5.9 Implementation of the Simulation Program of the HGCHP System

In accordance with the aforementioned work in chapters 3 and 4, the simulation models of the GHEs can determine the values of *EWT* and *ExWT* if the GHE loads are given. In reverse, the GHE loads can only be obtained from the simulation model of the HGCHP unit with the knowledge of *EWT*s. Based on the unique relationship between the GHE load and *EWT*, the GHE and HGCHP models can be coupled together to systematically estimate the performances of both the GHE and heat pump under specified operating conditions. The main program codes of the systemic model are listed in Appendix. The basic procedure of the simulation algorithm of the systematic model is shown in Figure 5.8.

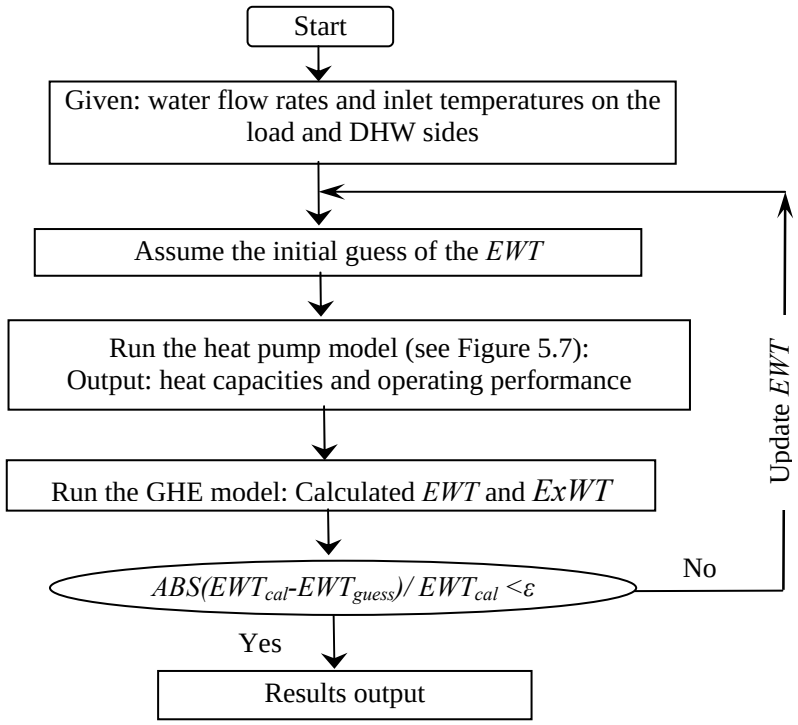

Figure 5.8 Flow chart of the simulation model of the HGCHP system

In this research, the comprehensive simulation algorithm has been written using *FORTRAN* language owing to its distinct advantage of the high speed of scientific computing over other compiling languages. To conveniently set the various parameters or different configurations of the individual components, a program with a friendly interface and visual graph has been developed under the *Delphi* Environment. In the visual interface, all the geometry parameters and inlet conditions can be set up in dialog boxes which can be popped up by clicking the component icons, as shown in Figure 5.9. When all the required parameters are set up, the pre-compiled program using *FORTRAN* will begin to simulate under the specific conditions just by clicking the "Simulate" icon.

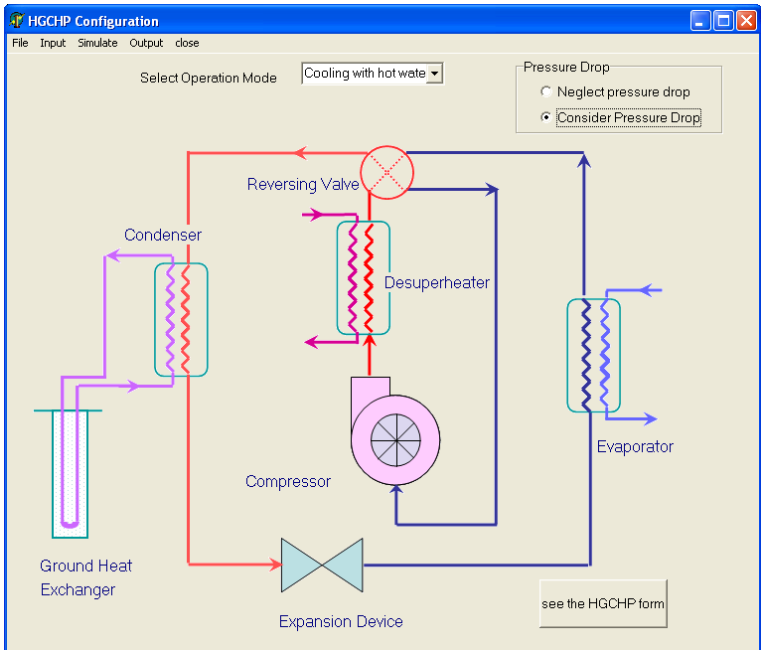

Figure 5.9 Interface of the simulation program

5.10 Discussion of the Simulation Results

Based on the simulation model developed in preceding sections, the system performance under various operation modes are analyzed in this section. It should be noticed that the heating only mode will not be discussed here in view of the following two factors: 1) both the operating principle and the performance of the heating mode are generally similar to those of the DHW heating mode; 2) the possibility of operating the heating only mode is quite little in cooling-dominated buildings in southern China. Thus, this section mainly discusses four operation modes, i.e. cooling only, cooling with DHW, heating with DHW, and DHW heating modes.

The pilot project of the HGCHP system which is presented in Chapter 6 is selected to be the basic case for a variety of simulations. The basic parameters in the simulation model including the refrigerant type (R22), refrigerant charge, and the component geometries, can be found in Table 6.1. Although a number of variables may affect the system performance in the four cases of operation modes, the inlet DHW temperature to the desuperheater ($T_{dsp,\ in}$), EWT, and the heat transfer area ratio of the desuperheater to the condenser cause more significant effects on the system performance over other parameters. The following discussion is therefore focused on the three critical variables.

Prior to analyzing the system performance, a set of parameters are defined as the benchmark, as shown in Table 5.1.

Table 5.1 Benchmark parameters of the HGCHP System

Parameter	Value
The water mass flow rate in evaporator:	m_{evp}=0.93 m^3/h
The water mass flow rate in desuperheater:	m_{dsp}=0.93 m^3/h
The water mass flow rate in condenser:	m_{con}=1.01m^3/h
Heat transfer area ratio of the desuperheater to the condenser:	A_{dsp}/A_{con}=0.7
Chilled water return temperature:	$T_{evp,1}$=12˚C
Ground temperature:	22 ˚C

5.10.1 Comparisons of the cooling only and cooling with DHW modes

With the known parameters that are defined as Table 5.1 and the pre-specified $T_{dsp,in}$ ranging from 25˚C to 50˚C, the cooling with DHW heating mode was continuously simulated for nearly 9 hours. On the other hand, the simulation for the cooling only mode was also made during the same period for comparison.

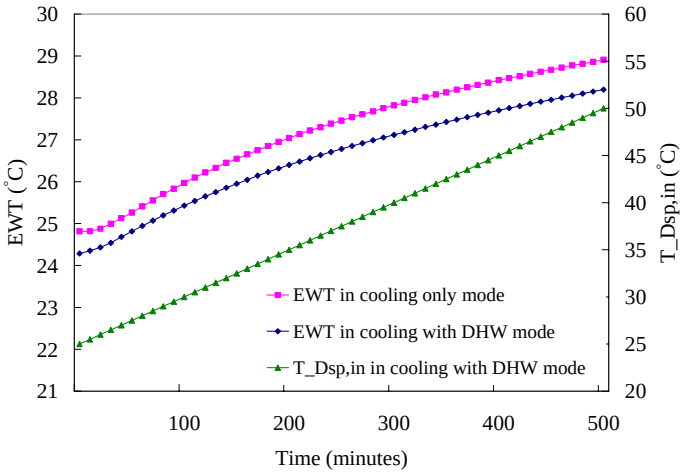

Figure 5.10 Variations of *EWT* and $T_{dsp,\,in}$ with time under different operation modes

Figure 5.10 compares the variations of *EWT* under the cooling with DHW and cooling only modes, respectively. As expected, the *EWT* in the cooling with DHW mode was distinctly lower than that in cooling only mode, resulting in a reduction of anywhere between 0.5˚C to 1˚C during the nine-hour simulation. This is due to the partly shift of condensation heat from the GHE to the desuperheater. The less heat rejection into the ground can greatly improve the heat transfer performance in the GHE, which correspondingly leads to a high operating performance of the system.

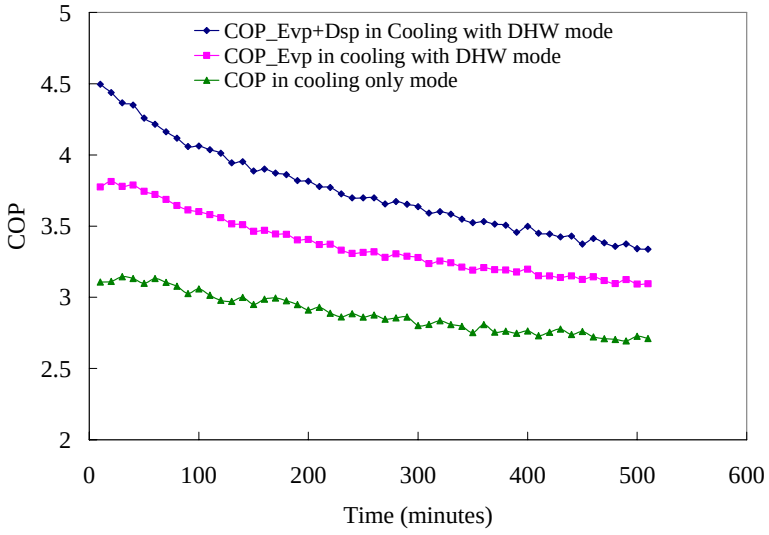

Figure 5.11 Comparisons of *COP* in different operation modes

The variations of the COP for the two cooling modes are illustrated in Figure 5.11. The $COP_{Evp+Dsp}$ that is defined in Equation 5.24 is used to evaluate the overall performance of the HGCHP system, which takes the heat gain of the DHW into account, while COP_{Evp} is the conventional expression, which is the ratio of the cooling capacity to the compressor power input. It can be found that, even neglecting the heat gain of the DHW, the cooling with DHW mode still contributed a large energy saving of 7~16% as compared with the cooling only mode. When

considering the useful output of the DHW, the cooling with DHW mode offered more substantial savings, resulting in approximately 23-40% over the cooling only mode in the case study.

5.10.2 Cooling with DHW heating mode

For the HGCHP system, the heat transfer area of the desuperheater and the DHW inlet temperature ($T_{dsp,in}$) are significantly critical for the system performance, especially under the condition of the cooling with DHW heating. In this section, the effects of the $T_{dsp,in}$ and the heat transfer area ratio of the desuperheater to condenser (A_{dsp}/A_{con}) on the system performance are discussed.

Figure 5.12 shows the variations of the desuperheater heat-transfer percentage of the total condensation heat (Q_{dsp}/Q_{con}) against $T_{dsp,in}$ and A_{dsp}/A_{con}. The corresponding variations of *EWT* and *COP* are illustrated in Figure 5.13 and Figure 5.14, respectively.

In general, as observed in Figures 5.12 and 5.13, the heat transfer rate of the desuperheater was effectively enhanced with the increase of its heat transfer area, which correspondingly reduced the heat rejection into the ground, resulting in lower *EWT*s. For the design condition of A_{dsp}/A_{con}=0.7, the desuperheater can capture 10 to 27 percent of the total condensation heat whereas the *COP* varied from 4.6 to 3.9 over the range of $T_{dsp,in}$ = 25˚C ~40˚C.

It can be found from Figure 5.14 that, for the cases with lower $T_{dsp,in}$ (e.g. 25˚C or 30˚C, which is comparable to *EWT*s), the *COP* consistently rose with the increase of the area ratio A_{dsp}/A_{con}. On the contrary, for the higher DHW temperatures (e.g. 35

˚C or 40˚C, which is much higher than *EWT*s), the *COP* was slightly increased at the beginning of the simulation and then gradually reduced at certain point with the increase of desuperheater size. This is attributed to the fact that the higher DHW temperature in the larger desuperheater may cause a much higher condensing temperature which considerably increases the compressor power consumption.

The analysis of the *COP* demonstrates that only increasing the desuperheater size may enhance or, reversely, deteriorate the operating performance which primarily depends on the inlet water temperature of the desuperheater. Actually, an optimum size of the desuperheater should be determined by several related factors, such as the building loads, the heat pump performance and the DHW demands. The results indicate that the HGCHP system can offer a maximum operating performance under the circumstance of using the desuperheater only to preheat the DHW at a relatively lower temperature.

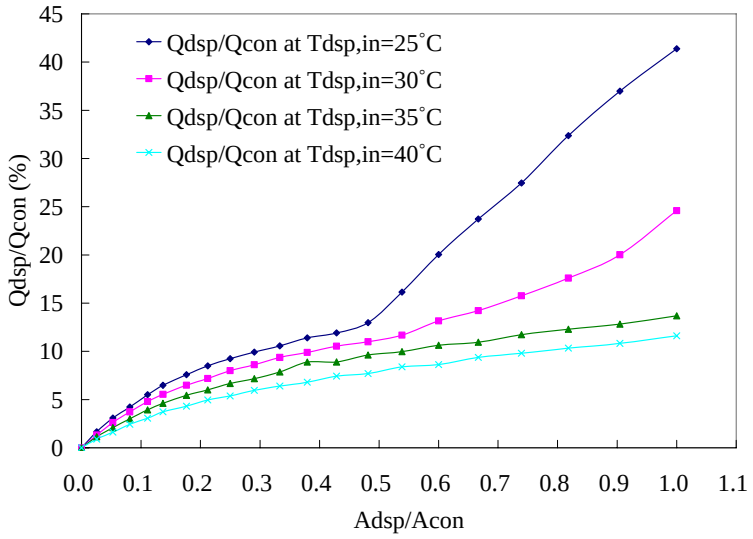

Figure 5.12 Variations of the heat rate ratio Q_{dsp}/Q_{con} against $T_{dsp,in}$ and A_{dsp}/A_{con} (cooling with DHW mode)

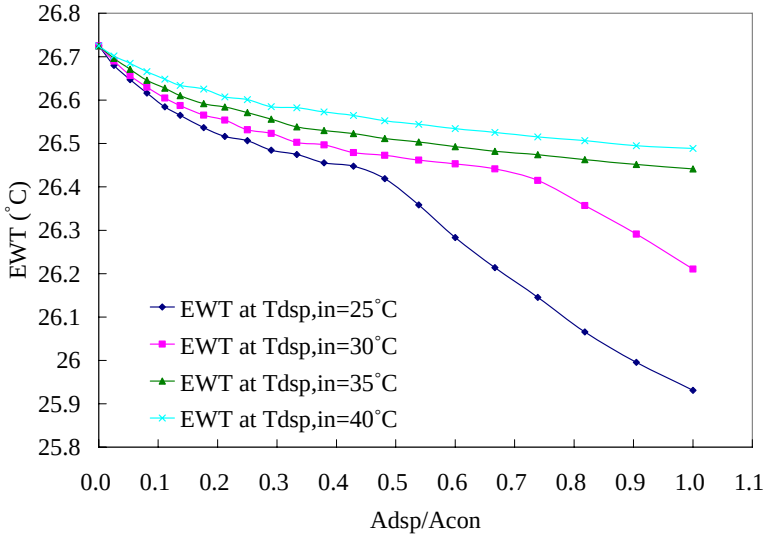

Figure 5.13 Variations of *EWT* against $T_{dsp,in}$ and A_{dsp}/A_{con} (cooling with DHW mode)

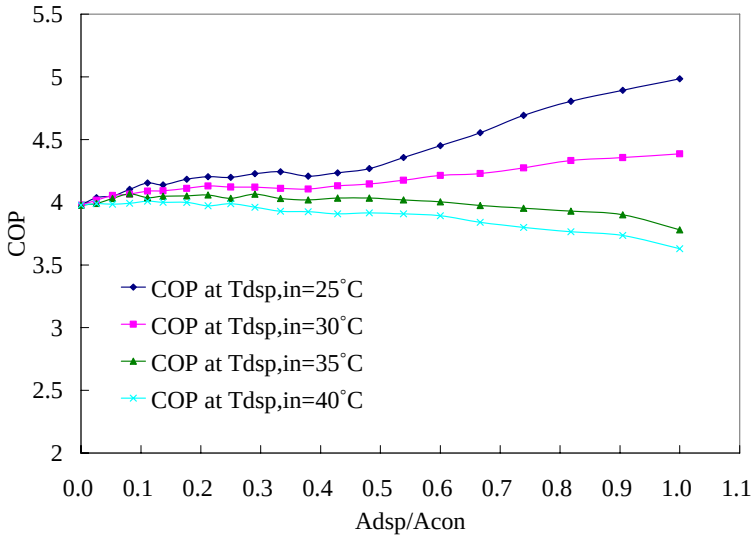

Figure 5.14 Variations of *COP* against $T_{dsp,in}$ and A_{dsp}/A_{con} (cooling with DHW mode)

5.10.3 Heating with DHW heating mode

The system operating performance of the heating with DHW mode is discussed under the conditions of $T_{con,\ in}$=45˚C and $T_{dsp,in}$=20˚C ~45˚C. The detailed simulation results are presented in Figures 5.15-5.16.

Figure 5.15 illustrates the variations of the heat transfer rates in the condenser, desuperheater and evaporator (connected with the GHE in this case) with $T_{dsp,in}$. The heat transfer rate in the desuperheater was significantly reduced as the $T_{dsp,in}$ rose, owing to the gradual decrease of the temperature difference between the DHW and refrigerant. Correspondingly, a greater heat-transfer rate in the condenser was observed with the increase of $T_{dsp,in}$. In general, the heat transfer rate in the desuperheater accounted for a significant percentage of the total heat transfer of condensation, approximately within a range of 15~50% in the simulation case.

As is shown in Figure 5.16, the power consumption of the compressor was increased from 1.55kW to 1.82kW, while the *COP* was decreased from 3.8 to 2.8 when the $T_{dsp,in}$ was heated from 20˚C to 45˚C.

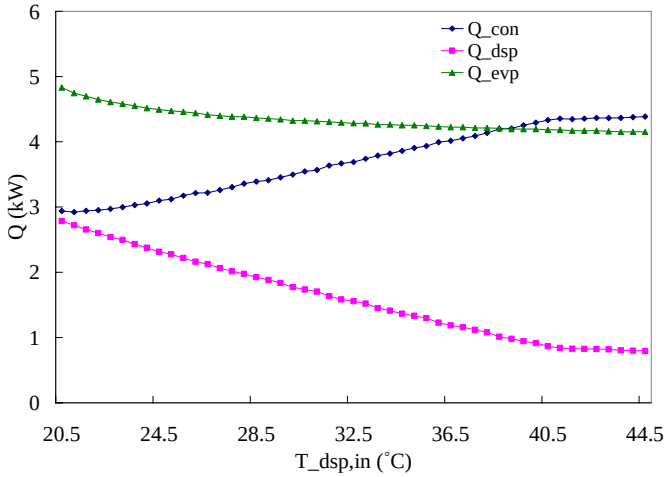

Figure 5.15 Variations of heat transfer rates vs. $T_{dsp,in}$ (heating with DHW mode)

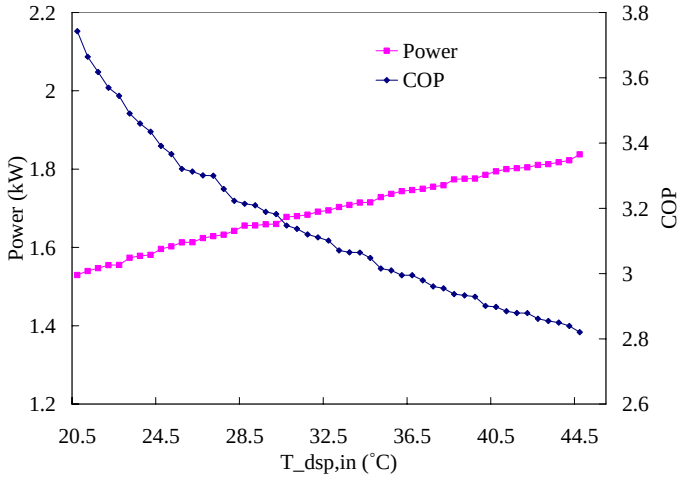

Figure 5.16 Variations of *COP* and *Power* vs. $T_{dsp,in}$ (heating with DHW mode)

5.10.4 DHW heating mode

Basically, the DHW heating mode exhibits the similar operating characteristics, related to the system performance and the GHE heat transfer, as the heating with DHW mode. The only difference between them is that the condenser in the DHW heating mode is used to preheat DHW instead of providing space heating. In this section, the HGCHP system was simulated under the condition of $T_{dsp,in}$ =16˚C ~47˚C in the DHW heating mode.

It can be seen from Figure 5.17 that the *COP* reached a maximum value of about 6 when $T_{dsp,in}$=16˚C at the beginning of the simulation. The average *COP* was nearly 4.0 under a wide range of $T_{dsp,in}$ (16˚C ~47˚C), which indicates a much higher performance than the conventional DHW heating systems.

To investigate closely the pressure losses in the heat pump unit and their impacts for the system, parts of the simulated refrigerant properties mainly related to the temperature and pressure are listed in Table 5.2, along with the relative inlet water temperature of the desuperheater. The meanings of the notations in Table 5.2 are corresponding to those in Figure 5.2.

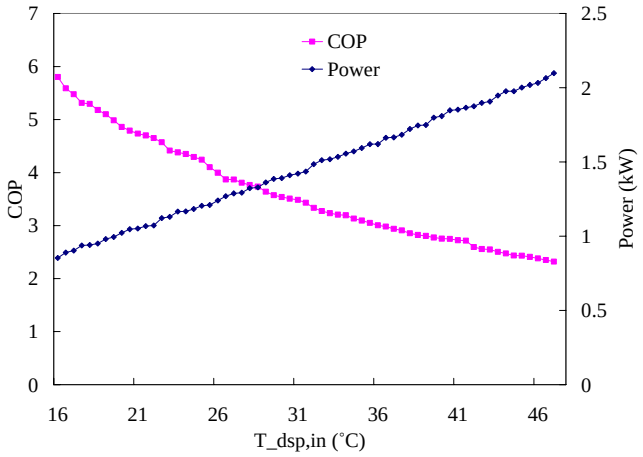

Figure 5.17 Variations of *COP* and *Power* vs. $T_{dsp,in}$ (DHW heating mode)

Table 5.2 Simulated refrigerant temperature and pressure

Tdsp,in (℃)	T1(℃)	T2 (℃)	T5(℃)	Tc (℃)	T3c (℃)	T3 (℃)	T4 (℃)	Te (℃)	Pe (kPa)	Pc (kPa)	dPcon (kPa)	dPevp (kPa)
20.00	13.35	50.89	30.44	30.24	29.81	22.70	9.80	8.35	647.64	1199.43	13.25	29.13
20.50	13.34	52.43	31.17	31.17	30.75	22.72	9.80	8.34	647.48	1229.07	13.43	29.12
21.00	13.31	54.27	32.29	32.29	31.88	22.73	9.76	8.31	646.79	1264.85	13.61	29.09
21.50	13.27	56.65	33.73	33.74	33.25	22.76	9.72	8.27	646.02	1312.41	16.09	29.06
22.00	13.36	54.65	32.79	32.55	32.13	24.31	9.81	8.36	647.85	1273.28	13.97	29.03
22.50	13.53	56.64	33.87	33.87	33.44	24.26	9.69	8.53	651.19	1316.65	14.15	23.21
23.00	13.46	59.01	35.29	35.30	34.88	24.27	9.62	8.46	649.87	1365.18	14.34	23.16
23.50	13.55	57.14	34.39	34.18	33.75	25.80	9.70	8.55	651.59	1327.30	14.52	23.14
24.00	13.52	58.78	35.18	35.18	34.75	25.82	9.68	8.52	651.09	1361.28	14.71	23.12
24.50	13.48	61.02	36.54	36.55	36.13	25.85	9.63	8.48	650.13	1408.53	14.90	23.09
25.00	13.56	59.37	35.94	35.57	35.13	27.37	9.71	8.56	651.82	1374.46	15.09	23.06
25.50	13.53	60.97	36.65	36.54	36.25	27.39	9.68	8.53	651.30	1408.41	10.35	23.04
26.00	13.49	63.21	37.91	37.92	37.63	27.42	9.63	8.49	650.33	1457.13	10.32	23.01
26.50	13.60	61.62	37.50	36.98	36.69	28.96	9.75	8.60	652.64	1424.03	10.45	22.98
27.00	11.72	61.21	37.35	35.79	35.44	30.99	11.30	6.72	616.16	1381.93	11.91	91.82
27.50	11.88	61.88	37.89	36.28	35.94	31.49	11.46	6.88	619.13	1399.13	12.06	92.25
28.00	13.58	63.97	38.96	38.43	38.06	30.37	10.02	8.58	652.31	1475.96	13.57	28.79
28.50	13.43	66.09	39.87	39.67	39.38	30.30	9.86	8.43	649.26	1521.55	10.99	28.60
29.00	13.39	68.32	41.04	41.04	40.75	30.35	9.82	8.39	648.45	1573.21	11.13	28.57
29.50	13.47	66.46	40.58	39.93	39.63	31.81	9.89	8.47	650.05	1531.01	11.27	28.53
30.00	13.46	68.27	41.43	41.05	40.75	31.86	9.88	8.46	649.77	1573.48	11.41	28.52
30.50	13.41	70.49	42.42	42.42	42.13	31.91	9.83	8.41	648.90	1626.18	11.55	28.48

It can be seen from Table 5.2 that the pressure drop in the evaporator was nearly 30kPa, resulting in an evaporation temperature drop of about 1.5˚C. On the other hand, the pressure loss in the condenser was slightly lower as compared with the evaporator, owing to the relatively small specific volume of the high-pressure refrigerant. As shown in Table 5.2, the corresponding condensing temperature drop was only 0.3˚C or so, which can be completely neglected in practice.

5.11 Summary

A detailed steady-state simulation model for a water-to-water heat pump unit equipped with a desuperheater has been developed based on the basic conservation laws of mass, energy and heat transfer correlations as well. In addition, a comprehensive simulation algorithm of the HGCHP system which incorporates the heat pump and GHE models has been developed in this chapter. Finally, a program with a friendly interface for the simulation algorithm has been implemented under the *Delphi* environment.

Based on the discussions associated with varying parameters under the various operating modes, the following conclusions are obtained.

1) The HGCHP with DHW system can offer considerable energy savings in cooling with DHW heating mode, especially in the case of using the desuperheater only to preheat the DHW. In addition, it can greatly alleviate the heat buildup in the ground through adding the desuperheater to produce DHW. The heat transferred to the desuperheater accounted for 10 to 27

percent of the total condensation heat in the case study.

2) For the heating with DHW mode, the heat transfer rate in the desuperheater contributed a significant percentage of total heat transfer of condensation, approximately within a range of 50~15% corresponding to the $T_{dsp,in}$ range of 20˚C and 45˚C.

3) The HGCHP system exhibited a higher average *COP* of as much as 4.0 over the range of $T_{dsp,in}$ =16˚C ~47˚C in DHW heating mode, which indicates a much higher performance than the conventional DHW heating systems.

In summary, the simulation model of the HGCHP with DHW system can provide a useful and effective tool to analyze the system performance in a variety of operating modes. Furthermore, the simulation program can be utilized to better design a HGCHP unit with high efficiency through searching an optimal combination of components.

Based on the substantial simulation results, it is feasible and desirable to apply this kind of system to cooling-dominated buildings in southern China.

CHAPTER 6 DESCRIPTION OF THE HGCHP SYSTEM AND EXPERIMENTAL APPARATUS

6.1 Introduction

A pilot project of the HGCHP with DHW supply system was built to offer space cooling/heating and domestic hot water for a wooden house in a renewable theme park in Hong Kong in 2006. The on-site photo of the project is shown in Figure 6.1. The primary purposes of the pilot project are to investigate the operating characteristics of the system in warm-climate areas and to experimentally validate the simulation model of the HGCHP system. It has now become an important role to introduce the technology of the renewable geothermal energy to the public and improve the application of the GCHP for space cooling and DHW heating as well in Hong Kong. An experimental rig has been set up in the pilot project in order to test the system performance.

In this chapter the detailed descriptions of the pilot project and its major components are firstly presented. Then it is followed by describing the experimental devices and data acquisition system. Finally, the uncertainty analysis is investigated in terms of the measuring devices and the data acquisition system.

Figure 6.1 Photograph of the project

6.2 Project Description

Figure 6.2 illustrates the schematic diagram of the pilot project of the HGCHP system in cooling with DHW heating mode. Five major components are included in the system, which are a water-to-water heat pump, a GHE, a thermal water tank, a fan coil unit and circulating-water pumps. The water-to-water heat pump unit with the cooling and heating capacity of 4.5 kW and 4.9 kW respectively was mounted in the plant room. Three circulation pumps are of the constant flow rates (Model: UPS 25-125 180). The capacity of the thermal storage tank is 260 liter with a pressure rating of 7MPa. The fan coil unit is located on the wall of the wooden house, which has three levels of wind speed with the maximum capacity of 4.5 kW in cooling mode.

As seen from Figure 6.2, the heat pump unit consists of five basic components: a rolling piston compressor, a thermostatic expansion valve and three heat exchangers (i.e. desuperheater, evaporator and condenser). All the three heat exchangers within

the heat pump are copper tube-in-tube heat exchangers, where refrigerant flows through the inner tube and water flows across the tubes. Other components are neglected in this study due to the comparatively little contribution to the thermodynamic analysis of the entire system. The working fluid employed in the system is refrigerant R22.

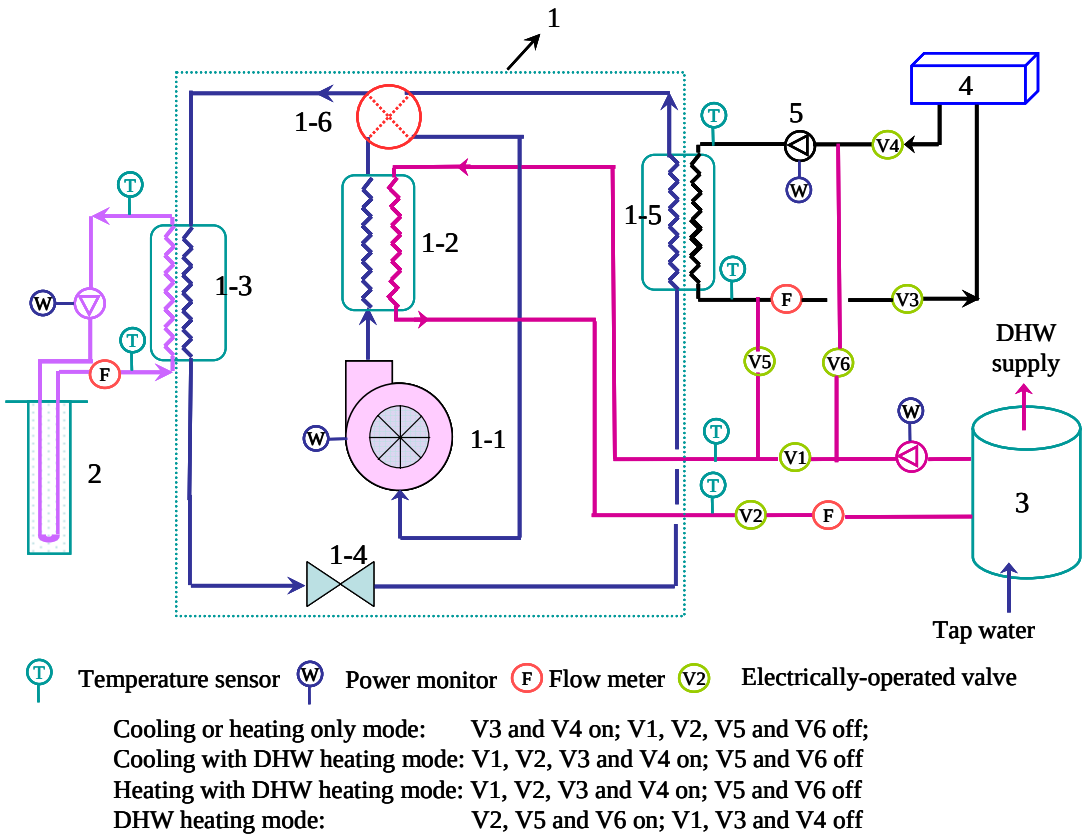

1: water-to-water heat pump; 2: GHE; 3: thermal storage tank; 4: FCU; 5: water pump

For heat pump, 1-1: compressor; 1-2: desuperheater; 1-3: condenser; 1-4: expansion valve; 1-5: evaporator; 1-6: reversing valve

Figure 6.2 Schematic diagram of HGCHP with DHW heating system

The desuperheater, also called hot water heater, was installed between the compressor outlet and the reversing valve. The main function of the desuperheater is

to absorb excess heat to produce or preheat DHW, which can reduce the heat rejection into the ground and consequently balance the annual heating and cooling loads of the GHE. The only difference between the HGCHP system and a conventional GCHP system is that the additional heat exchanger (i.e. a desuperheater) and a hot water tank are supplemented to the system.

In general, the pilot project can offer a total of five different operation modes according to owner's requirements, which include cooling or heating only; cooling with DHW heating, heating with DHW heating, and DHW heating modes. All the operation modes can be accomplished through changing the flow directions of the external water loops by means of the electrically-operated valves installed in the water loops, which are noted in Figure 6.2.

Table 6.1 Basic Parameters of components in the heat pump unit

Components	**Parameter**
Rolling piston compressor (R22)	Displacement : 6.1 m^3/h Refrigerant charge inventory: 1.15 kg
Evaporator	On the copper tube-in-tube heat exchanger, there is an outside tube of a length of 4.5 m and outer diameter of 28 mm, where six inner tubes of outer diameter of 7.94 mm were installed in parallel.
Desuperheater	On the copper tube-in-tube heat exchanger, there are two outside tubes of a length of 2.52 m and outer diameter of 28 mm. One inner tubes of outer diameter of 19 mm was installed in each outside tube.
Condenser	Identical with the evaporator.
Expansion valve	

In cooling mode, the condenser is connected to the GHE while the evaporator is connected to the fan coil unit and vice versa in heating mode as the refrigerant flow direction is changed reversely by the reversing valve. In the DHW heating mode, the hot water first goes through the condenser before entering the desuperheater in order to improve the heat transfer rate within the condenser and desuperheater.

The specifications of each component in the system are summarized in Table 6.1.

6.3 GHE with Inclined Boreholes

The following figures are the photos of the on-site drilling boreholes and pipe installation.

Figure 6.3 (a) Drilling inclined borehole

Figure 6.3 (b) Drilling vertical borehole

Figure 6.3 (c) Pipe installation

Figure 6.3 Photos of the drilling and installation of the boreholes

The GHE in the project consists of two vertical and two inclined boreholes with a tilted angle of 20º arranged in a rectangular configuration. The deviation direction of

the inclined boreholes is away from each other along their depth. The distance between two adjacent boreholes on the ground surface is about 4 m (seen Figure 3.13). Each borehole has the diameter of 110mm and the depth of 30m. The U-tubes are the high-density polyethylene pipe with the outer diameter 32mm (SDR 11). The horizontal supply and return headers were buried at a depth of 1 meter.

To prevent the surface water penetration and potential groundwater contamination, the boreholes were completely backfilled with a kind of thermally enhanced grout which was mixed with cement, quartz sand and bentonite according to specific proportions. The thermal conductivity of this special grout was tested to be approximately 2.0 W/ (m ºC) in laboratory.

The local average ground temperature a few meters below the ground surface is about 22 ºC. According to the geological report which was offered by the drilling contractor, the major stratum in the local area is fine ash tuff. The thermal conductivity and the thermal diffusivity of the local ground were estimated to be 1.7 W/ (m ºC) and 1.0e-6 m^2/s, respectively.

6.4 Experimental Rig and Data Acquisition System

In order to investigate the performance of the HGCHP system applied in the warm-climate area, an experimental rig was established in the system. As is shown in Figure 6.2, six three-wire thermal sensors (Pt100) are located in the water pipes to measure the water temperatures at the inlet and outlet of the three water loops. All the Pt100 sensors have an accuracy of ±0.2℃. Three turbine flow meters (model: LW15) are used to measure the water flow rates in the three water loops. The flow

meters, whose flow range is within 0.6-6 m^3/h, have been calibrated by the manufacturer to ±0.5% of full scale. The energy electricity consumed by the compressor and the water pumps is measured using a power monitor which has an accuracy of ±0.5% of its rated value.

A number of Pt100 temperature sensors with an accuracy of ±0.2℃were attached tightly on the down and up pipes of the U-tubes in the four boreholes. The purpose of these sensors is to investigate the thermal performance of the GHE in the ground and to validate the heat transfer model of the GHE in short-time scale. Figure 6.4 shows the distribution of the temperature sensors along the U-tubes in the boreholes.

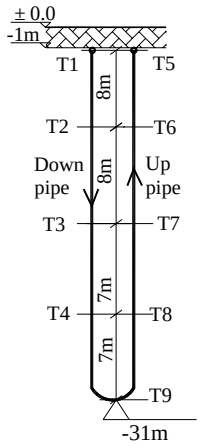

Figure 6.4 Distribution of temperature sensors along the U-tube

All sensors and transducers used in this test rig can output analog signals of direct current (DC) in the forms of voltage, resistance, or frequency. These analog signals can then be converted into the digital signals by a data acquisition system which consists of a PCI card (Model PCI-8360V), and some transformers. Finally, the data acquisition system can scale the digital signals into the real physical values of the measured parameters using a pre-compiled program inside the module. The time

interval of collecting data can be optionally set according to actual conditions or research functions. Figure 6.5 shows the visual interface of the data collection program.

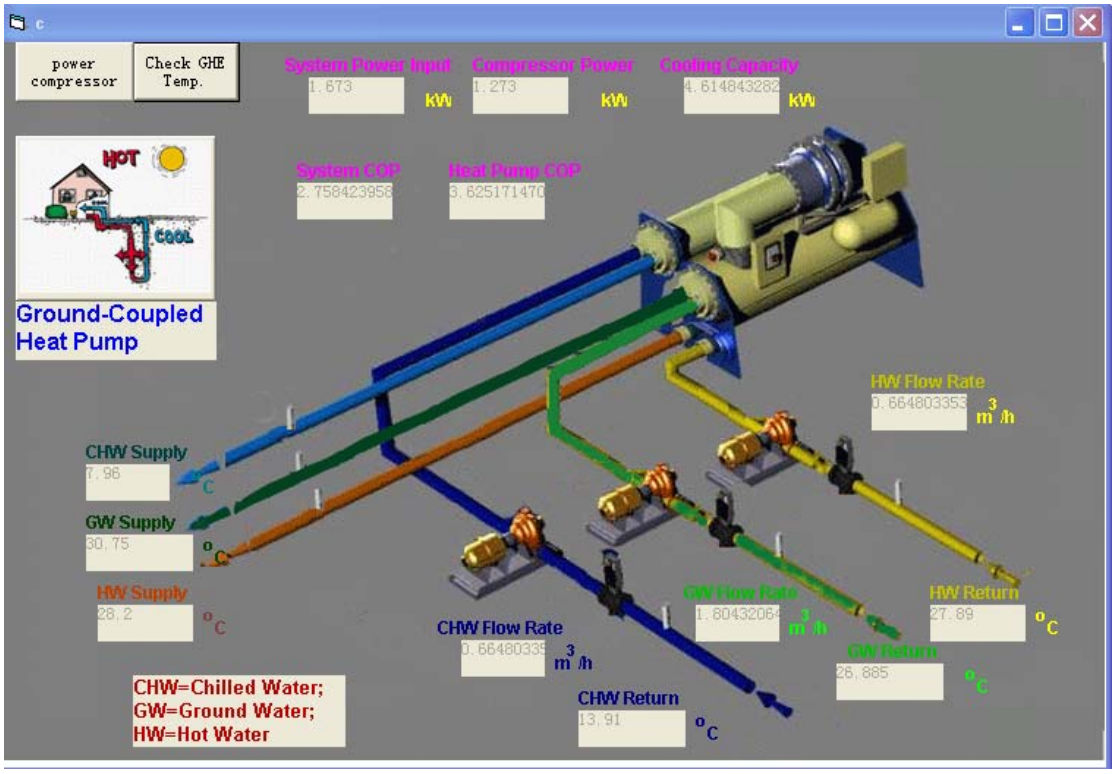

Figure 6.5 Schematic diagram of the visual interface of the Data collection system

6.5 Uncertainty Analysis

An uncertainty analysis is performed to evaluate the errors of the indirectly measured parameters using the classic root-sum-square formula described by Holman (1989) and Treado and Snouffer (2001). Suppose the calculated variable R is a function of the independent variables $x_1, x_2, \ldots, x_n$. Based on the uncertainties of independently measured variables ($w_1, w_2, \ldots, w_n$), the relative uncertainty of the calculated variable can be estimated using the classic root-sum-square formula:

$$\sigma_R = \frac{\left[\left(\frac{\partial R}{\partial x_1} w_1\right)^2 + \left(\frac{\partial R}{\partial x_2} w_2\right)^2 + \ldots + \left(\frac{\partial R}{\partial x_n} w_n\right)^2\right]^{1/2}}{R} \tag{6.1}$$

where

w_i = the uncertainty of the independently measured variable x_i

$\frac{\partial R}{\partial x_i}$ = sensitivity coefficient, the partial derivative of the calculated variable R with respect to the measured variable x_i

Taking the heat transfer rate as an example, the cooling or heating capacity of the HGCHP system can be calculated by means of the measured values of water flow rate and water temperatures:

$$Q = m_w c_p (t_{w,in} - t_{w,out}) \tag{6.2}$$

According to Equation (6.1), the relative uncertainty of the cooling or heating capacity can be expressed as,

$$\sigma_Q = \sqrt{\left(\frac{w_m}{m_w}\right)^2 + \left(\frac{w_t}{t_{w,in} - t_{w,out}}\right)^2 + \left(\frac{w_t}{t_{w,in} - t_{w,out}}\right)^2} \tag{6.3}$$

Thus, the relative uncertainty of the cooling or heating capacity is predicted approximately at 6% under design conditions of m_w=1.5m^3/h and a temperature difference of 5℃. This value may vary slightly with the changes of the actual flow rate and temperatures in practical operation.

CHAPTER 7 MODEL VALIDATION

7.1 Description of Experiments

The simulation model of the HGCHP with DHW heating system presented in Chapter 5 can be used to analyze the system operating performance and to identify any potential mismatches among the components. Besides, it can design an optimal system when incorporating some optimum algorithms into the model. However, it is indispensable to validate the theoretical model using experimental methods before applying it either to engineering practice or other research fields. In view of this, the primary objective of this chapter is to experimentally verify the simulation model of the HGCHP system under a variety of operating conditions.

A series of tests were conducted on the basis of the pilot project as reported in Chapter 6 in order to validate the simulation model. A total of four operation modes (i.e. cooling only; cooling with DHW; heating with DHW; and DHW heating only) were investigated under different operating conditions. Table 7.1 summarizes the test periods and input parameters of the four sets of experiments.

Table 7.1 Test periods and input parameters of the four sets of experiments

Mode	Date	Time	$\dot{m}_{FCU}$ (m^3/h)	$\dot{m}_{GHE}$ (m^3/h)	$\dot{m}_{DHW}$ (m^3/h)
Cooling only	18 May 2007	13:20~15:00	0.7	1.22	N/A
Cooling with DHW	19 Jan 2007	11:30~15:00	0.88	1.0	1.4
Heating with DHW	16 Dec 2006	11:30~13:10	0.88	1.0	1.4
DHW heating only	11 Dec 2006	15:28~16:30	N/A	0.93	1.03

Throughout the experiments, the data collection system presented in Chapter 6 was used to automatically record the external operating parameters, including the inlet and outlet water temperatures, the water flow rates, and the power consumption of the compressor. Based on the uncertainties of the parameters directly measured, the uncertainties for the indirectly measured parameters can be calculated using the method described by Holman (1989), as presented in Chapter 6.

According to the operating range of the system during the four sets of tests, the relative uncertainty of the water temperature was found to be within 0.4%~4.6%. Whereas the relative uncertainty of the water flow rates was within 2.0%~4.8%. For the power consumption of the compressor, the relative uncertainty was found to be 0.7%~1.2%. The heat transfer rates showed a large relative uncertainty of 4.3%~7.6% as it took the uncertainties of the temperature and flow rate into consideration and the relative uncertainty of the *COP* was within 9%.

Once the necessary parameters and the inlet water temperatures of the load side, GHE side and the DHW side are given, the simulation model can determine the corresponding outlet parameters, heat transfer rates and the *COP* as well as the thermal loads of the GHE**.** It should be noted that the start-up period of system, which is usually considered as a dynamic process, is excluded from the following comparisons since the simulation model developed in this research is a steady state model.

7.2 Cooling Mode

This section validated the accuracy of the simulation model in terms of the cooling only mode using the experimental data. The system operating performance of the cooling only mode was also discussed.

Figures 7.1 through 7.5 illustrate the comparisons between the experimental measurements and model predictions in terms of the following parameters: 1) the outlet water temperature in the evaporator ($T_{evp,out}$); 2) *ExWT*; 3) heat transfer rate in the evaporator (Q_{evp}); 4) the power consumption of the compressor (*Power*) and 5) the *COP* of the heat pump.

In general, the simulation model was accurate to within ±10% of the experimental results, which is considered to be satisfactory for engineering applications. According to the results obtained from the continuous cooling operation of two and half hours, the measured *COP* was found to be fairly low (from 3.5 to 2.9). This demonstrates that the conventional GCHP system is not economically efficient if it is only used to provide space cooling in warm or hot climates, such as the climate in Hong Kong.

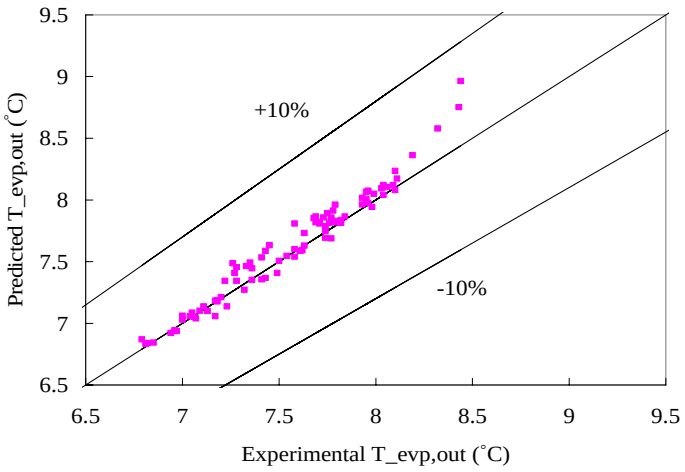

Figure 7.1 Comparison of experimental and predicted $T_{evp,out}$ (cooling mode)

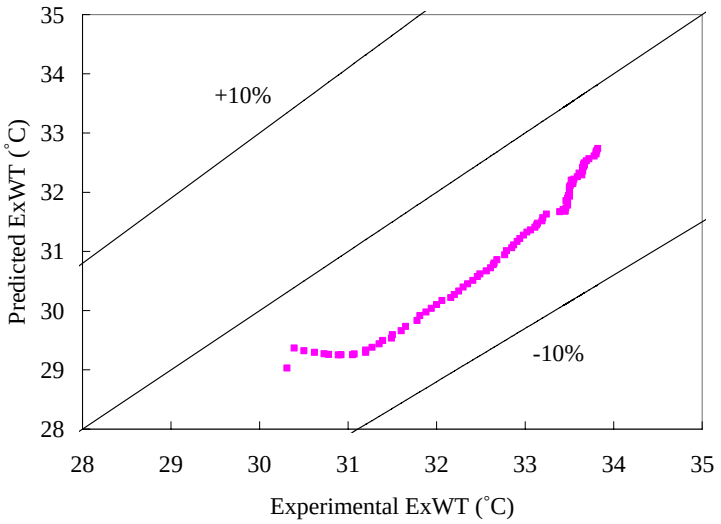

Figure 7.2 Comparison of experimental and predicted *ExWT* (cooling mode)

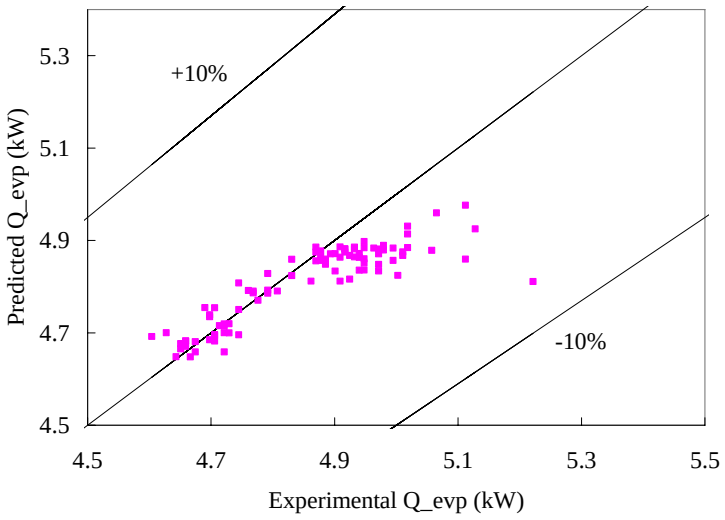

Figure 7.3 Comparison of experimental and predicted heat transfer rate in the evaporator (cooling mode)

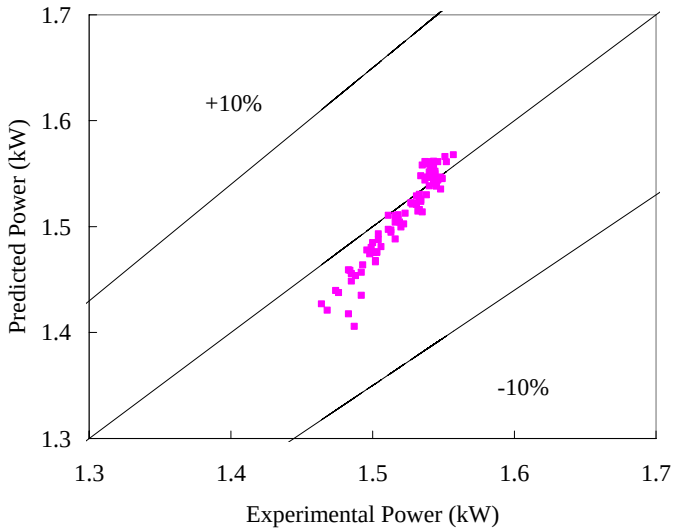

Figure 7.4 Comparison of experimental and predicted power consumption of the compressor (cooling mode)

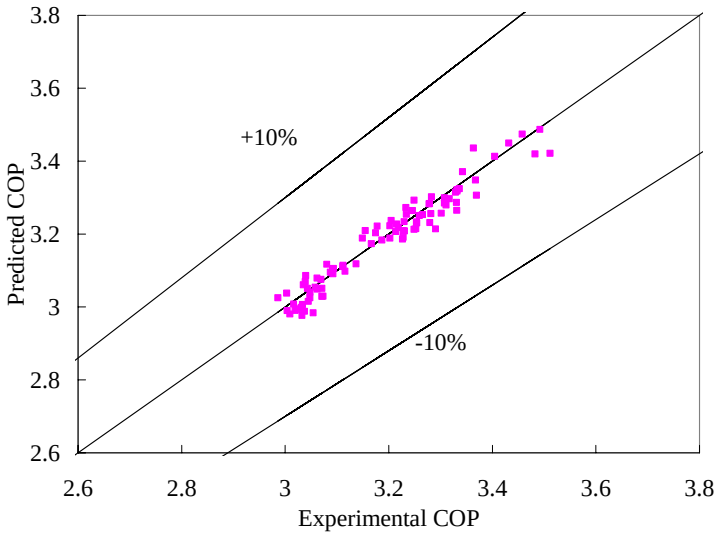

Figure 7.5 Comparison of experimental and predicted *COP* of the heat pump (cooling mode)

7.3 Cooling with DHW Heating Mode

The comparisons between the experimental and predicted results on the cooling with DHW heating mode were conducted and illustrated from Figures 7.6 to 7.13, with respect to $T_{evp,out}$, *ExWT*, outlet DHW water temperature from the desuperheater ($T_{dsp,out}$), heat transfer rates in the evaporator, condenser and desuperheater, the power consumption of the compressor and the *COP* of the heat pump.

As can be observed in Figure 7.6, the deviations of the predicted $T_{evp,\ out}$ from the measured values were within ±0.5℃. It can be found from Figures 7.7 to 7.13 that the most predicted data fell well within ±15% bands of the experimental data except the heat transfer rate occurred in the desuperheater (Q_{dsp}). The large errors of the predicted Q_{dsp} (about ±20%) were attributed primarily to the relatively smaller absolute values of Q_{dsp} which was caused by the small temperature rise.

In this test, the desuperheater possessed a considerable percentage of the total condensation heat, ranging from 57% to 10%, under the condition of $T_{dsp,in}$= 20℃~ 37℃. Corresponding to the same range of $T_{dsp,in}$, the actual *COP* was varied from 5 to 3, which was obviously greater than that in the cooling only mode.

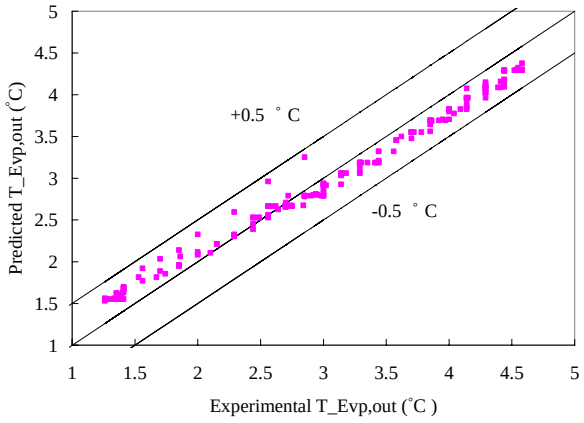

Figure 7.6 Comparison of experimental and predicted $T_{evp,out}$ (cooling with DHW mode)

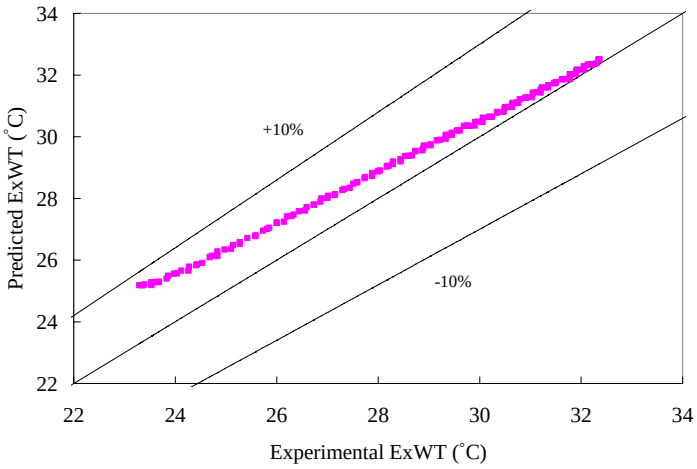

Figure 7.7 Comparison of experimental and predicted *ExWT* (cooling with DHW mode)

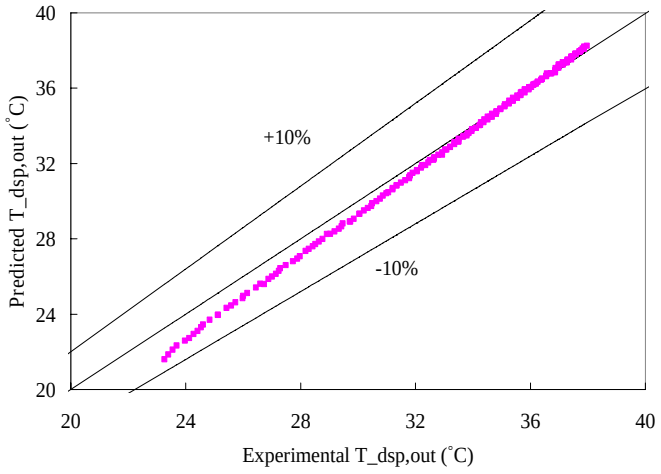

Figure 7.8 Comparison of experimental and predicted $T_{dsp,out}$ (cooling with DHW mode)

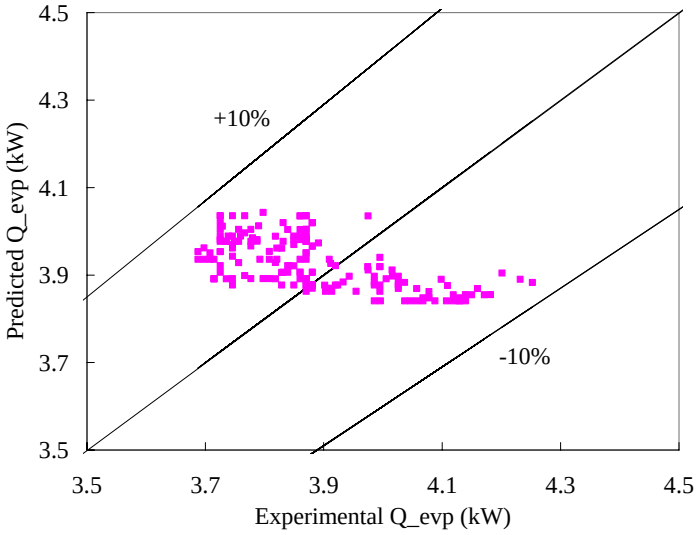

Figure 7.9 Comparison of experimental and predicted Q_{evp} (cooling with DHW mode)

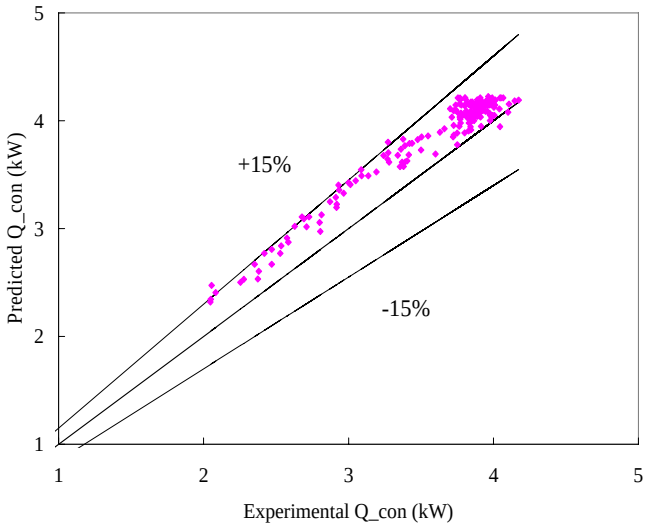

Figure 7.10 Comparison of experimental and predicted Q_{con} (cooling with DHW mode)

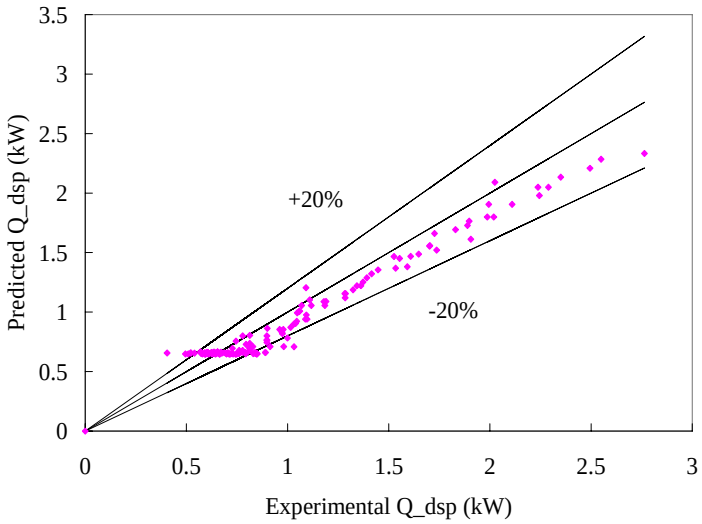

Figure 7.11 Comparison of experimental and predicted heat transfer rate in desuperheater (cooling with DHW heating mode)

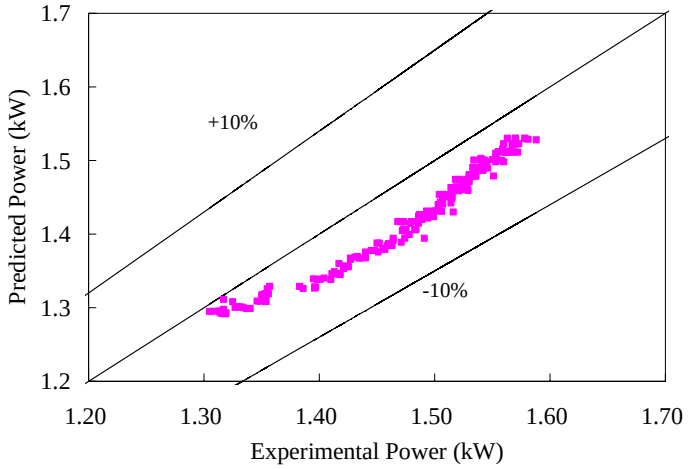

Figure 7.12 Comparison of experimental and predicted power consumption in compressor (cooling with DHW heating mode)

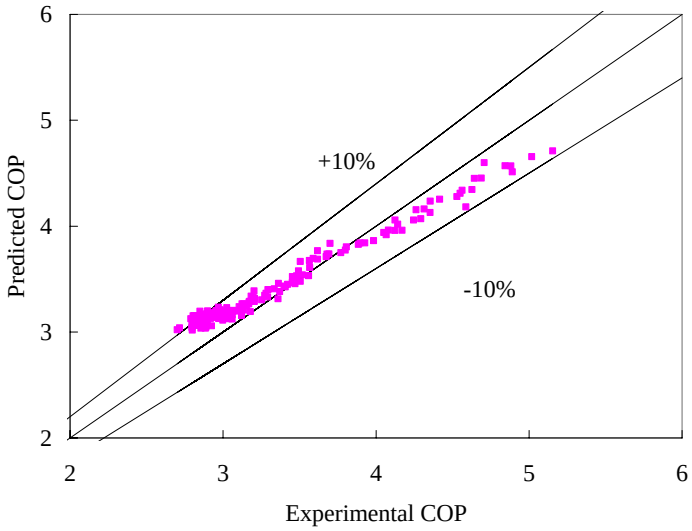

Figure 7.13 Comparison of experimental and predicted *COP* of the heat pump (cooling with DHW heating mode)

7.4 Heating with DHW Heating Mode

The comparisons of the experimental and predicted data under the heating with DHW mode were discussed and presented from Figures 7.14 to 7.20, which include the outlet condenser water temperature ($T_{con,out}$), *ExWT*, $T_{dsp,out}$, heat transfer rates in the evaporator, condenser and desuperheater, the power consumption of the compressor and the *COP* of the heat pump.

In general, the simulation model showed an acceptable accuracy of ±15% of the experimental data; however, some points of *COP* existed with large errors of above 15% at the early beginning of the test. It is estimated that the DHW absorbed a large amount of heat in the range of 40% to 20% of the total heat released from the high-pressure refrigerant side, which correspondingly increased the DHW temperature from 30℃ to nearly 55℃. At the same time, the outlet condenser water

temperature to the indoor FCU was increased from 26℃ to 45℃. The overall *COP* showed a maximum value of 4.6 at first and then steadily reduced with the increase of the temperatures of the DHW and condenser water. The average value of the *COP* was found to be 4 over the period of the test.

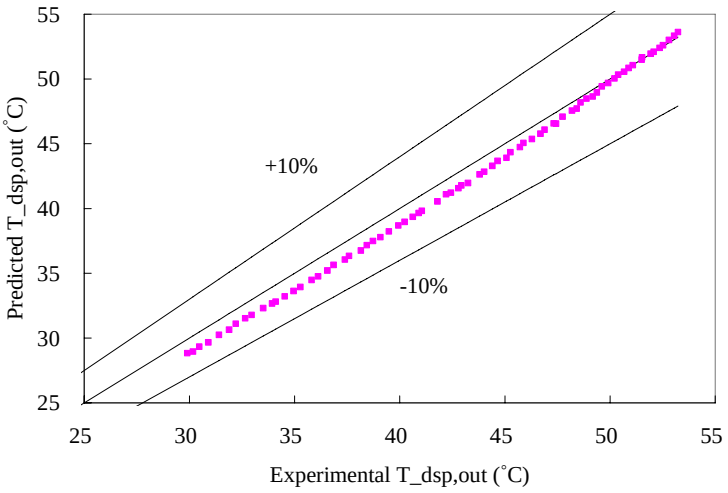

Figure 7.14 Comparison of experimental and predicted $T_{dsp,\,out}$ (heating with DHW heating mode)

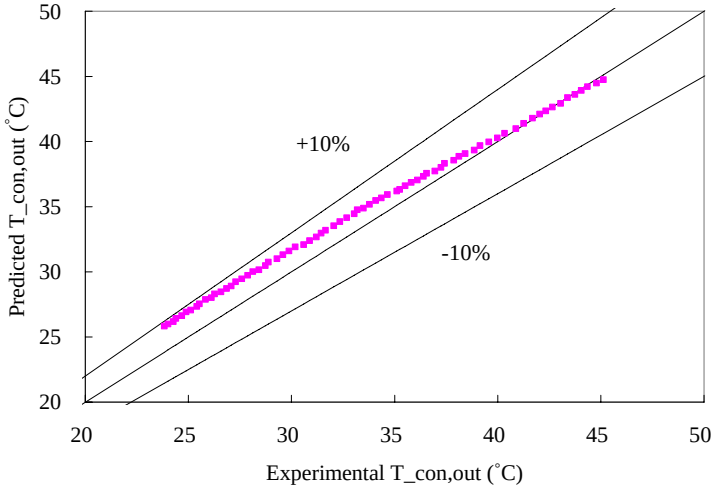

Figure 7.15 Comparison of experimental and predicted $T_{con,\,out}$ (heating with DHW heating mode)

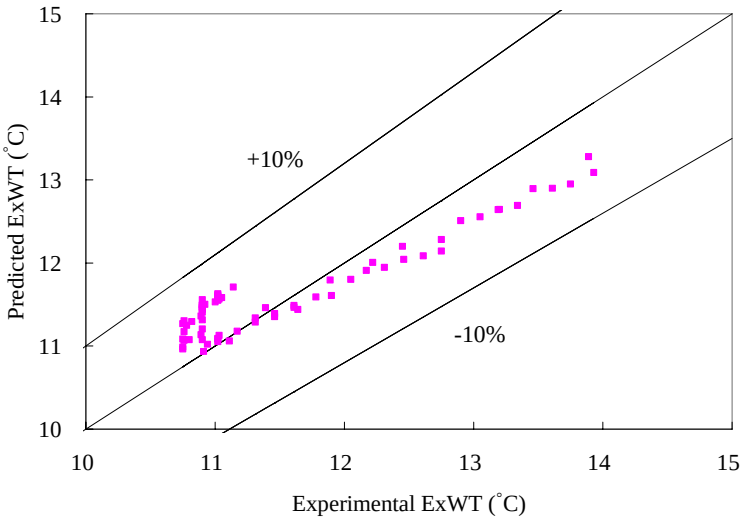

Figure 7.16 Comparison of experimental and predicted *ExWT* (heating with DHW heating mode)

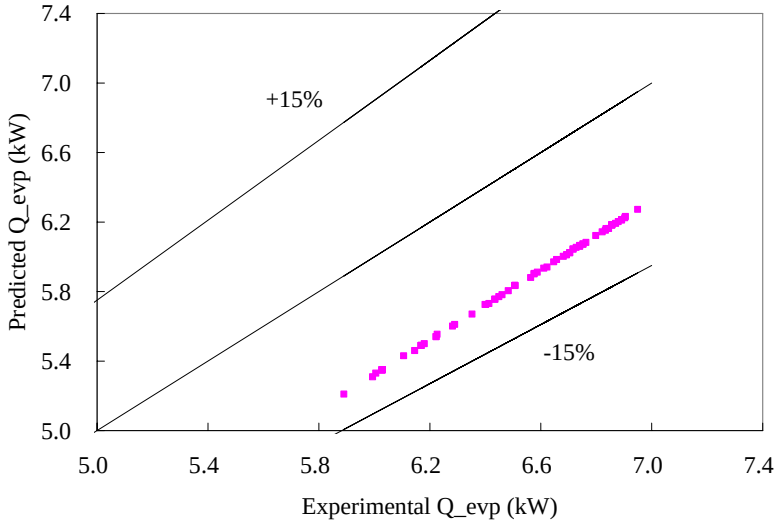

Figure 7.17 Comparison of experimental and predicted Q_{evp} (heating with DHW heating mode)

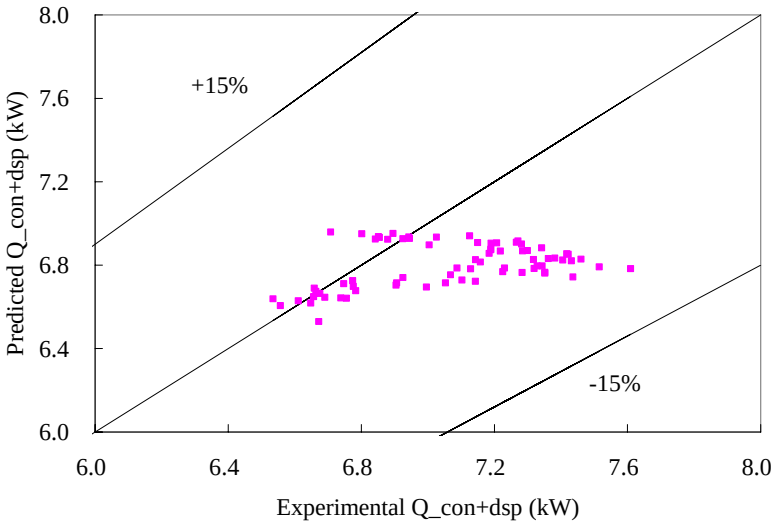

Figure 7.18 Comparison of experimental and predicted $Q_{con+dsp}$ (heating with DHW heating mode)

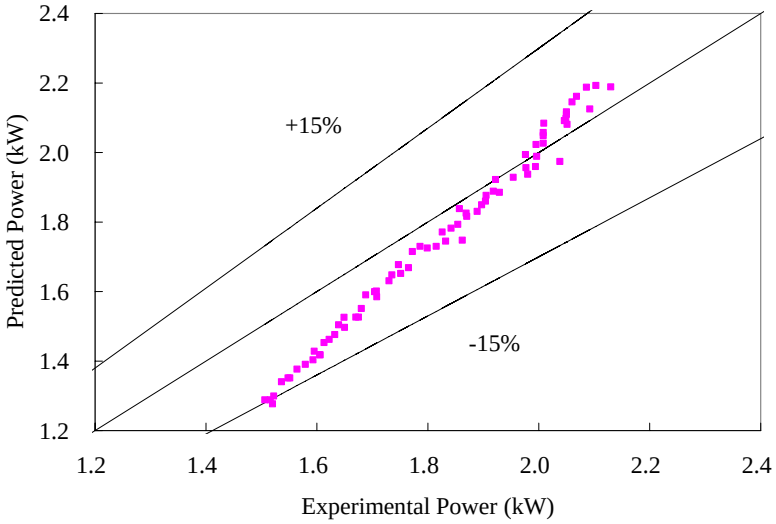

Figure 7.19 Comparison of experimental and predicted power consumption of the compressor (heating with DHW heating mode)

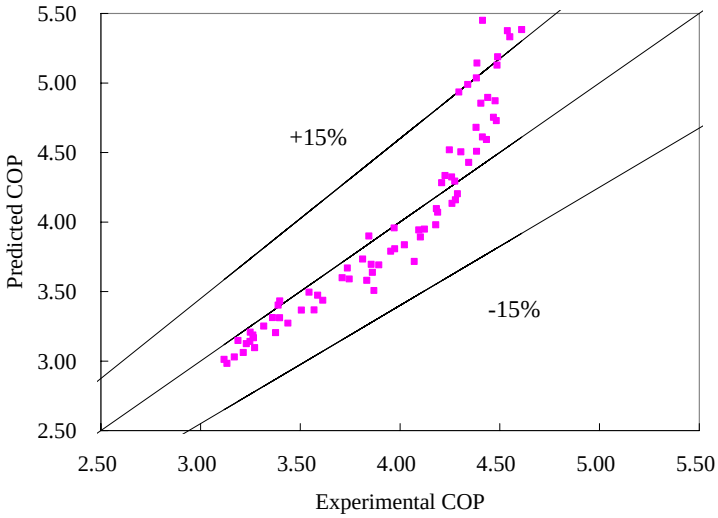

Figure 7.20 Comparison of experimental and predicted the *COP* of the heat pump (heating with DHW heating mode)

7.5 DHW Heating Mode

This section validated the simulation model using the experimental data with respect to the DHW heating mode. The comparison results of the experimental and predicted data were illustrated in Figures 7.21 through 7.26, which include $T_{dsp,out}$, *ExWT*, heat transfer rates in the evaporator, condenser and desuperheater, the power consumption of the compressor and the *COP* of the heat pump.

Similar to the heating with DHW mode, the majority of the predicted points fell well within the bands of ±15% of the experimental data. The DHW temperature was heated rapidly from 32℃ to about 58℃over the heating operation period of less than two hours. The *COP* reached a maximum value of about 4.2 at the beginning of the test, then gradually reduced with the increase of the DHW temperature, and finally

ended up with a low value of about 2.6. The average *COP*, however, was 3.5 which is much higher than the conventional DHW heating systems.

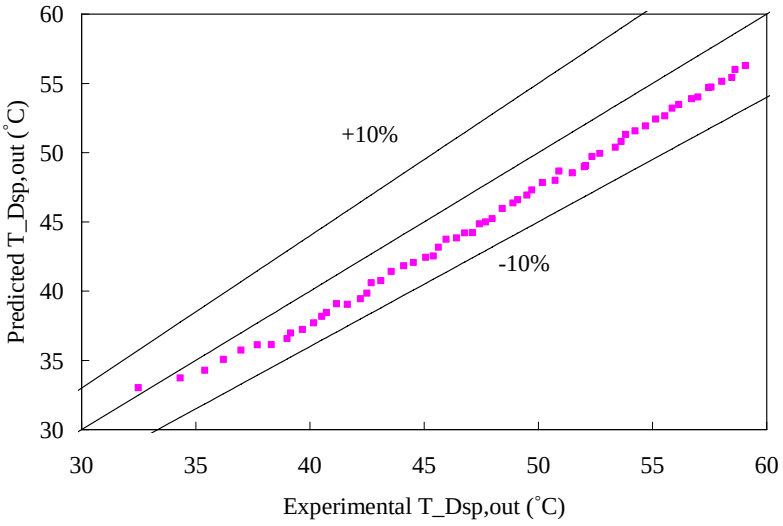

Figure 7.21 Comparison between experimental and predicted $T_{dsp,\,out}$ (DHW heating mode)

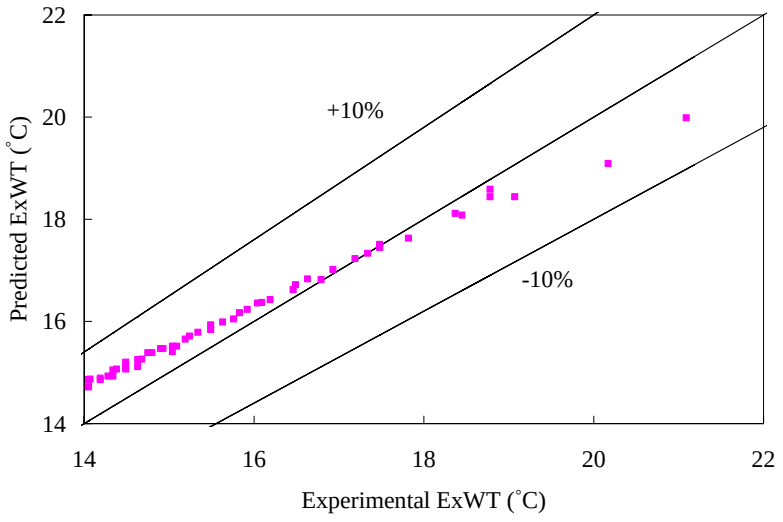

Figure 7.22 Comparison between experimental and predicted *ExWT* (DHW heating mode)

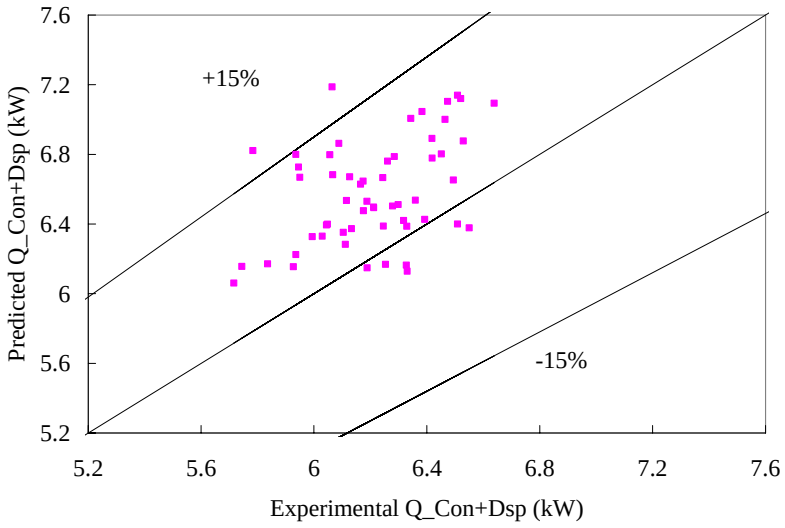

Figure 7.23 Comparison of experimental and predicted $Q_{con+dsp}$ (DHW heating mode)

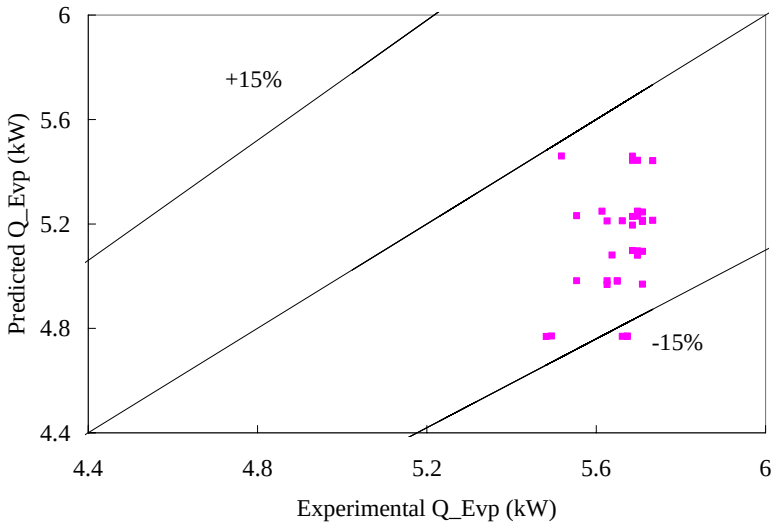

Figure 7.24 Comparison between experimental and predicted heat transfer rate in the evaporator (DHW heating mode)

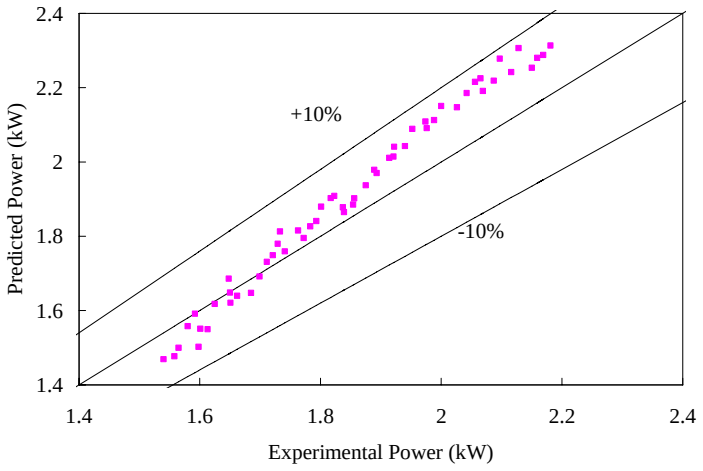

Figure 7.25 Comparison between experimental and predicted power consumption (DHW heating mode)

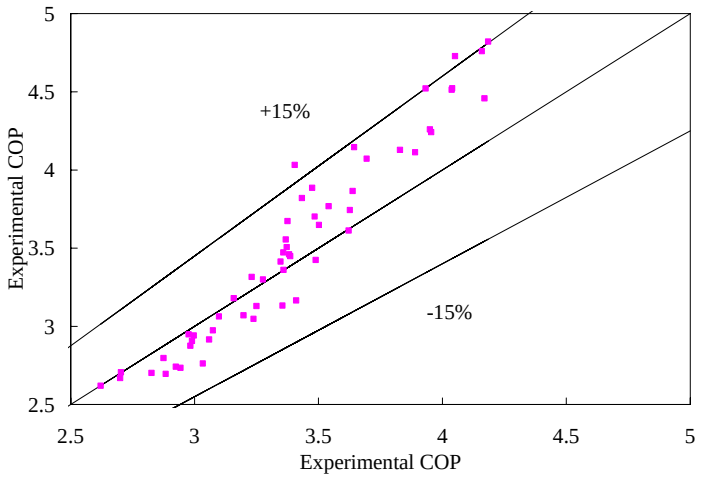

Figure 7.26 Comparison between experimental and predicted *COP* of the heat pump (DHW heating mode)

7.6 Summary

The simulation model of the HGCHP system has been extensively validated by the experiments that were conducted in the pilot project, covering four different

operation modes which are commonly used in practice (i.e. cooling only, cooling with DHW, heating with DHW and DHW heating modes). A comprehensive comparison between the experiments and model predictions has been carried out in terms of outlet water temperatures, heat transfer rates and the compressor power consumption. The operating performance (*COP*) under different operation modes was also discussed in this chapter.

In general, most of the deviations of the predicted data from the experimental data were found to be within $\pm 15\%$ except some points either simulated at the early beginning of the tests or predicted with a relatively smaller measured value, such as the heat transfer rate in the desuperheater. This demonstrates that the simulation model is suitable for research study and engineering applications with a satisfactory accuracy.

In the concerned tests, the desuperheater generally captured a significantly large percentage of the total heat in the HGCHP unit, ranging from 10%~57%, depending mainly on the inlet DHW temperature to the heat pump.

Finally, the experimental results obtained from the four different operation modes indicate that the HGCHP system can achieve a relatively higher performance in all the operation modes with DHW heating, for example, an average *COP* of 3.5 in the cooling with DHW mode, and about 4 in heating with DHW and 3.5 in DHE heating mode. However, the average *COP* of the cooling only mode was only 3 in the test. It should be noted that a higher DHW temperature can evidently reduce the system performance.

CHAPTER 8 ENERGY AND EXERGY ANALYSIS OF HGCHP WITH DHW SYSTEM

8.1 Introduction

Majority of the current approaches to evaluate the performance of GCHP systems are limited in energy analysis, i.e. the first law of thermodynamics, where the total energy is conserved in energy transformations. The coefficient of performance (*COP*) becomes the unique measure to assess the operating efficiency of the systems. However, the *COP* can only compare the desired energy output to the required energy input since it is directly derived from the first law of energy conservation principle. In other words, it cannot represent the quality of energy and indicate the irreversibility or the energy losses in the components of a thermal system (Wark, 1995). An effective method is to combine the conservation of energy principle with the second law of thermodynamics (i.e. exergy analysis) for the design and analysis of energy systems (Dincer, 2002; Ren, 2001). This method can also identify the optimal operating conditions and consequently provide an optimal design for any thermal devices when simultaneously taking into account the thermodynamic and economic characteristics.

Thus, it is essential to evaluate the performance of the HGCHP system using the exergy analysis, which can inherently detect the inefficient parts of the system and lead to the optimum operating conditions.

In recent years, some exergy or thermodynamic analysis has been gradually incorporated into the investigations of the GCHP or other heat pump systems. A solar-assisted heat-pump system was analyzed using the first and second laws of thermodynamics by Chaturvedi et al. (1991). The performance of the solar-assisted heat-pump system was compared with that of a solar system without a heat pump. Cervantes and Torres-Reyes (2002) evaluated the exergy losses for a solar-assisted heat pump based on experimental study and concluded that the main source of irreversibility occurred in the evaporator.

Hepbasli and Akdemir (2004) presented the energy and exergy analysis of a GSHP system which provided heating and cooling services for a 65 m^2 room. Ozgener and Hepbasli (2005) investigated the capital cost and the thermodynamic losses for a solar assisted ground-source heat pump greenhouse heating system and pointed out that there was a systematic correlation between the capital cost and the thermodynamic losses. The performance of a typical GCHP system for district heating was conducted in terms of energy and exergy aspects by Hepbasli (2005), which demonstrated that the exergy analysis was a useful approach to detect and quantitatively evaluate any causes of energy degradation or exergy loss. The energetic and exergetic efficiencies of the ground-coupled heat pump systems with two horizontal ground heat exchangers have been investigated by Hikmet et al. (2007). The results showed that the energetic and exergetic efficiencies of the

systems increased when increasing the heat source (ground) temperature in heating season.

However, few studies have been done for analyzing the operating performance of the HGCHP with DHW supply system in terms of exergy analysis. The aim of this chapter is therefore to evaluate the energy and exergy efficiencies of the HGCHP system based on experimental studies and thermodynamics principles. Another objective is to compare the operating performance of the system for DHW supply with other DHW heating systems with respect to energy and exergy efficiencies.

8.2 Energy and Exergy Analysis of the HGCHP System

In order to comprehensively investigate the exergy performance of the HGCHP system, the four common operating modes (i.e. cooling only, cooling with DHW, heating with DHW and DHW heating modes) are analyzed, respectively, with the aid of the experimental data obtained from the pilot project. Figure 8.1 illustrates the operating principle of the HGCHP system in DHW heating mode.

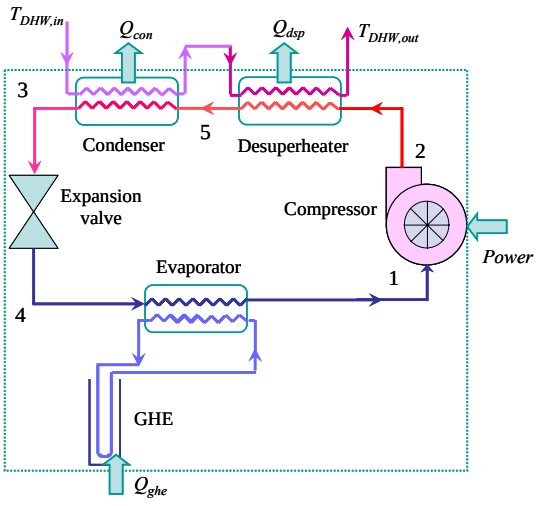

Figure 8.1 Schematic diagram of the HGCHP system in DHW heating mode

8.2.1 Energy analysis

The energy analysis of the HGCHP system, involving the energy balance and the energy performance, has been described in detail in Chapter 5, as follows:

Energy balance: $$Q_{dsp}+Q_{con}= Q_{evp}+Power \quad (8.1)$$

COP in cooling modes: $$COP=\frac{Q_{evp}+Q_{dsp}}{Power} \quad (8.2a)$$

COP in heating modes: $$COP=\frac{Q_{dsp}+Q_{con}}{Power} \quad (8.2b)$$

The energy balance in Equations (8.1) and (8.2) shows that the *COP* only relates to the energy transferred between the different components in the system. It gives equal weighting to both the electric energy supplied to the compressor and the low-grade thermal energy in the heat exchangers. No information on the quality changes of the different energy resources is illustrated in the energy analysis. Hence, it is necessary to further investigate the performance of the HGCHP system using exergy analysis.

8.2.2 Exergy analysis

For a thermal system, a detailed exergy analysis is usually conducted with respect to its surrounding environment. When a system and its environment are in equilibrium each other, the system can then be assumed to be in its dead state at T_{env} and P_{env} (Rosen and Dincer, 2004; Kotas, 1985). In this study, all the thermal processes are occurred in the surrounding environment, including the GHE which has an indirectly heat transfer process with the outdoor air. Besides, the exergy analysis is focused on the concerned period of the experiment in the local area. Therefore, a more

reasonable dead state is taken as the local average atmospheric air during the experiment.

Based on the definition of exergy, the specific stream exergy of a fluid in a steady-flow process with kinetic- and potential-energy changes neglected can be expressed as:

$$e = h - h_{env} - T_{env}(s - s_{env}) \tag{8.3}$$

Then, the exergy change of a fluid with mass flow rate $\dot{m}$ between the two states is:

$$\dot{E}_2 - \dot{E}_1 = \dot{m}\ \left(h_2 - h_1 - T_{env}(s_2 - s_1)\right) \tag{8.4}$$

The exergy associated with the heat transfer on the control surface is determined by the maximum work that could be obtained using the environment as a reservoir of thermal energy (Kotas, 1985). For a heat transfer rate Q_r and a temperature T_{rsv} on the control surface where the heat transfer takes place, the heat exergy is:

$$\dot{E}_Q = Q_r\left(1 - \frac{T_{env}}{T_{rsv}}\right) \tag{8.5}$$

The exergy balance for a control region can be written as:

$$\sum \dot{E}_{in} = \sum \dot{E}_{out} + \dot{I} \tag{8.6}$$

where $\sum \dot{E}_{in}$ is the sum of all exergy transfers making up the input, and $\sum \dot{E}_{out}$ is the sum of all exergy transfers making up the output; $\dot{I}$ is the total irreversibility, i.e. the exergy losses.

There are several definitions for the exergy effectiveness to formulate the criteria of the system performance, among which, two typical formulas are widely used in the exergy analysis of thermal plants. One of them is defined as the ratio of the exergy output to the work input:

$$\varepsilon = \frac{rate\ of\ exergy\ output}{rate\ of\ work\ input} \tag{8.7}$$

The other one is the ratio of the exergy output (or gain) over the exergy input (Kotas, 1985; Wark K. 1995).

$$\varepsilon = \frac{rate\ of\ exergy\ output}{rate\ of\ exergy\ input} \tag{8.8}$$

It is worth noticing that employing the first definition to analyze the GCHP systems may draw some unreasonable conclusions, especially when the temperature of the low thermal reservoir is higher than that of the environment. Taking an ideal heat pump cycle as an example, the work input in heating mode can be expressed as follows,

$$Power = Q_H - Q_L \tag{8.9}$$

And, the exergy of the heating rate is given by

$$E_{QH} = Q_H\left(1 - \frac{T_{env}}{T_H}\right) \tag{8.10}$$

where, $Q_H = \Delta S T_H$ is the heat transfer rate to the high thermal reservoir at T_H; $Q_L = \Delta S T_L$ is the heat transfer rate from the low thermal reservoir at T_L; and ΔS is the entropy change.

Therefore, the exergy efficiency related to the first definition can be deduced as,

$$\varepsilon = \frac{E_{QH}}{Power} = \frac{T_H - T_{env}}{T_H - T_L} \tag{8.11}$$

For the GCHP system in heating mode, the low thermal source is the ground, which always satisfies $T_L > T_{env}$. In this case, the exergy efficiency obtained from Equation (8.11) is greater than unity, which obviously conflicts with the second law of thermodynamics. In view of this, the latter exergy effectiveness, which is more reasonable for the GCHP system than the former one, is adopted in this study.

Table 8.1 Exergy analysis for the system components

Component	Exergy input $\dot{E}_{in}$ (kW)	Exergy output(or gain) $\dot{E}_{gain}$ (kW)	Irreversibility (destruction) $\dot{E}_{in} - \dot{E}_{gain}$ (kW)
Compressor	$Power$	$\dot{m}_r e_2 - \dot{m}_r e_1$	$Power + \dot{m}_r e_1 - \dot{m}_r e_2$
Desuperheater	$\dot{m}_r (e_2 - e_5)$	$\dot{m}_{dsp}(e_{dsp,f2} - e_{dsp,f1})$	$\dot{m}_r (e_2 - e_5) - \dot{m}_{dsp}(e_{dsp,f2} - e_{dsp,f1})$
Condenser	$\dot{m}_r (e_5 - e_3)$	$\dot{m}_{con}(e_{con,f2} - e_{con,f1})$	$\dot{m}_r (e_5 - e_3) - \dot{m}_{con}(e_{con,f2} - e_{con,f1})$
Expansion valve	$\dot{m}_r (e_3 - e_4)$	0	$\dot{m}_r (e_3 - e_4)$
Evaporator	$\dot{m}_r (e_4 - e_1)$	$\dot{m}_{evp}(e_{evp,f2} - e_{evp,f1})$	$\dot{m}_r (e_4 - e_1) - \dot{m}_{evp}(e_{evp,f2} - e_{evp,f1})$
GHE	$Q_{evp}\left(1 - \frac{T_{env}}{T_{soil}}\right)$	$\dot{m}_{evp}(e_{evp,f1} - e_{evp,f2})$	$\dot{m}_{evp} e_{evp,f2} + Q_{evp}\left(1 - \frac{T_{env}}{T_{soil}}\right) - \dot{m}_{evp} e_{evp,f1}$

On the basis of the aforementioned formulations related to the exergy analysis and the operating principle of the system, it is convenient to deduce the exergy

destructions and gains for each of the HGCHP components, which are summarized in Table 8.1.

Taking the DHW heating mode as an example, the total exergy input of the whole system (denoted by the dashed frame in Figure 8.1) can be readily calculated from:

$$\dot{E}_{in,system} = Power + \dot{E}_Q = Power + Q_{evp}\left(1 - \frac{T_{env}}{T_{soil}}\right) \tag{8.12}$$

It is worthwhile to notice that the thermal exergy $\dot{E}_Q$ is associated with the heat transfer in the GHE due to the temperature difference between the soil and the environment. The overall exergy gain of the system is the sum of the exergy gains in the desuperheater and condenser:

$$\dot{E}_{gain,system} = \dot{E}_{gain,dsp} + \dot{E}_{gain,con} = \dot{m}_{dsp}\left(e_{dsp,f2} - e_{dsp,f1}\right) + \dot{m}_{con}\left(e_{con,f2} - e_{con,f1}\right) \tag{8.13}$$

Since $\dot{m}_{dsp} = \dot{m}_{con}$, a more straightforward formula of the system exergy gain can be further deduced in terms of the heat exergy.

$$\dot{E}_{gain,system} = \left(Q_{dsp} + Q_{con}\right)\left(1 - \frac{T_{env}}{\overline{T}_{DHW}}\right) \tag{8.14}$$

where $\overline{T}_{DHW}$ means the average DHW temperature in the desuperheater and condenser. Hence, the irreversibility of the system is:

$$\dot{I} = \dot{E}_{in,system} - \dot{E}_{gain,system} \tag{8.15}$$

As a result, the overall exergy effectiveness can be obtained from Equations (8.12) and (8.14):

$$\varepsilon_{HGCHP} = \frac{\left(Q_{dsp} + Q_{con}\right)\left(1 - \frac{T_{env}}{\overline{T}_{DHW}}\right)}{Power + Q_{evp}\left(1 - \frac{T_{env}}{T_{soil}}\right)} \tag{8.16}$$

Substituting Equations (8.1) and (8.2b), i.e. the energy balance and *COP,* into Equation (8.16) yields:

$$\varepsilon_{HGCHP} = \frac{\left(\overline{T}_{DHW} - T_{env}\right) \cdot COP \cdot T_{soil}}{\left(T_{soil} \cdot COP - COP \cdot T_{env} + T_{env}\right)\overline{T}_{DHW}} \tag{8.17}$$

The relative irreversibility of each component can be expressed as the ratio of its irreversibility rate to the overall exergy input of the system.

8.3 Case Study

As discussed in Chapter 7, four different experiments, which are corresponding to the different operation modes have been conducted based on the pilot project. To better investigate the actual exergy and energy performances of the HGCHP system, the actual exergy efficiencies of the four different experiments together with the *COP*s are calculated using Equations (8.2) and (8.8) according to the experimental data. The detailed experimental conditions and schedule have been presented in Chapter 7.

The overall effects of the measurement uncertainties of individual variables on the *COP* and ε can be analyzed using the classic root-sum-square formula which has been described in Chapter 6. Based on the measured data and their uncertainties, the relative uncertainty of the *COP* was within 9% and the relative uncertainty of ε varied from 8% to 10% in the concerned experiments.

Figures 8.2 and 8.3 illustrate the variations of the *COP* and ε in the two cases of the cooling and cooling with DHW heating modes, respectively. In general, compared with the cooling only mode, the cooling with DHW mode behaved a distinctly higher operating performance associated with the energy and exergy efficiencies due to the useful energy gain of the DHW. The exergy efficiency of the cooling only mode was decreased from 17% to 15.5% with operating time. For the cooling with DHW mode, whereas, its exergy efficiency was found to be firstly increased to a high value of 25% during a short period and then decreased with the increase of the DHW temperature. This is due to the fact that the increase rate in the exergy gain of the DHW was larger than the relative increase rate of power input at the beginning of the test and, after some time, the power consumption played a dominant role in determining the exergy efficiency.

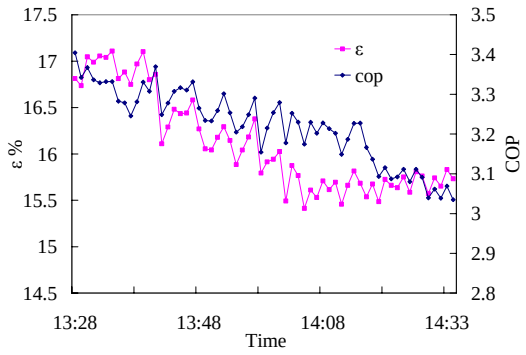

Figure 8.2 Variations of ε and *COP* vs. time (cooling only mode)

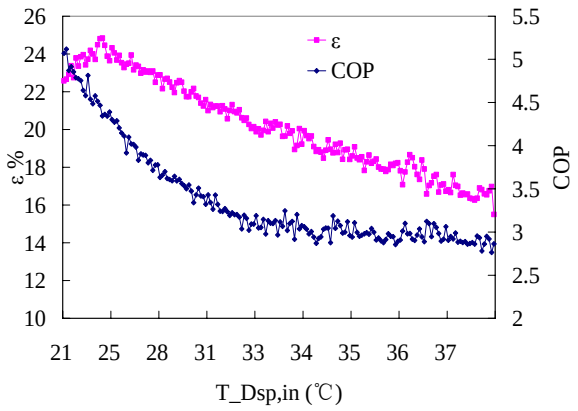

Figure 8.3 Variations of ε and COP vs. $T_{dsp,in}$ (cooling with DHW mode)

The variations of the exergy efficiencies of the heating with DHW and DHW heating modes together with the *COP*s are presented in Figures 8.4 and 8.5. It can be seen from the figures that the two cases showed the quite similar variation trends of both the *COP* and exergy efficiency. Therefore, the following discussion is mainly focused on the DHW heating mode. The average value of the *COP* was above 3 during the test periods, which is relatively higher than that of the conventional hot water heaters. For the DHW heating mode, the *COP* was clearly decreased with the increase of the DHW temperature because of continual rise in compressor power consumption, whereas the exergy efficiency was increased from 22% to 32% with DHW temperature ranging from 28℃ to 50℃. The contrary variations between the *COP* and the exergy efficiency reveal that higher *COP* of a HGCHP system may not represent a higher exergy efficiency which should be further investigated by co-analysis of exergy and energy.

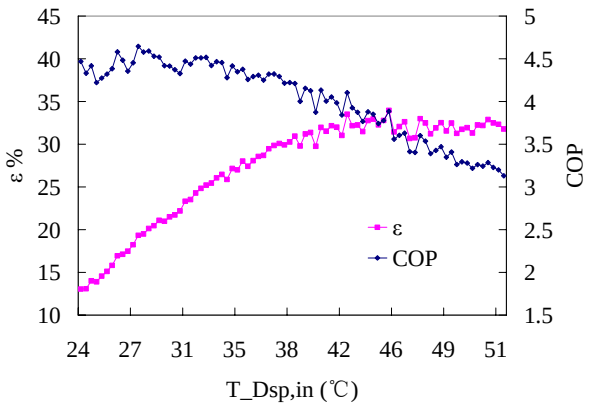

Figure 8.4 Variations of ε and COP vs. $T_{dsp,in}$ (heating with DHW mode)

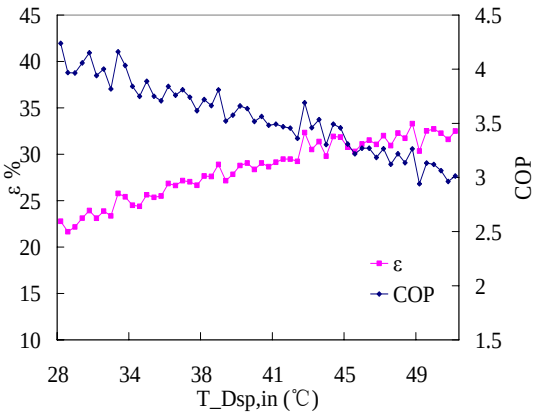

Figure 8.5 Variations of ε and COP vs. $T_{dsp,in}$ (DHW heating mode)

8.4 Exergy Analysis in DHW Heating Mode

To further detect the detailed exergy losses in the system, an operation point was chosen from the test data of the DHW heating mode for exergy analysis. The exergy changes in the water side can be easily determined using the experimental data. However, the refrigerant thermal properties cannot be measured in-situ since no test equipment was installed in the refrigerant cycle at this time. Therefore, the

simulation program developed in Chapter 5 is employed here to evaluate the refrigerant properties.

Using the simulation program together with the recorded data such as the inlet water temperatures and water flow rates, the outlet conditions and refrigerant properties at the selected point can be determined, as shown in Table 8.2. Based on the aforementioned exergy equations and the measured data from the experiment, the exergy gain and loss of each component can be calculated and the proportion of exergy flux distribution in the system can be consequently obtained, as shown in Figure 8.6 (the Grassmann diagram). Obviously, the Grassmann diagram gives the quantitative information regarding the proportion of exergy input which was dissipated in the different components of the system.

Table 8.2 The property data of the operating point in DHW heating mode

Water side (recorded data) with $\dot{m}_{evp} = 0.26$ kg/s and $\dot{m}_{dsp} = \dot{m}_{con} = 0.28$ kg/s						
	$T_{evp,f2}$	$T_{evp,f1}$	$T_{con,f1}$	$T_{con,f2}$	$T_{hot,f1}$	$T_{hot,f2}$
T (℃)	*20.4*	*15.74*	*39.03*	*44.54*	*44.5*	*45.53*
e (kJ/kg)	*0.21*	*0.004*	*3.99*	*5.957*	*5.934*	*6.349*
Refrigerant side (Simulated values) with flow rate $\dot{m}_r$ =0.04 kg/s and *Power*=1.92 kW						
state	1	2	3	4	5	
T (℃)	*16.09*	*88.04*	*44.98*	*11.09*	*51.37*	
h (kJ/kg)	*414.54*	*453.58*	*256.31*	*256.31*	*422.12*	
s (kJ/kgK)	*1.764*	*1.789*	*1.187*	*1.198*	*1.705*	
e (kJ/kg)	*48.24*	*79.99*	*56.3*	*52.94*	*72.87*	

It can be found from Figure 8.6 that the largest irreversibility in the system occurred in the compressor, about 36.5% of the total exergy input, which was caused by the electric, mechanical and polytropic efficiencies of the compressor. The second largest exergy loss of 11.2% existed in the evaporator. The exergy losses in the condenser and desuperheater exhibited similar magnitudes of 6.9% and 8%, respectively. The losses in the heat exchangers were mainly caused by the temperature differences between the refrigerant side and water side. The exergy destruction in the expansion valve was found to be 6.1%, which was largely attributed to the pressure drop of the refrigerant. This is generally regarded as an inherently dissipative process. The smallest irreversibility of all the components occurred in the GHE, only 3.4% of the total exergy input. The ratios of exergy gains in the desuperheater and the condenser were 4.8% and 23%, respectively. A higher exergy gain of the latter is primarily owing to its large heat transfer area over the desuperheater. Therefore, the overall exergy efficiency of the system was found to be 27.8%.

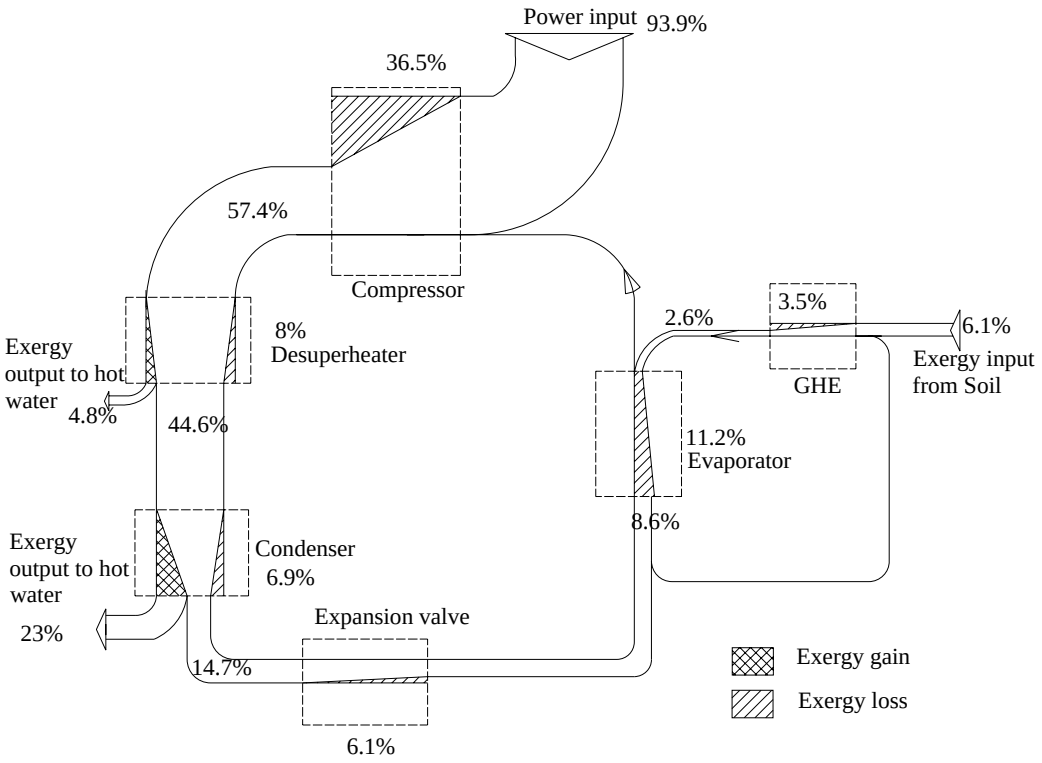

Figure 8.6 Exergy flux distribution (Grassmann diagram) of the HGCHP system

8.5 Energy and Exergy Comparisons with Other DHW Systems

To better investigate the operating performance of the HGCHP system with respect to DHW supply, a meaningful comparison of energy and exergy efficiencies has been undertaken between the HGCHP system and other three kinds of conventional DHW systems, i.e. air-source heat pump (ASHP) system, electric heater (ElcH) and gas-fired boiler (GasB).

Based on the second law of thermodynamics, the exergy efficiency of an ElcH system can be expressed as:

$$\varepsilon_{elc} = \frac{Q_{DHW}\left(1-\frac{T_{env}}{\overline{T}_{DHW}}\right)}{\left(Q_{DHW}/\eta_{elc}\right)} = \left(1-\frac{T_{env}}{\overline{T}_{DHW}}\right)\cdot\eta_{elc} \tag{8.18}$$

The exergy efficiency of the GasB is evaluated by:

$$\varepsilon_{gas} = \frac{Q_{DHW}\left(1-\frac{T_{env}}{\overline{T}_{DHW}}\right)}{\left(Q_{DHW}/\eta_{gas}\right)\cdot\varphi} = \left(1-\frac{T_{env}}{\overline{T}_{DHW}}\right)\cdot\eta_{gas}\Big/\varphi \tag{8.19}$$

where Q_{DHW} is heat gain by the DHW; η_{elc}=98% means the energy efficiency of the ElcH system (Tso and Yau, 2003); η_{gas} is the energy efficiency of the GasB (78%), and φ is the ratio of specific chemical exergy of the gas to its net calorific value (1.04) (Kotas, 1985).

The exergy analysis of the ASHP system can be deduced from Equation (8.17) when using outdoor air temperature (T_{env}) instead of soil temperature (T_{soil}).

$$\varepsilon_{ASHP} = \left(1-\frac{T_{env}}{\overline{T}_{DHW}}\right)\cdot COP_{ASHP} \tag{8.20}$$

Actually, the relationship between the COP_{ASHP} and the average DHW temperature of a heat pump unit can be obtained through a linear regression of the catalog data provided by manufacturers. In this case, the water-to-water heat pump unit in the pilot project and an air-to-water heat pump unit with the same nominal capacity as the water-to-water heat pump are selected for comparison. A third order polynomial regression is adopted to fit the correlations of the *COP* and $\overline{T}_{DHW}$ in the HGCHP and ASHP units.

For the water-to-water heat pump unit, the fitted equation is given,

$$COP_{HGCHP} = 13.34572 - 0.60805\overline{T}_{DHW} + 0.01241\overline{T}_{DHW}^{2} - 9.25e-5\overline{T}_{DHW}^{3} \quad (EWT=20℃)$$

(8.21)

For the air-to-water heat pump unit,

$$COP_{ASHP} = 11.79517 - 0.55578\overline{T}_{DHW} + 0.0118\overline{T}_{DHW}^{2} - 9.02e-5\overline{T}_{DHW}^{3} \quad (EAT=15℃)$$

(8.22)

where, *EWT* is the entering water temperature to the HGCHP system from the GHE loop; *EAT* is the entering air temperature to the ASHP unit from the outdoor air.

The energy efficiencies of the ElcH and GasB systems, which are assumed as constant (0.98 and 0.78 respectively), are also called the system *COP*. Using Equations (8.17) through (8.22) the energy and exergy efficiencies of the four different DHW heating systems were calculated under the specific conditions of T_{soil}=22℃ and T_{env}=15℃ over the wide range of $\overline{T}_{DHW}$=15~55℃. The simulation results are illustrated in Figures 8.7 and 8.8.

It can be observed from Figure 8.7 that the HGCHP system resulted in the highest energy efficiency, ranging from 6.7 to 2.1, followed by the ASHP (5.8~1.9), the ElcH (0.98) and the GasB systems (0.78). When compared with the ASHP system, the HGCHP system can save about 7.2% energy, and significantly more energy can be saved as compared with the ElcH (109%) and the GasB (163%), at the operating point of $\overline{T}_{DHW}$=55℃.

Similarly, as shown in Figure 8.8, the HGCHP system offered the highest exergy efficiency of about 26%, followed by the ASHP system, which had a relatively

higher value of 21%, while the maximum efficiencies of the ElcH and the GasB were only 11% and 9%, respectively.

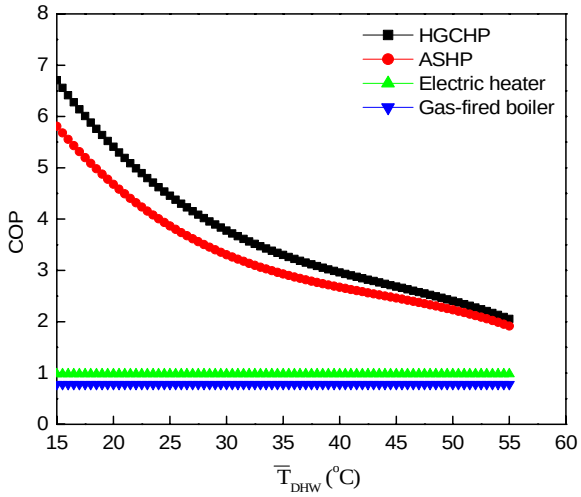

Figure 8.7 Comparisons of the *COP*s between the four DHW systems

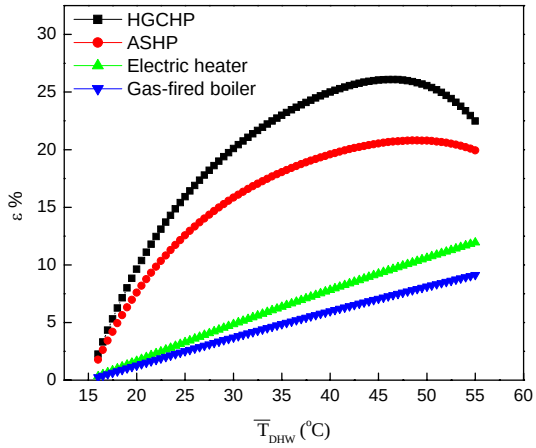

Figure 8.8 Comparisons of exergy efficiencies between the four DHW systems

It is noted that the exergy efficiencies of the HGCHP and ASHP systems were kept increasing until $\overline{T}_{DHW}$ reached approximately 46˚C and then began to be decreased with the increase of $\overline{T}_{DHW}$. The reduction can be explained through the fact that the increase of the power consumption dominated a major role in the exergy efficiency rather than the increase of the exergy gain in the case of the high temperature of $\overline{T}_{DHW}$. On the other hand, the exergy efficiencies of the ElcH and the GasB were always increased with the rise of $\overline{T}_{DHW}$ owing to the gradually reduced difference of energy quality between the energy supplied to the system and system output (hot water). Unfortunately, their exergy efficiencies were still much lower than those of the HGCHP and ASHP systems, even at the highest DHW temperature.

The presence of the high exergy losses in the ElcH and the GasB systems indicates a poor match between the quality of energy supplied to the system and the quality of output produced by the system. Taking a simple example of the GasB, the high-quality gas flame is at about 1000˚C while the low-quality hot water is always less than 60˚C. This mismatch obviously results in considerable irreversible losses because of the large irreversible heat transfer.

8.6 Summary Exergy analysis for the HGCHP with DHW supply has been presented and the energy and exergy performances of the HGCHP project in the four different operating modes have been evaluated based on the experimental data. A simplified expression of the exergy efficiency for DHW systems is proposed. Comparisons between the HGCHP system and other three kinds of DHW systems

have been made in terms of energy and exergy efficiencies. Some specific conclusions of this study are given as follows.

The detailed exergy analysis for each component in the HGCHP system indicated that the largest exergy loss occurred in the compressor in the case study. More attention should be devoted to reducing the exergy losses in compressors. The external exergy loss in compressors due to the electrical and mechanical efficiencies can be significantly reduced by improving the performance of the motors, valves or lubrication systems. The internal exergy loss due to the fluid friction and the pressure difference in the compressor can be progressively reduced by decreasing the condensing and evaporation pressure difference. In view of this, the GCHP's exergy efficiency is higher than that of the ASHP system because of the relatively moderate ground temperature which produces smaller pressure difference between the condensing and evaporation processes. The exergy destructions in the heat exchangers in this study were also significant, which can be reduced through increasing the heat transfer coefficient or the heat transfer area.

The results obtained from the comparisons showed that the HGCHP system had the highest energy and exergy efficiencies among the four DHW heating systems. The significantly low exergy efficiencies of the ElcH and GasB systems are caused by the mismatch of the high quality energy supply and low quality energy demand.

Finally, an optimum condition can be obtained for the HGCHP system to achieve high energy efficiency and simultaneously to keep high exergy efficiency through the co-analysis of the first and second laws of thermodynamics.

CHAPTER 9 ANNUAL HOURLY SIMULATION OF THE HGCHP WITH DHW SYSTEM

9.1 Introduction

Usually, a great number of factors affect the HGCHP performance, such as the heat pump capacity, various profiles of the DHW usage, the continuously changing environmental conditions, the building loads and the long-term heat transfer of the GHE. Therefore, an annual hourly simulation of this hybrid system is very important for analyzing the hourly operating performance of this system for a given building under given weather conditions. The main purpose of this chapter is to develop an hour-by-hour simulation model for the complex system including its all major components within a component-based modeling environment (HVACSIM+). The annual power consumption of the whole system will be calculated and meaningful comparisons with a conventional GCHP system and an electric hot water heater will be made.

9.2 System Description

As presented in Chapter 6, a small prototype HGCHP with DHW heating system was developed to provide space heating, space cooling and hot water heating. As is shown in Figure 6.2, this system consists of a water-to-water heat pump equipped with a desuperheater, a GHE, a thermal storage water tank and water pumps. The

heat pump has the capacities of 4.5kW in cooling mode and 4.9 kW in heating mode respectively. An apartment of 30m^2 in Hong Kong is used for the simulation with the heat pump providing the heating/cooling source.

The thermal tank, which is used to store DHW, is installed with an electric resistance element as a backup water heating source. The volume of the thermal tank is 120 liters. According to ASHRAE handbooks and the local DHW usage profile, the average daily DHW demand per person for a typical residential apartment is about 60 liters. Hence, generally speaking, the sample system with DHW heating can basically meet the requirements of space cooling, heating and DHW demand for a family of two persons.

The detailed configuration and specifications of the GHE in the system can be referred to Chapter 6.

The major components including the heat pump (with desuperheater), GHE, thermal storage tank and pumps are modeled individually in the following section.

9.3 Component Models

9.3.1 Heat pump model

A simple equation-fit model of the heat pump unit with a desuperheater is developed using the experimental data. The following assumptions are made prior to fitting the model equations.

1) The water flow rates through the heat pump unit are assumed constant since the thermophysical changes of pure water with temperature are relatively insignificant and neglected in the simulation model.

2) The water supply temperature to the conditioned space is assumed to be constant at 7˚C in cooling mode and 45 ˚C in heating mode.

Based on the aforementioned assumptions and experimental data, the parameters including the heat pump power consumption, load side heat transfer rate (Q_{load}) and DHW side heat transfer rate (Q_{DHW}) can be expressed as a function of heat pump entering water temperature (EWT) from the GHE and entering DHW temperature ($T_{dsp,in}$) from the thermal tank.

A second-order polynomial regression is employed here to identify the coefficients in the fitted equations of all the parameters. Taking the example of the heat pump power consumption, the equation is given as follows:

$$Power = a_1 + a_2 EWT + a_3 EWT^2 + a_4 T_{dsp,in} + a_5 T_{dsp,in}{}^2 + a_6 EWT \cdot T_{dsp,in} \qquad (9.1)$$

where, a_1 to a_6 are the coefficients fitted using the experimental data from the manufacturer, which are listed in Table 9.1.

A correction factor, which is defined as the ratio of the actual cooling/heating loads of the building to the heat transfer rate of the fitted load, is introduced to offset the deviation of the fitted values from the actual ones.

$$f = \frac{Q_{act,load}}{Q_{fit,load}} \qquad (9.2)$$

The heat pump power consumption fitted from experimental data should be corrected by multiplying the correction factor. Then, the system COP can be determined by:

$$COP = \frac{Q_{act,load} + Q_{DHW}}{Power} \tag{9.3}$$

The source side heat transfer rate (Q_{source}) can be consequently obtained using energy balance.

Table 9.1 Summary of the identified coefficients in the fitted equations

Modes/Variables		*a1*	*a2*	*a3*	*a4*	*a5*	*a6*	*Relative Error*
Cooling with DHW	Q_{DHW}	*0.076945*	*0.045974*	*0.002079*	*-0.01616*	*0.001043*	*-0.00321*	*2.6%*
	Power	*0.47217*	*0.031362*	*0.000142*	*-2.44E-05*	*3.77E-06*	*-7.32E-06*	*0.44%*
	Q_{load}	*5.0172*	*-0.02421*	*-3.96E-05*	*0.003788*	*-8.37E-05*	*5.32E-05*	*1.48%*
Heating with DHW	Q_{DHW}	*4.4432*	*0.030681*	*2.73e-4*	*-0.13562*	*0.001179*	*-4.5e-4*	*8.9%*
	Power	*1.5417*	*0.012303*	*-2.69e-4*	*0.0078664*	*-2.98e-5*	*1.52e-4*	*1.16%*
	Q_{load}	*-0.6583*	*0.079218*	*3.24e-4*	*0.14139*	*-1.21e-3*	*3.97e-4*	*2.88%*
Cooling	*Power*	*0.44939*	*0.03268*	*0.00012*	*0*	*0*	*0*	*0.82%*
	Q_{load}	*4.9079*	*-0.01191*	*-0.00017*	*0*	*0*	*0*	*0.37%*
Heating	*Power*	*2.128*	*0.018806*	*7.60e-05*	*0*	*0*	*0*	*1.2%*
	Q_{load}	*4.15*	*0.10815*	*0.001059*	*0*	*0*	*0*	*0.31%*

9.3.2 GHE model

Chapter 3 and Chapter 4 have elaborately developed the analytical (inclined finite line source) and numerical (finite element method) models of the inclined GHEs. It should be noticed that the short time-steps model based on the finite element numerical approach is utilized in the first ten hours simulation as an extension of the

long time-step model. Combined the heat transfer models outside and inside the boreholes, the temperatures of the circulating water to/from the heat pump can be determined, as shown in Equation (3.28). The entire GHE model also uses the techniques of spatial superimposition for multiple boreholes and sequential temporal superimposition for arbitrary heating/cooling loads of the system as proposed by Eskilson (1987).

9.3.3 Thermal storage tank model

The following assumptions are made in the thermal storage tank model.

- The water in the tank is assumed to be well-mixed and equal to the outlet water temperature;
- The radiation heat loss on the tank surface is neglected.

The governing equation for the tank model is given:

$$\rho V c_p \frac{dT}{dt} = UA\left(T_{ambient} - T\right) + \dot{m} c_p \left(T_{in} - T\right) \tag{9.4}$$

where ρ and c_p denote the water density and specific heat capacity at temperature T; V and $\dot{m}$ are the tank volume and water mass flow rate through the tank; UA is the overall heat transfer coefficient of the tank (5 W/K in this case); $T_{ambient}$ means the ambient air temperature.

To simplify the simulation process, the daily DHW usage time is set to be within 9:00~10:00 p.m. for shower and the thermal tank is refilled with make-up water at ambient temperature before 10 p.m. This means the HGCHP system will stop heating the DHW from 9 p.m. to 10 p.m. no matter whether the DHW temperature

achieves the set point or not. The resistance heating element can automatically operate when a thermostat detects the DHW supply temperature is still below the set value (50℃) until 9 p.m.

9.3.4 Circulation water pump model

A simplified simulation model for water pumps is employed because of their constant water flow rate and relatively small power consumption compared with that of the heat pump.

$$Power = \dot{m}\,\Delta p/(\rho\eta) \tag{9.5}$$

where, Δp and η denote the pressure increase and the efficiency of the water pump.

9.4 Building Loads and Ambient Air Temperature

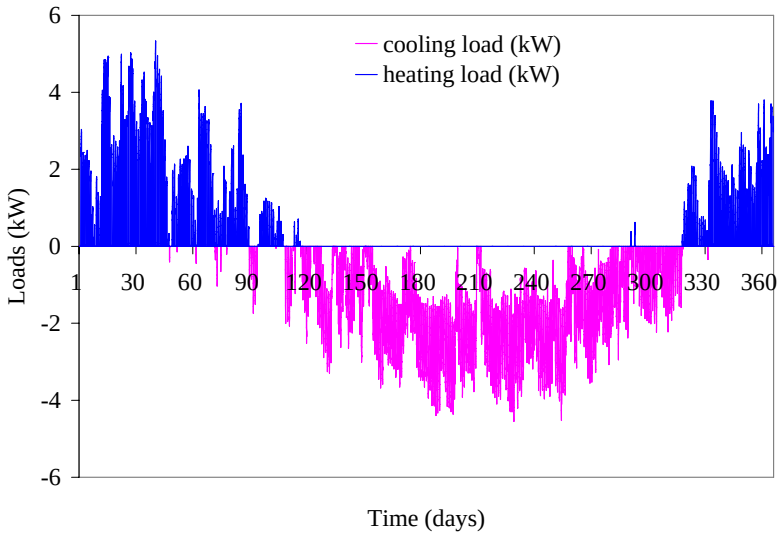

Figure 9.1 Annual building loads in the TMY in Hong Kong

(Cooling loads are negative and heating loads are positive)

The annual hourly loads of the sample building in the typical meteorological year (TMY) of 1989, as shown in Figure 9.1, were calculated using the building energy simulation software, HTB2 (Alexander, 1994). Figure 9.2 illustrates the average hourly ambient air temperature during the TMY.

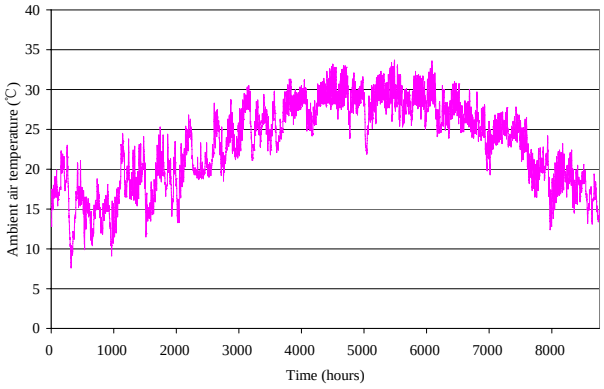

Figure 9.2 Annual ambient air temperatures in the TMY in Hong Kong

9.5 Simulation of HGCHP with DHW Using HVACSIM+

The system is constructed in the HVACSIM+ modeling environment, which stands for 'HVAC Simulation Plus other systems'. It was initially developed by the National Institute of Standards and Technology (NIST) (Clark 1985) and updated to a visual interface version using an event driven approach (Varanasi 2002). It is capable of modeling HVAC systems, HVAC controls, buildings, energy management systems and other thermal systems. The HVACSIM+ represents HVAC elements as individual component (e.g. fans, pumps, pipes, etc.) connected to form a complete system, which allows users to develop new models and introduce them in the package to simulate them in various configurations. A number of

modular components related to ground source heat pump systems have been developed by a research group in U.S.A (Yavuzturk and Spitler 1999; Ramamoorthy, et al., 2001; Jin and Spitler 2002).

The entire system is configured in the visual modeling environment (HVACSIM+), as shown in Figure 9.3. All the components in the system are represented as icons and pictures. The boundary parameters include the cooling/heating loads, ambient air temperature, and water flow rates in the GHE and DHW loops. The input variables of each component are connected either to the output variables of other components or to specified boundary conditions according to the system operation principle.

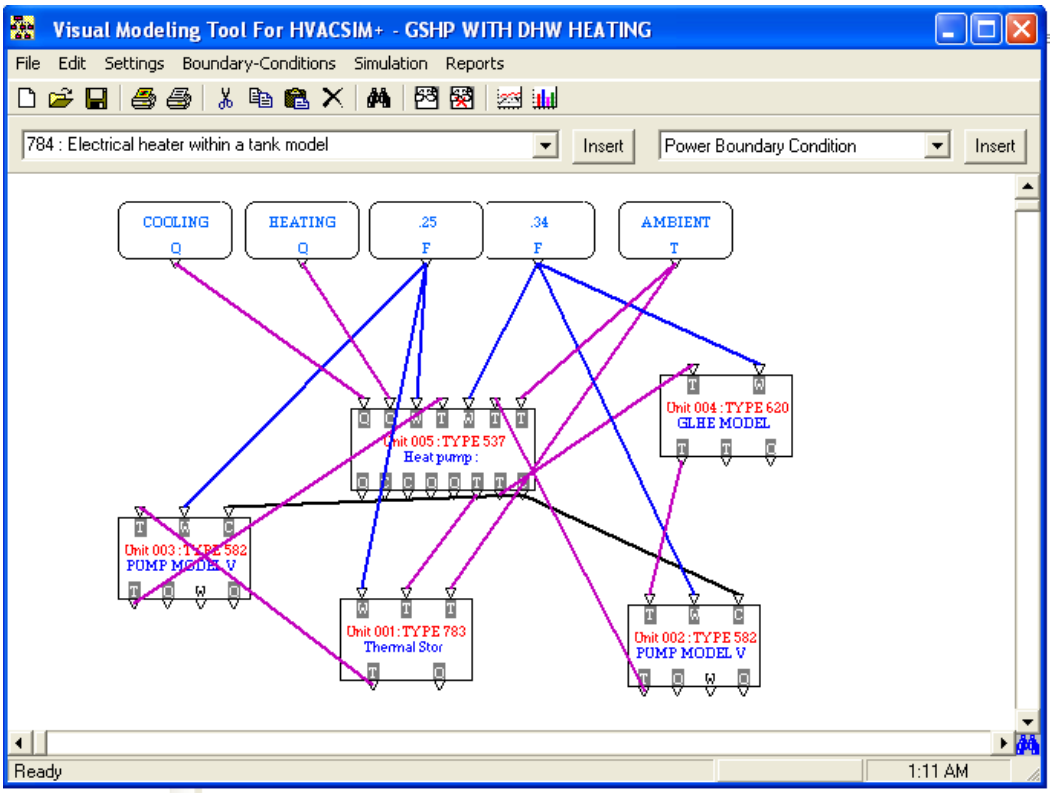

Figure 9.3 System configuration in the visual HVACSIM+ environment

9.6 Simulation of GCHP System and Electric Heater Using HVACSIM+

A conventional GCHP system for space heating/cooling and an electric heater commonly used for DHW heating in Hong Kong are also constructed and simulated in HVACSIM+ for the sake of comparisons with the HGCHP system. The combination of the GCHP system and the electric heater is referred to as a base case.

9.7 Simulation Results and Discussion

The annual simulations of the HGCHP system and the base case are conducted under the HVACSIM+ environment. Some critical performance parameters are obtained and plotted in Figures 9.4-9.7.

9.7.1 GHE thermal performance

Figures 9.4 and 9.5 illustrate the variations of hourly heat pump entering and exiting water temperatures (*EWT/ExWT*) from/to the GHE, respectively, in one simulation year. The maximum value of the *EWT* for the HGCHP system was about 37˚C, whereas the *EWT* of the base case reached a peak of 52˚C. As can be seen from the curves, the *EWT* for the HGCHP system almost returned back to its initial value after the first year of a heating/cooling circle. By contrast, a temperature increase of 3˚C for the base case was observed after one year operation.

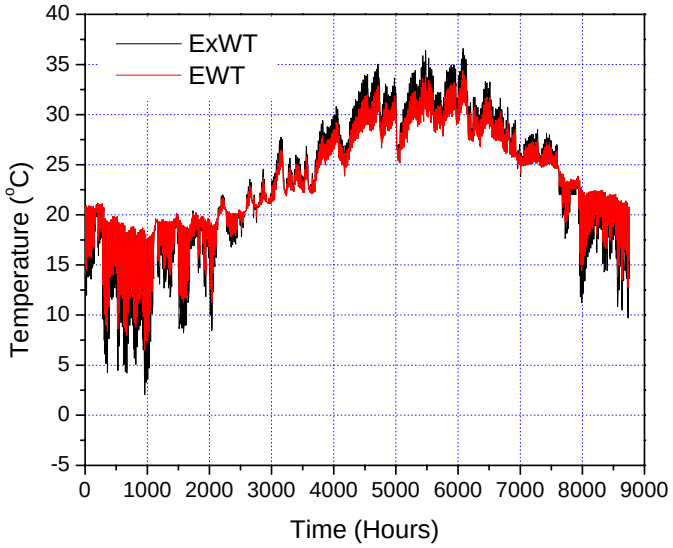

Figure 9.4 Hourly variations of *EWT* and *ExWT* for the HGCHP system

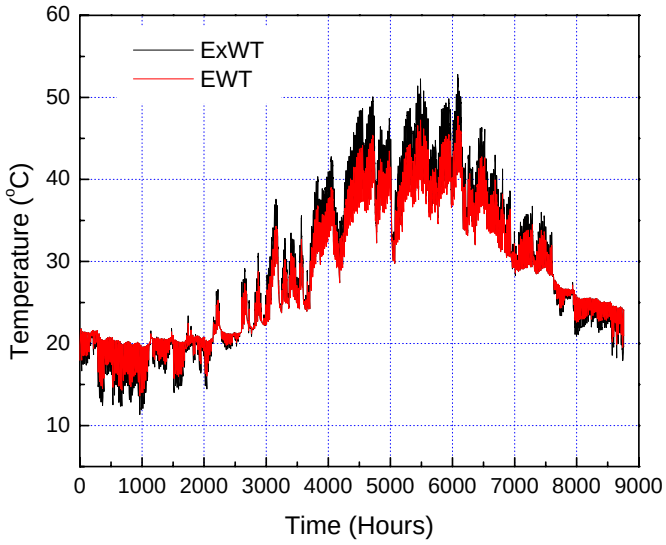

Figure 9.5 Hourly variations of *EWT* and *ExWT* for the GCHP system (base case)

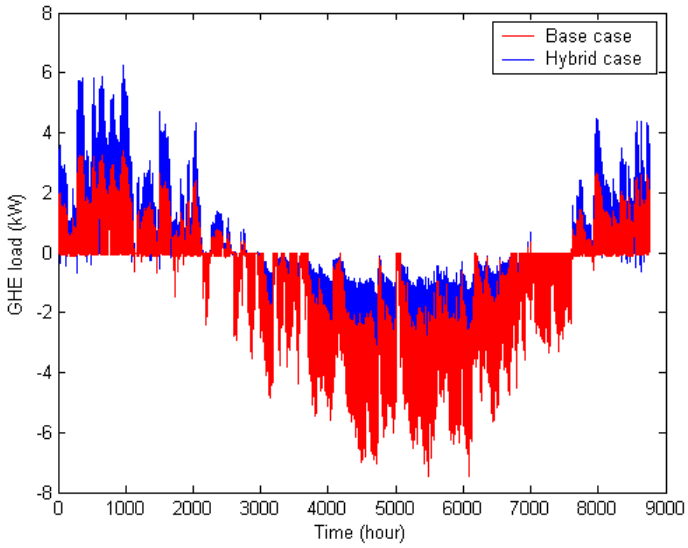

Figure 9.6 comparisons of GHE loads between the HGCHP system and the base case

The hourly variations of the GHE loads (i.e. heat rejection or extraction to/from the ground) of the HGCHP system and the conventional GCHP system (base case) are described in Figure 9.6. As expected, the HGCHP system rejected much less heat to the ground in cooling season and, on the other hand, extracted more heat from the ground in heating season than the base case owing to the favorable function of the DHW heating.

Based on the comparisons associated with the GHE loads and values of *EWT/ExWT* between the HGCHP and the base case, it is concluded that the HGCHP system can effectively alleviate the thermal imbalance of the GHEs by means of adding a desuperheater in the system to produce DHW.

9.7.2 Energy consumptions

The monthly accumulative energy consumptions of the HGCHP system and the base case, which include the energy consumed by the heat pump, water pumps and electric heater, are calculated according to the hourly simulation results, as shown in Figure 9.7.

As can be found from the two bars in each month (the left is HGCHP system and right is the base case), the energy consumption of the HGCHP system was significantly lower than that of the base case in cooling season due to the lower EWT of the HGCHP system. For the heating mode, the heat pump power consumption of the HGCHP system was slightly higher as compared with the base case, because of the greater heat extraction from the GHE to heat DHW. However, the total energy consumed by the DHW in the HGCHP system was distinctly lower than the base case.

As a whole, the annual total energy consumption of the HGCHP system for space cooling and heating achieved a reduction of nearly 10% as compared with the base case. For the energy consumption by the DHW heating (including the circulation DHW pump and the supplemental electricity), the HGCHP system offered a considerable energy saving of 67% of the base case (the electric heater) during the first year of operation. In addition, it is estimated that the HGCHP system can offer almost 95% of the DHW demand for two persons all the year round.

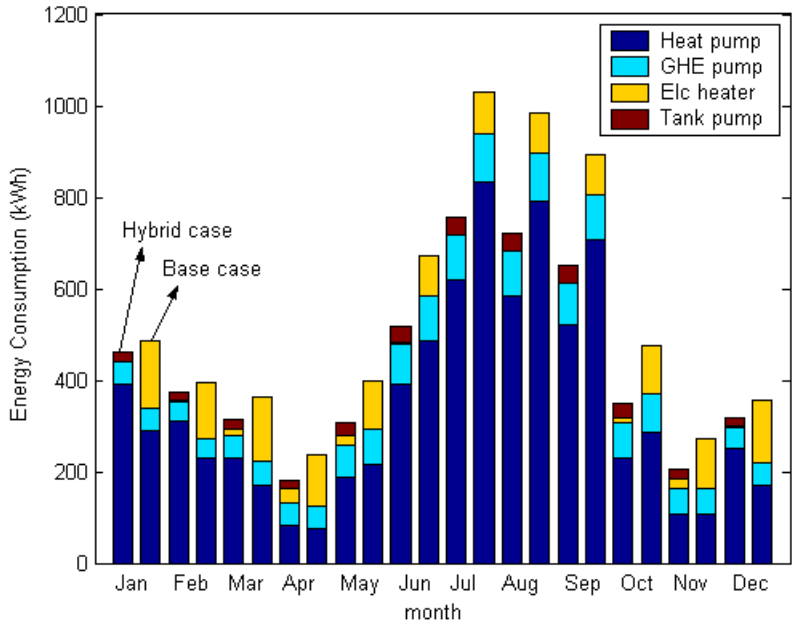

Figure 9.7 Energy consumptions of the HGCHP system and the base case

9.8 Summary

A simulation model of the HGCHP with DHW heating system has been developed within the HVACSIM+ environment. Since the DHW usage and the building loads are strongly influenced by the ambient air temperature, an annual hourly simulation for the hybrid system has been performed for a small residential apartment in Hong Kong. To compare the HGCHP system performance with conventional systems, a GCHP system for space cooling/heating and an electric heater for DHW supply are also modeled and simulated on an hourly basis within the HVACSIM+ as a base case. Some specific conclusions obtained from this case study are described as follows:

1. The HGCHP system can effectively alleviate the imbalanced loads of the GHE which exhibits lower *EWT* to the heat pump than that of the GCHP system.
2. The general energy saving of the HGCHP system for space cooling/heating was about 10% compared with the GCHP system in the first simulation year.
3. The HGCHP can offer almost 95% of total DHW demand in this case study along with about 67% energy saving compared with the electric heater.

An analysis of the simulation data shows that the HGCHP with DHW supply system has significantly high performance compared with the conventional systems, which is thus a good option to provide space cooling/heating and DHW as well for residential buildings in warm-climate areas.

CHAPTER 10 CONCLUSIONS AND RECOMMENDATIONS FOR FUTURE WORK

A new hybrid GCHP system incorporated with a desuperheater and an inclined GHE has been proposed to provide space cooling, heating and DHW heating for residential buildings in warm-climate areas. This thesis focuses on developing the simulation model of the HGCHP system and investigating the operating performance in terms of the energetic and exergetic efficiencies in different operation modes. In this chapter, only the main points are highlighted as the concluding remarks have been given at the end of each chapter.

10.1 Simulation Models of the Inclined GHEs

An inclined finite line-source model in a semi-infinite medium has been developed to describe the transient and steady-state heat conduction processes in GHEs for long-term operation.

- The representative temperature of a specific point on the middle cross-section circle of the borehole wall was proposed for the design of GHEs instead of the integral average temperature along the cross-section circle and the borehole depth, which can greatly simplify the calculation and reduce the computing time.
- The thermal interference between two inclined boreholes can be approximately simplified to that of two supposed vertical boreholes

disposed at a distance between the middle points of the inclined boreholes. The representative temperature obtained from this approximate method is recommended for engineering design.

- A semi-empirical function with satisfactory accuracy has been proposed to substitute the steady-state integral average temperature of the inclined borehole wall.
- Comparisons between the inclined and vertical GHEs with typical rectangular patterns show that the temperature rise on the borehole wall of the inclined GHE can be 10%~35% lower than that of the vertical GHE for long-term performance under commonly encountered conditions in engineering practice.
- Finally, the accuracy of the analytical model of the inclined finite line source was experimentally validated through the pilot project under the cooling mode.

A finite element numerical model was developed as an extension of the finite line source to deal with the heat transfer of the GHEs in short-time scale operation.

- Experimental validation of the numerical model was conducted by means of the measured U-tube wall temperatures under various operating modes during a short-time period. The results illustrate that the finite element numerical model is quite suitable for analyzing the heat transfer behavior of the GHEs in short time scale instead of the typical finite line-source model.

- Furthermore, the variation of the U-tube pipe wall temperatures illustrates that the alternative cooling/heating modes can effectively alleviate the heat buildup in surrounding soil, which can ultimately improve the system performance.

To sum up, inclusion of inclined boreholes in the GHE configuration can improve its thermal performance especially for the systems with imbalanced annual loads and limited land allowance to install the GHE. In order to achieve high efficiency, the alternative cooling/heating modes and the discontinuous operation mode which can reduce the GHE loads (such as operating during daytime while shut down at night or vice versa) are recommended and it is feasible for commercial or residential buildings.

10.2 Simulation Model of the HGCHP with DHW System

A detailed steady-state simulation model for a water-to-water heat pump unit equipped with a desuperheater has been developed based on the basic conservation laws of mass and energy as well as heat transfer correlations. In addition, a comprehensive simulation program of the HGCHP system which incorporates the heat pump and GHE models was also developed, including a user-friendly interface for the convenience of flexibly changing or setting up various parameters.

The simulation model of the HGCHP system was extensively validated using the experiments, covering the four different operation modes which are commonly used in practice (i.e. cooling only, cooling with DHW, heating with DHW and DHW

heating modes). The results show, on the whole, the simulation model is generally accurate to within ±15% of the experimental data.

According to the experimental results, the desuperheater can capture a significantly large percentage of the total heat in the HGCHP unit, ranging from 10%~57%, depending strongly on the inlet DHW temperature to the heat pump. The experiments also indicate that the HGCHP system can achieve a relatively high performance in all the operation modes with DHW heating, for example, an average *COP* of 3.5 in the cooling with DHW mode, and about 4 in heating with DHW and 3.5 in DHE heating mode. However, the average *COP* of the cooling only mode was only 3 in the test. It should be noted that a high DHW temperature can evidently reduce the system performance. Therefore, in order to achieve higher operating performance, it is recommended to use a desuperheater to preheat DHW if possible.

In summary, the simulation model for the HGCHP with DHW supply can provide a useful and effective tool to analyze the system performance in a variety of operating modes. In addition, it is also suitable for research study and engineering applications with an acceptable accuracy.

10.3 Exergy and Energy Analysis of the HGCHP System

Exergy and energy performances of the HGCHP system in the four different operating modes has been evaluated based on experimental data and the simulation results.

The detailed exergy analysis for each component in the HGCHP system indicates that the largest exergy loss was made in the compressor in the case study. The

exergy destructions in the heat exchangers in this study were also significant, which can be improved through increasing the heat transfer coefficient or the heat transfer area of the equipment.

Comparisons between the HGCHP system and other three kinds of DHW systems have been made in terms of energy and exergy efficiencies. The results show that the HGCHP system had the highest energy and exergy efficiencies among the four DHW heating systems. An optimum condition may be obtained for the HGCHP system to realize high energy efficiency and simultaneously to keep high exergy efficiency through the co-analysis of the first and second laws of thermodynamics.

Finally an annual hourly simulation of the hybrid system for a small residential apartment in Hong Kong has been performed within the HVACSIM+ environment. To compare the HGCHP system performance with conventional systems, a GCHP system for space cooling/heating and an electric heater for DHW supply were also modeled and simulated on an hourly basis within the HVACSIM+ as a base case. Some specific conclusions drawn from this case study are described as follows:

- The HGCHP system can effectively alleviate the imbalanced loads of the GHE which exhibits lower *EWT* to the heat pump than that of the GCHP system.
- The general energy saving of the HGCHP system for space cooling/heating was about 10% compared with the GCHP system in the first simulation year.
- The HGCHP can offer almost 95% of the total DHW demand in this case study along with about 67% energy saving compared with the electric heater.

An analysis of the simulation data shows that the HGCHP with DHW supply system can achieve significantly high performance compared with conventional systems. The results demonstrate that it is feasible and desirable to apply the HGCHP with DHW supply system to cooling-dominated buildings in Hong Kong and other areas in Southern China.

10.4 Recommendations for Future Work

It is worthwhile and necessary to make further investigations on the HGCHP systems.

Due to limitations of the experimental rig, the accuracy of the simulation model for the HGCHP system was verified only using the external water parameters together with the power consumptions of the compressor in this thesis. Actually, the simulation model should be further validated through the measured internal refrigerant properties, such as temperature and pressure, which can identify any default or improper settings in the simulation model.

Furthermore, it may be extremely time-consuming to employ the simulation program to design an efficient system with an optimal combination of components, since the simulation model developed in this study is limited to analyze the operating performance of the HGCHP systems. This is realizable if a specific optimum method can be incorporated into the simulation program, such as Genetic Algorithm.

Finally, it is of importance to introduce economic analysis to further investigate the lifecycle cost of the system along with the exergy cost, which can comprehensively evaluate the performance of the HGCHP systems.

REFERENCES

Alexander, D.K. 1994. HTB2 user manual version 2.0. Welsh School of Architecture, University of Wales College of Cardiff.

Allen, J.J. and J.F. Hamilton. 1983. Steady-state reciprocating water chiller models. ASHRAE Transactions, 89(2A): 398-407.

ASHRAE, 1995. Commercial/Institutional Ground-Source Heat Pump Engineering Manual. American Society of Heating, Refrigeration and Air-Conditioning Engineers. Inc., Atlanta.

ASHRAE, 1999. ASHRAE Handbook, HVAC applications. American Society of Heating, Refrigeration and Air-Conditioning Engineers, Inc., Atlanta.

ASHRAE. 2000 ASHRAE Handbook, HVAC Systems and Equipment. Atlanta: American Society of Heating, Refrigerating, and Air-Conditioning Engineering, Inc., Atlanta.

ASHRAE, 2005. Handbook: Fundamentals. American Society of Heating, Refrigerating and Air-conditioning Engineers, Inc., Atlanta.

Ball, David A.; Robert D. Fischer, David L. Hodgett. 1983. Design methods for ground-source heat pumps. *ASHRAE Transactions*, 89(2B): 416-440.

Beck, J., K. Cole, A. Haji-Sheikh, and B. Litkouhi. 1992. Heat Conduction Using Green's Functions, published by Hemisphere.

Bensafi, A., S. Borg, D. Parent. 1997. CYRANO: a computational model for the detailed design of plate-fin-and-tube heat exchangers using pure and mixed refrigerant. *International Journal of Refrigeration*, 20(3): 218-228.

Bernier, Michel A. 2001. Ground-Coupled Heat Pump System Simulation. ASHRAE Winter Meeting CD, Technical and Symposium Papers, ASHRAE, 739-750.

Bose, J.E., J.D. Parker and F.C. McQuiston. 1985. Design/data manual for closed-loop ground coupled heat pump systems, Oklahoma State University for ASHRAE.

Bose, J.E., M.D. Smith, J.D. Spitler. 2002. Advances in Ground Source Heat Pump Systems - An International Overview. Proceedings of the Seventh International Energy Agency Heat Pump Conference. 1:313-324. Beijing.

Cane, R.L.D., D.A. Forgas. 1991. Modeling of ground-source heat pump performance. *ASHRAE Transactions*, n pt 1: 909-925

Caneta Research Inc., 1995. Commercial/Institutional Ground-Source Heat Pump Engineering Manual, ASHRAE, Atlanta.

Carslaw, H. S. and J. C. Jaeger. 1946. Conduction of Heat in Solids. Oxford, U.K.: Claremore Press.

Cervantes, J.G., and E. Torres-Reyes. 2002. Experiments on a solar-assisted heat pump and an exergy analysis of the system. *Applied Thermal Engineering*, 22(12): 1289-1297.

Chaturvedi, S.K., T.O. Mohieldin, D.T. Chen. 1991. Second-law analysis of solar-assisted heat pumps. *Energy*, 16 (6): 941-949.

Chi J., D. Didion. 1982. A simulation model of the transient performance of a heat pump. International Journal of Refrigeration, 5(3): 176-184.

Chiasson, A.D., C. Yavuzturk, and W.J. Talbert. 2004. Design of school building HVAC retrofit with hybrid geothermal heat-pump system. *Journal of Architectural Engineering*, Vol. 10, No. 3, pp: 103-111.

Clark, D.R. 1985. HVACSIM+ building systems and equipment simulation program reference manual. NBSIR 84-2996. National Bureau of Standards.

Cui, P., H.X. Yang, Z.H. Fang. 2007. The simulation model and design optimization of ground source heat pump systems. HKIE Transactions, 14(1): 1-5.

Deerman, J. D., S.P. Kavanaugh. 1991. Simulation of vertical u-tube ground coupled heat pump systems using the cylindrical heat source solution. *ASHRAE Transactions* 97(1): 287-295.

Deng, S.M., Y.Q. Jiang. 2003. Retrofitting hot water supply in Hong Kong luxury hotel. *ASHRAE Journal*, 45(12): 52-55.

Diao, N.R., Q.Y. Li, Z.H. Fang. 2003. An analytical solution of the temperature

response in geothermal heat exchangers with groundwater advection, *Journal of Shandong Institute of Architecture and Engineering*, 18(3):1–5.

Diao, N.R., H.Y. Zeng, Z.H. Fang. 2004. Improvement in modeling of heat transfer in vertical ground heat exchangers: *HVAC and R Research*, 10(4): 459-470.

Diao, N.R., H.Y. Zeng and Z.H. Fang. 2004. Heat transfer in ground heat Exchangers with groundwater advection. *International Journal of Thermal Sciences*, 43 (12): 1203-1211.

Dincer, I., 2002. The role of exergy in energy policy making, *Energy Policy*, 30(2): 137-149.

Domanski, P., and D. Didion. 1983. Computer modeling of the vapor compression cycle with constant flow area expansion device. *NBS Buidling Science Series* 155.

Eckert, E.R.G and R.M Drake. 1972. Analysis of heat and mass transfer, *McGraw-Hill*, New York, 104-106.

Electrical and Mechanical Services Department, Hong Kong Energy End-use Data 2006. *Hong Kong Special Administrative Region*, China: http://www.emsd.gov.hk/emsd/e_download/pee/hkeeudb_2006full_20070328.pdf

Eskilson, P. 1987. Thermal analysis of heat extraction boreholes. Ph.D. thesis, *University of Lund*, Sweden.

Fang, Z.H., N.R. Diao and P. Cui. 2002. Discontinuous operation of geothermal heat exchangers, *Tsinghua Science and Technology*, 7(2):194-197.

Fanney, A.H., B.P. Dougherty. 1992. Performance of a residential desuperheater. *ASHRAE Transactions*, 98(1): 489-499.

Incropera, F.P., D.P. DeWitt. 1990. Fundamentals of heat and mass transfer. *New York: Wiley,* P508.

Geoffrey, K.F., K.K. Tso, W. Yau. 2003. A study of domestic energy usage patterns in Hong Kong, ***Energy***, 28(15): 1671-1682.

Gu, Y., D.L. O'Neal 1998. Development of an equivalent diameter expression for vertical U-Tubes used in ground-coupled heat pumps. *ASHRAE Transactions* 104: 347-355.

Hackner, R.J., P.J. Hughes, R.A. O'Neil. 1987. Design of ECHP Systems in Northern Climates. *ASHRAE Transactions*, 93.

Hamilton, J.F., J.L. Miller. 1990. A simulation program for modeling an air-conditioning system. *ASHRAE Transactions*, 96(1), pp. 213-221.

Hart, D. P., R. Couvillion. 1986. Earth coupled heat transfer. *Publication of the National Water Well Association*.

Hellstrom, G. 1989. Duct ground heat storage model manual for computer code. *Department of Mathematical Physics, University of Lund,* Sweden.

Hellstrom, G. 1991. Ground heat storage : Thermal Analyses of duct storage systems. Sweden :Department of Mathematical Physics University of Lund .

Hepbasli, A., O. Akdemir. 2004. Energy and exergy analysis of a ground source (geothermal) heat pump system. *Energy Conversion and Management*, 45(5): 737-753.

Hepbasli, A. 2005. Thermodynamic analysis of a ground-source heat pump system for district heating. *International Journal of Energy Research*, 29(7): 671-687.

Hikmet, E., I. Mustafa, E. Mehmet and P. Kazim. 2007. Energy and exergy analysis of a ground-coupled heat pump system with two horizontal ground heat exchangers. *Building and Environment*, 42 (10): 3606-3615.

Holman, J.P., 1989. Experimental methods for engineers (fifth ed.). *McGraw-Hill*, New York 41–49.

IGSHPA, 1988. Closed-loop/ground-source heat pump systems – Installation guide.

Ingersoll, L.R., O.J. Zobel, and A.C. Ingersoll. 1954. Heat conduction with engineering, geological, and other applications. New York: *McGraw-Hill*.

Ingersoll, L.R., H.J. Plass. 1948. Theory of the ground pipe source for the heat pump. *ASHVE Trans.* 54, 339-348.

Ingersoll, L.R., F.T. Adler, H.J. Plass & A.C. Ingersoll. 1950. Theory of earth heat exchangers for the heat pump. *ASHVE Trans*. 56, 167-188.

Jin, Hui, J.D. Spitler. 2002. A parameter estimation based model of water-to-water heat pumps for use in energy calculation programs. *ASHRAE Transactions*, 108(1):

3-17.

Kandlikar, S.G. 1983. An improved correlation for prediction two-phase flow boiling heat transfer coefficient in horizontal and vertical tubes. *ASME,* New York.

Kandlikar, S.G. 1990. A general correlation for saturated two-phase flow boiling heat transfer inside horizontal and vertical tubes. *Journal of Heat Transfer*, 112(2): 219-228.

Kavanaugh, S.P. 1985. Simulation and experimental verification of vertical groundcoupled heat pump systems. Ph.D. dissertation. Stillwater, Oklahoma: Oklahoma State University.

Kavanaugh, S.P. and K. Rafferty. 1997. Ground-source heat pumps, design of geothermal systems for commercial and institutional buildings. *ASHRAE*, Atlanta.

Kavanaugh, S.P. 1998. A design method for hybrid ground-source heat pumps. *ASHRAE Transactions*, 104(2): 691-698.

Kavanaugh, S.P. 1992. Field test of a vertical ground-coupled heat pump in Alabama. *ASHRAE Transactions*, 98, pt 2: 607-615.

Klein, S. A., et al. 1996. TRNSYS Manual, a transient simulation program. *Madison: Solar Engineering Laboratory*. University of Wisconsin-Madison.

Kotas T. J. 1985. The exergy method of thermal plant analysis. *Tiptree, Essex*: Anchor Brendon Ltd.

Lee, A.H.W. and J.W. Jones. 1996. Thermal performance of a residential desuperheater/water heater system. *Energy Conversion and Management*, 37(4): 389-397.

Liu, X.L., D.L. Wang and Z.H. Fang. 2001. Modeling of heat transfer of a vertical bore in ground-source heat pumps. *Journal of Shandong Institute of Architecture and Engineering*, (1), 47-51.

Lockhart, R.W., R.C. Martinelli. 1949. Proposed correlation data for isothermal two-phase two-component flow in pipes. *Chemical Engineering Progress*, 45(1): 39-48.

Mei, V.C. and C.J Emerson. 1985. New approach for analysis of ground-coil design for applied heat pump systems. *ASHRAE Transactions* 91(2): 1216–1224.

Miles, L.. 1994. Heat pumps: theory and service. Albany, *N.Y.: Delmar Publishers.*

Muller-Steinhagen, H. & K. Heck. 1986, A simple pressure drop correlation for two-phase flow in pipes, *Chem. Eng. Process*, 20: 297-308.

Muraya, N.K., D. L. O'Neal and W. M. Heffington. 1996. Thermal interference of adjacent legs in a vertical U-tube heat exchanger for a ground-coupled heat pump. *ASHRAE Transactions* 102(2):12-21.

Ozgener, O., A. Hepbasli. 2005. Exergoeconomic analysis of a solar assisted ground-source heat pump greenhouse heating system. *Applied Thermal Engineering*, 25(10):1459-1471.

Ramamoorthy, M., H. Jin, A.D. Chiasson and J.D. Spitler, 2001. Optimal sizing of hybrid ground-source heat pump systems that use a cooling pond as a supplemental heat rejecter-A system simulation approach. *ASHRAE Transactions*, 107 (1): 26-38.

Rawlings, R.H.D., J.R. Sykulski. 1999. Ground source heat pumps: A technology review. *Building Services Engineering Research and Technology*, 20(3): 119-129.

Ren, C.Q., G.F. Tang, N.P. Li; G.F. Zhang, J. Yang. 2001. Exergy analysis of moist air and energy saving potential in HVAC by evaporative cooling or energy recovery. *Proceedings of the International Conference on Energy Conversion and Application (ICECA'2001)*, Vol. 1: 120-124.

Rosen, M.A., I. Dincer. 2004. Effect of varying dead-state properties on energy and exergy analyses of thermal systems. *International Journal of Thermal Sciences*, 43:121–133.

Rottmayer, S.P., W.A. Beckman, and J.W. Mitchell. 1997. Simulation of a single vertical U-tube ground heat exchanger in an infinite medium. *ASHRAE Transactions* 103(2): 651-659.

Shao, S.Q., W.X. Shi, X.T. Li, J. Ma. 2004. A new inverter heat pump operated all year round with domestic hot water. *Energy Conversion and Management*, 45:

2255-2268.

Spitler, J.D.. 2005. Ground-source heat pump system research past, present and future. *HVAC and R Research*, 11(2): 165-167.

Stefanuk, N.B.M., J.D. Aplevich, M. Renksizbulut. 1992. Modeling and simulation of a superheat-controlled water-to-water heat pump. *ASHRAE Transactions*, 98(2): 172-184.

Tan, K.X. and S.M. Deng. 2002. A simulation study on a water chiller complete with a desuperheater and a reversibly used water cooling tower (RUWCT) for service hot water generation. *Building and Environment*, 37(7): 741-751.

Thornton, J.W., T.P. McDowell, J.A. Shonder, P.J. Hughes, D. Pahud, G. Hellstrom. 1997. Residential vertical geothermal heat pump system models: Calibration to data. *ASHRAE Transactions,* 103(2): 660-674.

Treado, S.J., T. Snouffer. 2001. Measurement considerations for the determination of central plant efficiency. *ASHRAE Transactions*, 107(1): 401–406.

Varanasi, A. 2002. Visual modeling tool for HVACSIM+. M.S. Thesis, Oklahoma State University, School of Mechanical and Aerospace Engineering. Available online at www.hvac.okstate.edu.

Wallis, G.B. 1969. One-dimensional two-phase flow: *McGraw-Hill,* 51-54.

Wark, K. 1995. Advanced thermodynamics for engineers, New York: *McGraw-Hill*.

Wu, Y.Z. 1997. Design guideline for the small refrigeration equipment. *Mechanical industry press,* Beijing, China.

Yavuzturk, C. 1999. Modeling of vertical ground loop heat exchangers for ground source heat pump systems. PhD thesis, Oklahoma State University, USA.

Yavuzturk, C., and J.D. Spitler, 1999. A short time step response factor model for vertical ground loop heat exchangers. *ASHRAE Transactions* 105(2):475-485.

Yavuzturk, C., J.D.Spitler, S.J. Rees. 1999. A Transient two-dimensional finite volume model for the simulation of vertical U-tube ground heat exchangers. *ASHRAE Transactions*, 105 (A): 465-474.

Yavuzturk, C., J.D. Spitler. 2001. Field validation of a short time step model for

vertical ground-loop heat exchangers. *ASHRAE Transactions*, 107(1): 617-625.

Yavuzturk, C., J.D. Spitler. 2000. Comparative study to investigate operating and control strategies for hybrid ground source heat pump systems using a short time-step simulation model. *ASHRAE Transactions*, 106(2):192-209.

Yu, M.Z., N.R. Diao, D.C. Su and Z.H. Fang. 2002. A pilot project of the closed-loop ground-source heat pump system in China, *Proceeding of IEA 7th Heat Pump Conference*, Beijing, 356-364.

Zeng, HY, N.R. Diao, Z.H. Fang. 2002. A finite line-source model for boreholes in geothermal heat exchangers. *Heat Transfer Asian Research*, 31(7): 558-567.

Zeng, H Y, N.R. Diao, Z.H. Fang. 2003. Efficiency of vertical geothermal heat exchangers in ground source heat pump systems. *Journal of Thermal Science*, 12(1): 77-81.

Zeng, H Y, N.R. Diao, Z.H. Fang. 2003. Heat transfer analysis of boreholes in vertical ground heat exchangers. International Journal of Heat and Mass Transfer, 46 (23): 4467-4481.

APPENDIX MAIN PROGRAM CODES

```
C MAIN PROGRAME for the HGCHP system with DHW heating and inclined borehole    *
C this program developed in 2006 Dec.: consist of submodels of Compressor, condenser,    *
C                                evaporator, desuperheater, expansion valve(cappliary), and GHE *
C    icool meaning: 1=cool; 2=cool with hot water; 3=hotwater and heat;4=hotwater;5=heat *
C    icom meaning : 0=rotary compressor; 1=reciprocating compressor                -     *
C    IDP=used to calculate pressure drop                                                 *
C     Compressor is a rotatory compressor                                               *
C    three heat exchangers are tube-in-tue, R is inside the pipe;Water is outside the pipe     *
C    WFR= water flow rate                                                              *
*************************************************************************

       implicit real(a-z)
      INTEGER IFLUID,N1,LSTOP,M1,M2,M3,BORENUMBER,npipe,tnumber,ih3,
       &              IFANTI,ANTISTOP,Ihot,JG,JM,ix,jy,nx,nxx,ny,nyy,icool,icom
       %              ,ivlv,ipressure,idp,AreaNo,JA
      COMMON /RTEMP/TRCON1,TRCON2,TREVP1,TREVP2,TRHOT1,TRHOT2
      COMMON /COMPRESULT/MR,win,QC,Q0,H1,H2,H3,H4,T1,T2,T3,T4,cop,
       &                              EER,HINEVP,HOUEVP,ih3,tcomout
      COMMON /MAIN/IFLUID,TE,TC,DTS,X,VTH,MFCON,MFEVP,TFCON1,TFEVP1
       &                    ,RIEVP,RICON,LANEVP,LANCON,MFHOT,TFHOT1,ICool,JG,dtu
      COMMON /CONX2/HSL,HSV,HIN,HOU
      common /com_pressure/ pp1,pp2,pe,pc,p1,p2,icom,ivlv
      COMMON /CONRESULT/ TFCON2,LCON1,LCON2,LCON3,
       &                          CONJUDGE1,CONJUDGE2,QCON,LCON,QSC,QTP,QSH
      COMMON /EVPRESULT/ TFEVP2,LEVPTP,LEVPSH,LEVP,QEVP
        COMMON /PANDUAN/LSTOP,XMIN,XMAX,H33
      COMMON /M/ MCONSC,MCONTP,MCONSH,MEVPTP,MEVPSH,MEVP,MCONPIPE,
       &                MEVPPIPE,MhotPipe,MHOT,MHotSc,MhotSH,MHotTP,m00,JM
      common /hotw/ LHOT0,LHOT,TFhot2,HhotOU,Qhot0,Qhot,QhotSC,QhotTP,
       &                    QhotSH,Lhot1,Lhot2,Lhot3,HotJUDGE1,HotJUDGE2
      common /DPressure/DpEvp,DpevpMin,DpEvpMax,Dpcon,DpconMin,DpconMax,
       $                           Pein,Pcout,t3c,DpEvp0,Dpcon0,HSL3,DPHOT,DPCONTP
       &                           ,ipressure
      COMMON /ANTI/ IFANTI,NONGDU
      COMMON /QGROUND/QGHE(1000),dist(100),EWT(1000),TFM(1000),OWT(1000)
       &                          ,TFCON0(1000),TFHOT0(1000),CONOWT(1000),
       &                          TotalTime(1000),pro(9),GHEload(1000)
      COMMON/VapPHT/FitA1,FitA2,FitA3,FitA4,FitA5,
       $                    FitA6,FitA7,FitA8,FitA9
        COMMON /EXERGY/ Tenv0,Henv0,Senv0,ExR1,ExR2,ExR3,ExR4,penv0,Venv0
       &                          ,v1,v2,s4l,s4q
        common /capillarytube/Dcap,Lcap,lcap0,mr0
      COMMON/COMP/ r,xiaob,a2,b2,c2,a3,b3,c3,a4,b4,c4,
       &                    a5,b5,c5,a6,b6,c6,k,alafa,xiaocc,XIAOtc,dc,t0,
       &                    a,b,c,d,e,f,g,d1,d2,d3,d4,d5,d6,xiaoc1,
       &                    xiaoc2,xiaoc3,xiaoc4,xiaoc5,xiaoc6
        DIMENSION GROUNDPRO(6),THOT2(1000),PHT(9),LenDsp(100),LenCon(100)
       $              ,datainput(1000),tchR(1000),tground(1000),thotR(1000)
      Namelist /inputdata / icool,ivlv,ipressure,Tsoil,Mfchill,GHEflow
       $                           ,MFhot,LCON0,LHOT0,LEVP0,dtime,tnumber,AreaNo
      Namelist /ComData /icom,ifluid,displacement,speed,m00
```

```
      Namelist /ExpData /Dcap,LcapC,LcapH
      external functionh,functions
C-------------------------------------------------------------------------------------------
      XMAX=0.40
      X=0.05
c-------------------------------------------------------------------------------------------
c          datat in the inputfile are parameters listed in namelist;
c          note: water flow rate (m3/h); dtime (minutes); calculation numbers -
c          tchillDelphi.txt    is inlet temp to HP on load side;
c          tgroundDelphi.txt is inlet temp to HP on source side, ie GHE;
c          thotDelphi.txt        is inlet temp to HP on hot water side;
c-------------------------------------------------------------------------------------------
         open(111,file='.\delphi_interface\inputdata\inputfile.txt')
         read(111,NML= inputdata)
         close(111)
         open(114,file='.\delphi_interface\inputdata\tchillDelphi.txt')
         open(117,file='.\delphi_interface\inputdata\tgroundDelphi.txt')
         open(118,file='.\delphi_interface\inputdata\thotDelphi.txt')
         open(101,file='.\delphi_interface\inputdata\GHEload.txt')
      i=1
115      read(114,*,end=116) tchR(i)
         read(117,*,end=116) tground(i)
      read(118,*,end=116) thotR(i)
      read(101,*,end=116) GHEload(i)
         i=i+1
         go to 115
116      close(114)
         close(117)
      close(118)
         close(101)
c-------------------consider the area of desp and condenser-----------
      open(102,file='.\delphi_interface\inputdata\AreaDsp.txt')
      open(103,file='.\delphi_interface\inputdata\AreaCon.txt')
         i=1
41    read(102,*,end=40) LenDsp(i)
         read(103,*,end=40) LenCon(i)
      i=i+1
      goto 41
40    close(102)
      close(103)

c-----SET THE INITIAL VALUES FOR EACH COMPOMENT-----------------------------------
c         Ten0 and Penv0 means temp and pressure of dead state use for exergy
c         TIND means indoor air temp;
c-------------------------------------------------------------------------------------------
      thotR(0)=thotR(1)
      tground(0)=tground(1)
      tchR(0)=tchR(1)
      JM=0
      if (icool.ne.1 .and. icool.ne.2) then
      Tenv0=15
      else
      Tenv0=30.
```

```
      endif
         Tenv0=Tenv0+273.15
      tind=15
      Penv0=101.325
c---------------------------------------- 1 GHE-----------------------------------------
c       TNUMBER=number of time steps£¬DELTTAO=time step (SECOND)
c         NPIPE=6 number of boreholes,distance=borehole space, GHEFLOW=total ground
WFR£¬m^/hr
c       GHEFlow=19.2/2.0
c         QGHE=the heat flux of the previous moment£¬equal to the condensation heat rejected in
HP
c         hpipe=borehole deep£¬rb=borehole radius£¬rpi=U pipe inside radius¡¢rp=pipe outside
radius,
c         Dpipe=half distance of the U pipes; kp=pipe conducivity
c         asoil=soil thermal diffusion; ksoil=soil conductivity; kb=grout conducivity;
c-------------------------------------------------------------------------------------------
      QGHE(0)=0.0
      totaltime(0)=0.0
C-------------------------------------- 2 compressor-----------------------------------------
c         displacement = 35.7ml/rotate£»rotating speed=2850 rpm,m00=charge (kg)
c           vth=35.7*1e-6*2850/60    pratical discharge
          open(112,file='.\delphi_interface\inputdata\comdata.txt')
          read(112,NML= comdata)
          close(112)
          vth=displacement*1e-6*speed/60*0.85
c
c----------------------------------------3    hot water-desuperheater MFhot: kg/s----------------
c               input values for three EX: inlet water temp, WFR(kg/s),
c               RICON=scale resistance, LANCON=pipe conductivity-
c-------------------------------------------------------------------------------------------
          if (icool.eq.1 .or. icool.eq.5 ) then
      MFHOt=0.0
      endif
      MFhot=MFhot/3.6
c
C--------------------------------------4 condenser-----------------------------------------
c note: the initial water inlet temp from source side=soil temp; LCON0 is the length of the inner
pipe
c         set the max and mim values of DTU and TC
          EWT(0)=Tground(1)
          if (icool.eq.1 .or. icool.eq.2 ) then
          TFcon1=Tground(1)
      MFCON=GHEFLOW/3.6
      else if (icool.eq.4) then
          MFCON=MFHot
          TFcon1= ThotR(0)
          else
      TFcon1=Tchr(1)
      MFCON=MFChill/3.6
      endif
      DtuMax=30.
      Dtumin=0.0
          TCMIN=20.
```

```
      TCMAX=80.
C
C--------------------------------- 5 evaporator-----------------------------------------
c         RIEVP=scale resistance; LANEVP=conductivity£¬DTS=superheated degree
          if (icool.eq.1.or. icool.eq.2) then
      TFevp1=Tchr(1)
          MFEVP=MFChill/3.6
      else
      TFevp1=Tground(1)
          MFEVP=GHEFlow/3.6
      endif
          DTS=5
          DtsMax=15
      Dtsmin=0.0
c
c----------------------------------6 capillary-----------------------------------------
c ::: two with 1.6mm ID and 450mm long. considering the assistant capillary, add the length
c       add the capillary length by 1.0 ;the actuall length of CT is 0.45 and assistant one
          open(119,file='.\delphi_interface\inputdata\EXpdata.txt')
          read(119,NML= Expdata)
          close(119)
          Dcap=Dcap*1.0e-3
      if (icool.eq.1 .or. icool.eq.2) Lcap0=Lcapc/1000.0
          if (icool.eq.3 .or. icool.eq.4 .or.icool.eq.5) Lcap0=LcapH/1000.0
          if (ifluid.eq.1) then
      Tcritical=96.14
      Pcritical=4990
      endif

c--------------------------------------set the output files----------------------------------
          OPEN(19,FILE='.\outfile\TESTCON.TXT')
          WRITE(19,224)'h2','hsv','hsl','h3','tc','lcon1','lcon2','lcon3'
          OPEN(27,FILE='.\outfile\CONHotwater.TXT')
          WRITE(27,224)'lh1','lh2','lh3','qhtp','qhsh','lc1','lc2',
       $                    'lc3','qconsc','qctp','qcsh'
          open(20,file='.\outfile\jieguo.txt')
      open(22,file='.\outfile\output.txt')
      OPEN(23,FILE='.\outfile\CHARGE.TXT')
          OPEN(24,FILE='.\outfile\RTemp.TXT')
          OPEN(25,FILE='.\outfile\Exergyout.txt')
      open(26,file='.\outfile\ExergyE.txt')
      open(30,file='.\outfile\TestT.txt')
      if (icool.eq.1) then
      WRITE(22,*)'cooling model only'
      WRITE(25,*)'cooling model only'
      else if (icool.eq.2) then
      WRITE(22,*)'cooling with hot water model'
      WRITE(25,*)'cooling with hot water model'
          else if (icool.eq.3) then
      WRITE(22,*)'heating with hot water'
      WRITE(25,*)'heating with hot water'
      else if (icool.eq.4) then
      WRITE(22,*)'hot water heating model only'
```

```
      WRITE(25,*)'hot water heating model only'
      else
      WRITE(22,*)'heating model only'
      WRITE(25,*)'heating model only'
        endif
      WRITE(20,225)'T1','T2','T3','tr2','T4','h1','h2','hhot','h3','mr'
      WRITE(22,225)'time','PWIN','Ptevp2','Ptevp1','Ptcon2','Ptcon1',
     $            'Pthw2','Pthw1','QCON','QHT','QEVP','cop','EER','EWT','OWT'
      write(23,225) 'mconsc','mcontp','monsh','mconpipe','mevptp',
     $              'mevpsh','mevppipe','mhottp','mhotsh','mhotpipe','m'
        WRITE(24,224)'t1','t2','t21','tc','t3c','t3','t4','Te','h1','h2',
     %     'hhot','h3','mr','dts','DTU','trhot2','DPcon','DPevp','pe','pc'
        write(25,225) 'ExR1','ExR2','ExR5','ExR3','ExR4','ExHot1','Exht2',
     $     'ExCon1','Excon2', 'ExEvp1', 'ExEvp2','s1','s2','s3','s4','s5'
        write(26,225) 'SLEtaCom','SLEtaHot','SLEtaCon','SLEtaEV',
     $       'SLEtaEvp','SLEtaFCU','SLEtaGHE','SGDesp','SGEVP','SGGHE',
     $       'SGCON','WthPercent', 'QGHEPercent'
224     Format(1x,20(a12))
225     Format(1x,21(a12))
c-------------------------------------Begin to calculate----------------------          -------------------*
C          ih3=0, no adjust condenser, use the initial value of DTU;                                        *
C          ih3=1 means have adjusted condenser                                                             *
C          h3 is given, dtu can be calculate in compressor;                                                 *
c          ihot=0 no adjust hotwater, use the initial value of hhotou;                                      *
C          ihot=1 menas have adjust hotwater                                                                *
C          hhotou is assumed for the first iteration                                                        *
c-------------------------------------------------------------------------------------------------------------*
c-------------------------consider the number of area of dsp/con-------------------------------
        Do 555 JA=1,AreaNo
        Lcon0=LenCon(JA)
      Lhot0=LenDsp(JA)
      if (Lhot0.eq.0.0) then
      icool=1
      else
      icool=2
      endif
        if (JA.eq.20) then
      write(*,*) JA
      endif
        DO 666 JG=1,TNUMBER
        ih3=0
        Ihot=0
      if (ivlv.eq.2) then
      dtu=5.0
      dts=5.0
        endif
        if (icool.eq.1 .or. icool.eq.2) then
c----------------cooling mode-------------------
        Tground(JG)=EWT(JG-1)
        TFcon1=Tground(JG)
      TFevp1=TchR(JG)
      TFHOT1=THOTR(JG)
      else if (icool.eq.3 .or. icool.eq.5) then
```

```
c----------------heating mode--------------------
          Tground(JG)=EWT(JG-1)
          TFEVP1=Tground(JG)
       TFcon1=TchR(JG)
       TFHOT1=THOTR(JG)
c----------------hot water mode-----------------
       else
          Tground(JG)=EWT(JG-1)
          TFEVP1=Tground(JG)
       TFcon1=TchR(JG)
          if (JG.eq.1) then
       TFHOT1=THOTR(JG)
       else
          TFHOT1=TFCON2
          endif
          endif
C-----------------assume the initial values of TE and T3C ----------------------------------------
C    T3C is useful when considered pressure drop; T3C=TC when no pressure drop in condenser
*
c    T3C is the condensation temperature at the left saturated line; TC is on the right saturated
line*
       T3C=TFcon1+8
       TE=TFEVP1-6
C--------------------TE must be less the outlet chilled water temp-------------------------
3         IF(TE.GE.TFEVP1-5) THEN
       TE=TE-0.5
          WRITE(*,*)'TE=',TE
          GOTO 3
       END IF
4         IF(T3C.LT.TFcon1+5.0) THEN
       T3C=T3C+0.5
       WRITE(*,*)'T3C=',T3C
          GOTO 4
       END IF
C-------------------------set the initial value of the pressure drop in evp and con--------------
C--------- ipressure=1 means to consider the pressure drop; =0 no pressure drop------------
          Dpevpmin=0
       DpconMin=0
          if (ipressure.eq.1) then
          if(ifluid.eq.1) then
          call r22ph(te,pro)
       DpevpMax=0.25*pro(2)
       call r22ph(t3c,pro)
       DpconMax=0.25*pro(2)
       endif
       DpEvp0=(Dpevpmin+DpevpMax)/2.0
          Dpcon0=(DpconMin+DpconMax)/2.0
       else
          pEvp0=0
       Dpcon0=0
       tc=t3c
          endif
```

```
2     LCON=0
        LEVP=0
        IF(TC.GT.100) THEN
      WRITE(1,*)'Condensation temp is too high, suggest to increase pipe
       %                or water flow rate or refrigerant charge.'
      GOTO 100
      ENDIF
C---------------------Compressor model---------------------------
C     judge if there is error in model, if do, then CALL ERROR and go back to the beginning
      CALL COMPRESSOR
        IF(LSTOP.NE.0) THEN
        if (ivlv.eq.1) then
      CALL ERROR(LSTOP,TE,TC,X,XMIN,XMAX)
      else
      CALL ERRORCap(LSTOP,TE,TC,dts,dtu,dtsMax,dtuMax)
      endif
      GOTO 2
      ENDIF

C----------------------evaporator model-----------------------------------
C-judge if there is error in model, if do, then CALL ERROR and go back to the beginning---
      CALL EVAPORATOR(IDP)
        write(1,*)'predicted EVP length',LEVP,'practical length',LEVP0
        IF(LSTOP.NE.0) THEN
        if (ivlv.eq.1) then
      CALL ERROR(LSTOP,TE,TC,X,XMIN,XMAX)
      else
      CALL ERRORCap(LSTOP,TE,TC,dts,dtu,dtsMax,dtuMax)
      endif
      GOTO 2
      ENDIF
        IF (IDP.EQ.1) GOTO 2

C--------------------------------adjust the value of TE-------------------------------------
C---if differecne between exceed allowance error£¬call MODERATEEVP to adjust TE----
      IF(abs(LEVP-LEVP0).GT.0.01)THEN
      IF (ABS(LEVPORIGIONAL-LEVP)/LEVP0.LE.0.0000001) GOTO 14
        LEVPORIGIONAL=LEVP
        CALL MODERATEEVP(LEVP,LEVP0,TE,EVPJUDGE1,EVPJUDGE2,DTS,TFEVP1)
      write(1,*)LEVP,LEVP0,TE,EVPJUDGE1,EVPJUDGE2,DTS,TFEVP1
      GOTO 2
        ENDIF
C       after Adjustment£¬set the original value
14    EVPJUDGE1=0
      EVPJUDGE2=0
      IDP=0
        write(*,*)'evaprator is right'
c-----------------------------------------------------------------------------------------
c --------------------hot water model Ihot£½0 first time to call the model
C       assume the max and min value of the refrigerant outlet enthalpy of Dsp£»

        if (icool.ne.1 .and. icool.ne.5) then
      mfhot0=mfhot
```

```
      mrhot=mr
22      call hotwater(Ihot,mfhot0,mrhot)
        IF(LSTOP.NE.0) THEN
        if (ivlv.eq.1) then
      CALL ERROR(LSTOP,TE,TC,X,XMIN,XMAX)
      else
      CALL ERRORCap(LSTOP,TE,TC,dts,dtu,dtsMax,dtuMax)
      endif
      GOTO 2
      ENDIF
C                                   adjust the outlet enthalpy of the Dsp
C if differecne between.. exceed allowance error£¬call MODERATEEVP to adjust HhotOu
      IF(abs(Lhot-Lhot0).GT.0.01)THEN
      IF (ABS(LHotORIGIONAL-LHot)/LHot0.LE.0.00000001) GOTO 11
      LHotORIGIONAL=LHot
C     tfhot1>=tc+0.01, means superheat regime;
      IF (TFHOT1.GE.TC) THEN
        IF(IFLUID.EQ.1) THEN
      open(3,file='.\parameter\r22fitvap.dat')
        ELSEIF(IFLUID.EQ.2) THEN
      open(3,file='.\parameter\r134afitvap.dat')
      ENDIF
        do 111 i=1,9
        read(3,*) PHT(i)
111     continue
        close(3)
        FitA1=PHT(1)
        FitA2=PHT(2)*0.001
        FitA3=PHT(3)*1e-6
        FitA4=PHT(4)
        FitA5=PHT(5)*0.1
        FitA6=PHT(6)*1e-4
        FitA7=PHT(7)
        FitA8=PHT(8)
        FitA9=PHT(9)*1e-3
        HIN=H2
C--assume HhotOu, max is the oulet enthalpy from compressor (HSV);-----------------------
C-- min is Max(H33,HSL) ----------------------------------------------------
C-----jj=0 means the first guessed HhotOu, if jj=1, use the updated value                *
C---IF TFHOT1>TC, IT MEANS SUPERHEAT ONLY; assume no subcool region in Dsp *
C--------TRHOT2>TFHOT1, min is enthalpy when R22 at the condition of Pc and TFHOT1;
C -------Usually H33<HSV      *
C-----------------------------------------------------------------------------------------------
      TC1=tc+273.15
      TF1=TFHOT1+273.15
      EPS=0.0001
      HHSV=HSV/10.
      HH2=HIN/10.
c     HH is relative to TFHot1
      CALL ROOTH(HHSV,HH2,EPS,HH,TF1,TC1,HHSV)
        HTFhot1=HH*10.
      HMIN=HTFHot1
      ELSE
```

```
      HMIN=Hsl
      ENDIF
        CALL MODERATEHot(LHot,LHot0,HotJUDGE1,HotJUDGE2,H2,HMIN,HhotOu)
      Ihot=1
      GOTO 22
        ENDIF
C       after adjustment, set the value back
11    HotJUDGE1=0
      HotJUDGE2=0
c ------------------consider the two parallel pipes in the HE-----------------------
        endif

c-------------------------------condenser model---------------------------------
c         judge cooling with HW or only HW
      CALL CONDENSER(IDP)
        IF(LSTOP.NE.0) THEN
        if (ivlv.eq.1) then
      CALL ERROR(LSTOP,TE,TC,X,XMIN,XMAX)
      else
      CALL ERRORCap(LSTOP,TE,TC,dts,dtu,dtsMax,dtuMax)
      endif
      GOTO 2
      ENDIF
        IF (IDP.EQ.1) GOTO 2

C---------------------- adjust the condensation temp TC--------------------------
C
        LCON=LCON1+LCON2+LCON3
      IF(abs(LCON-LCON0).GT.0.01)THEN
      IF (ABS(LCONORIGIONAL-LCON)/LCON0.LE.0.00000001) GOTO 12
      LCONORIGIONAL=LCON
        if (ivlv.eq.1) then
c-----------in expansion valve case, consider the pressure drop or not, to adjust T3C or
TC----------
          if (ipressure.eq.0) then
          CALL MODERATECON(LCON,LCON0,TC,CONJUDGE1,CONJUDGE2,TFcon1)
       else
          CALL MODERATECON(LCON,LCON0,T3C,CONJUDGE1,CONJUDGE2,TFcon1)
       endif
      else
c adjust the outlet enthalpy of the condenser; then calculate dtu in the compressur model;
        if (LCON.lt.LCON0) then
      if (hcon3.eq.h33) then
c       ---------this means the tfcon1 is nealy equal to trcon2, ------------
c       ****want to rise LCON, need to reduce hcon3, which will cause hcon3<h33,
c             this is impossble in practice*********
        write(*,*) 'tfcon1 approaches trcon2, no compute the condensate'
      goto 12
      endif
        endif
        CALL MdrtConCap(LCON,LCON0,Tc,CONJUDGE1,CONJUDGE2,
       $TFCON1,dtu,hcon3,h3,h33)
        ih3=1
```

```
      endif
      GOTO 2
        ENDIF
C         set the adjustment back
12    CONJUDGE1=0
      CONJUDGE2=0
      IDP=0
        write(*,*)'correct condenser'
c-------------------------------------------------------------------------------------
c                                      no expansion valve model
c    ----------------       capillary model: update condensate pressure/temp, ----------
        if (ivlv.eq.2)       then
        if (ipressure.eq.0) then
        DPCON=0
      DPEVP=0
      endif
      PCAPIN=PC-DPCON
      PCAPOUT=PE+DPEVP
      CALL capillary(ifluid,t3,PCAPIN,PCAPOUT,tc,te,mr,tcmin,tcmax,dtu
       $,h3,dts0,dts)
        IF(LSTOP.NE.0) THEN
          CALL ERRORCap(LSTOP,TE,TC,dts,dtu,dtsMax,dtuMax)
      GOTO 2
      ENDIF
        mcap=mr/2.0
      IF(ABS(mr0-mcap)/mcap.GT.0.005)THEN
      IF (ABS(Mr0ORIGIONAL-Mr0)/Mcap.LE.0.0000001) GOTO 15
        Mr0ORIGIONAL=mr0
        CALL MODERATECAPPc(Mr0,mcap,Tc,CAPJUDGE1,CAPJUDGE2,TCmin,TCmax)
        write(20,200)tc,hou,h33,mr0,mcap
        write(20,200)T1,T2,T3,trcon2,T4,x,te,tc,h2,h3,mr
      GOTO 2
        ENDIF
15    CAPJUDGE1=0
      CAPJUDGE2=0
        write(*,*)'capillary model right'
      endif

c ------------------------------------------------------------------------------------
c-------------------------------------------------------------------------------------
C                              -------adjust the refrigerant chargement-----------------
        MCON=MCONSC+MCONTP+MCONSH
        MCHARGE=(MCON+MEVP+MCONPIPE+MEVPPIPE+MHOT+MHOTPIPE)*1.1
      write(23,200) mconsc,mcontp,mconsh,mconpipe,mevptp,mevpsh,mevppipe
       $,mhottp,mhotsh,mhotpipe,mcharge
        write(30,200) t1-273,t2-273,t3,t4,dts,dtu,pe,pc,h2,h3,x
        dts0=dts
        IF(ABS((MCHARGE-m00)/m00).GT.0.01) THEN
      IF (ABS(MCHARGEORIGIONAL-MCHARGE)/m00.LE.0.0000001) GOTO 13
        MCHARGEORIGIONAL=MCHARGE
C---------------------ivlv=1 adjust X    ivlv=2 adjust dts--------------------------
C JM: JUDGE WHETHER ADJUST MCHARGE or not (make note in condenser) C JM=1
means
```

```
C have adjusted Mcharge,
C      if hou<h33, need to increase x;but if mcharge<m00, need to reduce x;
C    reduce X and increase Charge£»will result in hou<h33,then need to increase x again;
          if (ivlv.eq.1) then
          CALL MODERATEM(MCHARGE,m00,X,MJUDGE1,MJUDGE2,XMIN,XMAX)
       JM=1
       WRITE(11,*)'X=',X,MCHARGE,m00,MCONPIPE,MEVPPIPE
       else
          CALL
MODERATEMDts(MCHARGE,m00,dts,MJUDGE1,MJUDGE2,Dtsmin,DtsMax,
        $te)
             JM=1
       WRITE(11,*)'dts=',dts,MCHARGE,m00,MCONPIPE,MEVPPIPE
       endif
       GOTO 2
       ENDIF
          write(23,*)'CRT M=',mcharge,'Last m=',mchargeorigional,'m0=',m00
          write(30,200)t1-273,t2-273,t3,t4,dts,dtu,pe,pc,h3,x
       go to 16
13        write(23,*)'wrong charge,current m=',mcharge,'last m=',
         &                    mchargeorigional,'m0=',m00
          write(30,*)'wrong',t1-273,t2-273,t3,t4,dts,dtu

16     MJUDGE1=0
       MJUDGE2=0
c----------------------just for hotwater heating, as the water is first go into the
c-----------condenser and then desuperheater;however, in simulation, the desuperheater is first
modeled
          if (icool.eq.4) then
       if (abs(TFhot1-TFcon2).gt.0.1) then
       TFHOT1=(TFhot1+TFcon2)/2
          go to 2
       endif
       endif
C------------------------heat pump unit output and exergy analysis-------------------------------------
          call exergyAnalysis(tsoil,tind)
          THOT2(JG)=TFHOT1b
          EER=(Qevp+Qhot)/win
       cop=(Qcon+Qhot)/win
          qcom=mr*(H2-H3)
       wth=mr*(h2-h1)
       QCHot=Qcon+Qhot
       WRITE(*,*)'THE', JG, ' time IS RIGHT'

C-----------------------------Run GHE model-----------------------------------------

          if (icool.eq.3) then
          TFMGH=(TFEVP1+TFEVP2)/2.0
       else
          TFMGH=(TFcon1+TFcon2)/2.0
       endif
          call    R718LIQ(TFMGH,GROUNDpro)
       yiu=GROUNDpro(2)
```

```
      cp=GROUNDpro(3)*1000
c-------------dtime means how many minutes in each time interval-----------------------
      totaltime(jg)=dtime*jg*60
         if (icool.ne.1 .and. icool.ne.2) then
         QGHE(JG)=GHEFLOW/3600.*YIU*CP*(TFEVP2-TFEVP1)
      else
         QGHE(JG)=GHEFLOW/3600.*YIU*CP*(TFcon2-TFcon1)
      endif
         call GHETemp(JG,GHEFlow,TSOIL)
      write(27,200)LHOT1,LHOT2,LHOT3,QHOTTP,QHOTSH,
       $LCON1,LCON2,LCON3,QSC,QTP,QSH
         t3=t3c-dtu
      trcon2=trcon2
c--------------------------------------------------------------------------------
c-------------------------------OUTPUT-------------------------------------------
c
      write(24,200)t1-273.15,t2-273.15,tcomout,tc,t3c,t3,t4,Te,h1,h2
       %                  ,hhotou,h3,mr,dts,DTU,trhot2,dpcon,dpevp,pe,pc
666      write(22,200)totaltime(jg),WIN,tfevp2,tfevp1,tfcon2,tfcon1,tfhot2,
       $tfhot1,QCON,QHOT,QEVP,cop,EER,EWT(JG),OWT(JG)
555      continue

200      FORMAT(1X,20F12.4)
201      FORMAT(1X,11F12.4)
         close(19)
      CLOSE(20)
         close(22)
         close(23)
         close(24)
         close(25)
      close(26)
      close(27)
      close(30)
100   END
```